AD-A185 482 EXPLOITATION OF THE SOL-GEL ROUTE IN PROCESSING OF CERAMICS AND COMPOSITES(U) PENNSYLVANIA STATE UNIV UNIVERSITY PARK MATERIALS RESEARCH LA... R ROY 1/2

UNCLASSIFIED 10 JUL 87 AFOSR-TR-87-1193 F49620-85-C-0069 F/G 11/4 NL

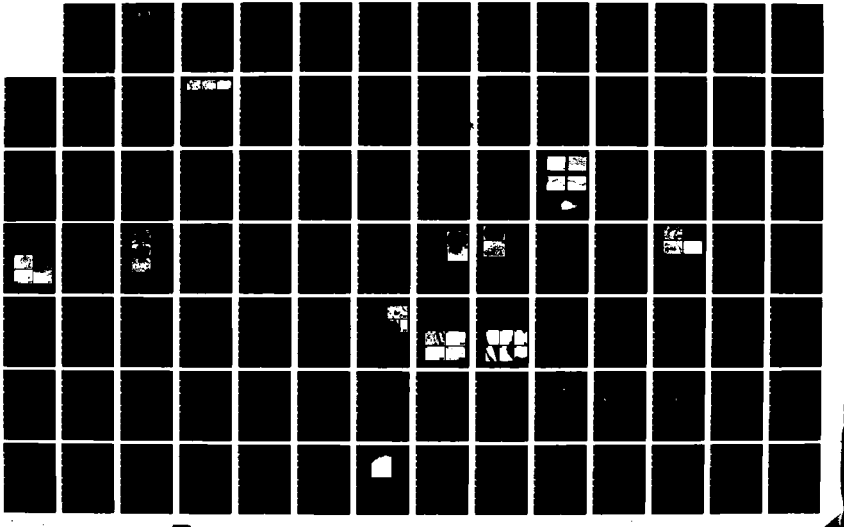

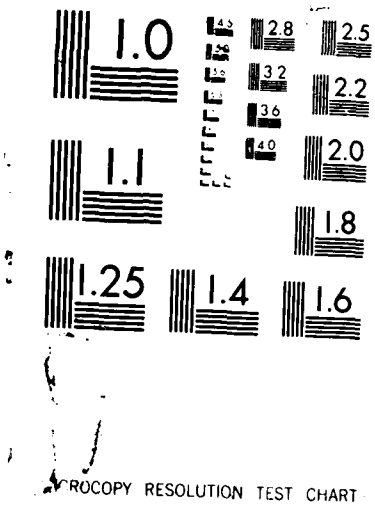
1.0
2.8
2.5
3.2
2.2
3.6
4.0
1.1
2.0
1.8
1.25
1.4
1.6
ROCOPY RESOLUTION TEST CHART

UNCLASSIFIED
SECURITY CLASSIFICATION OF THIS PAGE

DTIC FILE COPY

REPORT DOCUMENTATION PAGE

AD-A185 482 DTIC ELECTE OCT 0 2 1987 S D

	1b. RESTRICTIVE MARKINGS
2b. DECLASSIFICATION / DOWNGRADING SCHEDULE	3. DISTRIBUTION / AVAILABILITY OF REPORT Approved for public release; distribution unlimited
4. PERFORMING ORGANIZATION REPORT NUMBER(S) Final Report	5. MONITORING ORGANIZATION REPORT NUMBER(S) AFOSR-TR- 87-1193
6a. NAME OF PERFORMING ORGANIZATION The Pennsylvania State University	6b. OFFICE SYMBOL (If applicable)
6c. ADDRESS (City, State, and ZIP Code) Materials Research Laboratory University Park, PA 16802	7a. NAME OF MONITORING ORGANIZATION Air Force Office of Scientific Research
	7b. ADDRESS (City, State, and ZIP Code) Bolling Air Force Base Washington, DC 20332 BKG 410
8a. NAME OF FUNDING / SPONSORING ORGANIZATION Air Force Office of Scientific Research	8b. OFFICE SYMBOL (If applicable) NC
	9. PROCUREMENT INSTRUMENT IDENTIFICATION NUMBER Contract F49620-85-C-0069
8c. ADDRESS (City, State, and ZIP Code) Bolling Air Force Base Washington, DC 20332 BKG 410	10. SOURCE OF FUNDING NUMBERS

PROGRAM ELEMENT NO.	PROJECT NO.	TASK NO.	WORK UNIT ACCESSION NO.
61102F	2303	A3	

11. TITLE (Include Security Classification)
Exploitation of the Sol-Gel Route in Processing of Ceramics and Composites

12. PERSONAL AUTHOR(S)
Rustum Roy

13a. TYPE OF REPORT	13b. TIME COVERED	14. DATE OF REPORT (Year, Month, Day)	15. PAGE COUNT
FINAL	FROM 5/15/85 TO 5/14/87	July 10, 1987	103

16. SUPPLEMENTARY NOTATION

17 COSATI CODES			18. SUBJECT TERMS (Continue on reverse if necessary and identify by block number)
FIELD	GROUP	SUB-GROUP	

19. ABSTRACT (Continue on reverse if necessary and identify by block number)

Two years of this contract and two years of prior support through a grant have led to several important developments in the nanoheterogeneous sol-gel processing of ceramics. It is clear that such materials can reduce processing temperatures by 100-300°C, change the microstructure from 10μ to <1μ, and modify the morphology from equant to acicular.

1. Compositionally diphasic xerogels. These materials are very intimate mixtures composed of two solid phases each on the order of 10-20 nm. The two phases are only different in composition. Using the mullite ($3Al_2O_3 \cdot 2SiO_2$) system as the prototype model, we have shown that the compositionally diphasic materials sinter to a much lower temperature than the single phase gels. Such sintering of compositionally diphasic gels at much lower temperatures may be attributed, at least in part, to the heat of reaction of the two discrete phases at the sintering temperature. This notion was extended to other systems such as Al_2TiO_5, $ZrSiO_4$, $ThSiO_4$ and $Mg_2Al_4Si_5O_{18}$. Results to date on the Al_2TiO_5, $ZrSiO_4$ and $ThSiO_4$

20. DISTRIBUTION / AVAILABILITY OF ABSTRACT	21. ABSTRACT SECURITY CLASSIFICATION
☐ UNCLASSIFIED/UNLIMITED ☒ SAME AS RPT ☐ DTIC USERS	Unclassified

22a. NAME OF RESPONSIBLE INDIVIDUAL	22b. TELEPHONE (Include Area Code)	22c. OFFICE SYMBOL
Dr Donald R Ulrich	(202) 767-4963	NC

DD FORM 1473, 84 MAR 83 APR edition may be used until exhausted. All other editions are obsolete.

SECURITY CLASSIFICATION OF THIS PAGE

EXPLOITATION OF THE SOL-GEL ROUTE IN PROCESSING OF CERAMICS AND COMPOSITES

FINAL REPORT

to

AIR FORCE OFFICE OF SCIENTIFIC RESEARCH
Bolling Air Force Base, DC 20332

Contract F49620-85-C-0069

Period Covered:

May 15, 1985 - May 14, 1987

Submitted by

Rustum Roy
Materials Research Laboratory
The Pennsylvania State University
University Park, PA 16802

TABLE OF CONTENTS

ABSTRACT

Two years of this contract and two years of prior support through a grant have led to several important developments in the nanoheterogeneous sol-gel processing of ceramics. It is clear that such materials can reduce processing temperatures by 100-300°C, change the microstructure from 10μ to <1μ, and modify the morphology from equant to acicular.

1. Compositionally diphasic xerogels. These materials are very intimate mixtures composed of two solid phases each on the order of 10-20 nm. The two phases are only different in composition. Using the mullite ($3Al_2O_3 \cdot 2SiO_2$) system as the prototype model, we have shown that the compositionally diphasic materials sinter to a much lower temperature than the single phase gels. Such sintering of compositionally diphasic gels at much lower temperatures may be attributed, at least in part, to the heat of reaction of the two discrete phases at the sintering temperature. This notion was extended to other systems such as Al_2TiO_5, $ZrSiO_4$, $ThSiO_4$ and $Mg_2Al_4Si_5O_{18}$. Results to date on the Al_2TiO_5, $ZrSiO_4$ and $ThSiO_4$ systems do not show significant improvements in densification behavior although the use of diphasic gels led to a lowering in the crystallization temperatures of $ZrSiO_4$, $ThSiO_4$, etc. The diphasic $Mg_2Al_4Si_5O_{18}$ system exhibits metastable melting which could be used for enhanced densification of this low-expansion ceramic. Using the diphasic approach, we have also prepared translucent ultra-low expansion titania-silica glasses with 0 to 10% TiO_2. The coefficients of thermal expansion are intermediate between those of fused silica and a commercial titania-silica glass. The glass with 7.2% TiO_2 exhibited a zero thermal expansion coefficient at 150-210°C.

2. Structurally diphasic xerogels. These materials consist of two phases with the same composition but different structure. Examples include mixtures of crystalline seeds in amorphous or semicrystalline xerogels. The crystalline seeds are of the phase(s) expected in the final equilibrium assemblage. Using the system Al_2O_3 and Al_2O_3-MgO, we have demonstrated in detail the effects of α-Al_2O_3 and $MgAl_2O_4$ second phases (seeding) in lowering sintering temperature and enhancing densification. This approach was extended to $NiAl_2O_4/Al_2O_3$ composites for enhancing densification.

3. Natural models of gel-derived ceramics. The work of the past two years has revealed that the natural gel-derived ceramics such as opals, cherts, chalcedonies, flints, jaspers, etc., have mechanical properties superior to borosilicate or soda-lime glasses. The synthetic opal, gilsonite was found to be a diphasic material consisting of 3-5% tetragonal, spherical ZrO_2 in addition to spherical SiO_2. We have investigated the use of diphasic reaction bonding, γ-irradiation bonding and hydrothermal reaction bonding to mimic the natural as well as the synthetic gel-derived ceramics. We have made composites of glass by introducing second phases in porous glass.

Ten research papers supported by this project were presented during the past two years and nine papers appeared in print.

I. PROGRAM GOALS

The goal of this program was to explore and develop novel processing techniques for ceramics based on the solution-sol-gel route.

II. PROGRESS TO DATE

A. INTRODUCTION

The re-emergence of solution-sol-gel (SSG) technique as a versatile ceramic processing method is very recent although its original development occurred at Penn State some 30 years ago (1-4). The enormous value and versatility of this method can be gauged by its widespread use in industry for making coatings and films (5,6), glass and ceramic fibers (7,8), porous solids and microballoons (9,10), nuclear fuels and radioactive waste (11), and "bulk" ceramics (12) and glasses (13).

B. NEW DIRECTION FOR SOL-GEL RESEARCH

The worldwide goal of all sol-gel work has been ultrahomogeneity while our goal in this area has been switched to the preparation of materials which exhibit ultraheterogeneity or nanoheterogeneity. Our conceptual innovation, on which the present work rests, is a radically new direction for sol-gel research. Although we had utilized the idea of crystallographic seeding of gels with the equilibrium phase--specifically for example of adding α-Al_2O_3 or diaspore (Al.O.OH) seeds to boehmite gels in several of our early papers dating to 1949-50 we first presented the general idea of deliberately using the SSG route (14) to achieve heterogeneity on a nanoscale (1-100 nm units) in November 1982 (15) and have been developing this idea for processing ceramics under this contract. The work under this contract is focused on applications and processing, while the thermodynamics and structure of this family of nanoheterogeneous materials is studied under a parallel NSF grant. Both compositional heterogeneity and structural heterogeneity (seeding) have since been shown by us and continued by others to have profound effects on enhancing densification, sintering, and controlling microstructure and morphology in ceramics.

C. RESULTS

1. Compositionally Diphasic Xerogels for Enhanced Densification and Sintering

The work in the last two years of this contract has proved very successful. We have achieved theoretical density in the sintering of mullite, $3Al_2O_3 \cdot 2SiO_2$ using the compositionally diphasic xerogels approach where Al_2O_3 and SiO_2 sols have been used (see Reprint 1). This approach was shown to be superior to the heterocoagulation technique used by others. The use of compositionally diphasic gels in systems such as Al_2TiO_5, $ZrSiO_4$ and $ThSiO_4$ did not show detectable improvements in densification but showed a lowering in crystallization temperature. Metastable melting was observed in the cordierite, $Mg_2Al_4Si_5O_{18}$ system through the use of diphasic approach (see Manuscript 1).

2. Structurally Diphasic Xerogels for Enhanced Densification and Sintering

Structural 'seeding' has been shown to have profound effects on enhancing densification and sintering of Al_2O_3 and Al_2O_3-MgO gels. An example of the enormous value of structural heterogeneity is the use of α-Al_2O_3 seeds in the densification of boehmite sol-gels where 99% density has been achieved at 1200°C (see Reprint 2). The dramatic effects of α-Al_2O_3 seeding on the microstructural development upon sintering of boehmite gels were also shown (see Reprint 3). Microstructural characterization and density measurements of 93% Al_2O_3-7% MgO gels seeded with α-Al_2O_3 and $MgAl_2O_4$ revealed that this double seeding is superior to seeding with only one of them for densification of these gels (see Reprint 4).

3. Microwave Processing of Zeolites

Our earlier work has shown that gels can be melted in minutes in a microwave oven. We have now identified new materials which are highly susceptible to microwave radiation and can be used as thermal seeds for microwave processing of gels since the gels do not heat up rapidly in the beginning. These materials are zeolites, crystalline aluminosilicates with cage structures (see Reprint 5). A patent application on these materials has been submitted to the AFOSR.

4. Natural and Synthetic Models

The chemistry, microstructure and mechanical properties of a large representative set of naturally occurring and synthetic single and diphasic gel-derived ceramic materials have been

investigated in detail in order to understand the mechanism of consolidation at low temperatures. The synthetic opal, gilsonite, is a diphasic xerogel. The microstructure and mechanical properties of this synthetic opal were investigated to understand the consolidation process of this chemically bonded ceramic (see Reprint 6). Hardness and fracture toughness measurements indicate that jaspers, flints, cherts and agates are hard and very tough naturally formed, gel-derived ceramics which are harder and tougher than borosilicate or soda-lime glasses. Mechanical data was generated for this set of natural materials which will serve as a reference base for the next step of this work which is to find treatment methods to enhance the hardness and toughness of these materials (see Manuscript 2).

5. Diphasic Route to Ultra-Low Expansion (ULE) Glasses

A colloidal sol-gel process utilizing colloidal silica and stabilized or peptized titanium isopropoxide has been developed for making ultra-low expansion glasses. This, in principle, is the same as the compositionally diphasic route for making ceramics and glasses (see Reprint 7 and Manuscript 3).

REFERENCES

1. R. Roy and E.F. Osborn, "The System Al_2O_3-SiO_2-H_2O," Am. Mineral. 39 [11/12], 853-885 (1954).
2. V.G. Hill, R. Roy and E.F. Osborn, "The System Alumina-Gallia-Water," J. Am. Ceram. Soc. 35 [6], 135-142 (1952).
3. D.M. Roy and R. Roy, "An Experimental Study of the Formation and Properties of Synthetic Serpentines and Related Layer Silicate Minerals," Am. Mineral. 39 [11/12], 957-975 (1954).
4. R. Roy, "Aids in Hydrothermal Experimentation: II, Methods of Making MIxtures for Both 'Dry' and 'Wet' Phase Equilibrium Studies," J. Am. Ceram. Soc. 39 [4], 145-146 (1956).
5. H. Dislich and E. Hussmann, "Amorphous and Crystalline Dip Coatings Obtained from Organometallic Solutions: Procedures, Chemical Processes and Products," Thin Solid Films 77 [2], 129-139 (1981).
6. B.E. Yoldas and T.W. O'Keefe, "Antireflective Coatings Applied from Metal-Organic Derived Liquid Precursors," Applied Optics 18 [18], 3133-3138 (1979).
7. H.G. Sowman, "Alumina-Chromia-Metal (IV) Oxide Refractory Fibers Having a Microcrystalline Phase," U.S. Patent 4,125,406 (1978).
8. S. Yajima, H. Hasegawa, J. Hayashi and M. Iimura, "Synthesis of Continuous Silicon Carbide Fiber with High Tensile Strength and High Young's Modulus," J. Mat. Sci. 13 [12], 2569-2576 (1978).
9. B.E. Yoldas, "A Transparent Porous Alumina, " Am. Ceram. Soc. Bull. 54 [3], 286-288 (1975).
10. R.W. Wehrenberg, II Mat. Eng. (Oct. 1, 1978).
11. J.P. McBride, "Preparation of UO_2 Microspheres by Sol-Gel Techniques," Oak Ridge National Laboratory Report No. ORNL-3874 (1966).
12. W.D. Arnold, W.D. Bond and S.M. Robinson, Radioact. Waste Mgmt. Nucl. Fuel Cycle 3, 57 (1982).

13. I.M. Thomas, "Metal-Organic-Derived (MOD) Glass Compositions, Preparation, Properties, and Some Applications," Abstracts, Annual Meeting of the Materials Research Society, Boston, MA, p. 370 (1982).

14. R. Roy, "Sol-Gel Processes: Origins, Problems, Products," Am. Ceram. Soc. Bull. 60, 383 (1981).

15. R.A. Roy and R. Roy, "New Metal-Ceramic Hybrid Xerogels," Abstracts, Annual Meeting of Materials Research Society, Boston, MA, p. 377 (1982).

CUMULATIVE LIST OF PUBLICATIONS AND PRESENTATIONS

1. D. Hoffmann, R. Roy and S. Komarneni, "Diphasic Ceramic Composites via a Sol-Gel Method," Mat. Letters 2, 245-247 (1984).
2. D. Hoffmann, S. Komarneni and R. Roy, "Preparation of a Diphasic Photosensitive Xerogel," J. Mat. Sci. Letter 3, 439-442 (1984).
3. R. Roy, S. Komarneni and D.M. Roy, "Multiphasic Ceramic Composites Made by Sol-Gel Technique," in the Proceedings of the Symposium on "Better Ceramics Through Chemistry" (Eds. C.J. Brinker et al.), Elsevier, North-Holland, pp. 347-359 (1984) (jointly supported by NSF).
4. D.W. Hoffmann, R. Roy and S. Komarneni, "New Sol-Gel Strategies for Making Ceramic-Ceramic Composites," Abstracts, 1984 American Ceramic Society Meeting, Am. Ceram. Soc. Bull. 63, 459 (1984).
5. R. Roy, S. Komarneni and D.W. Hoffmann, "Sol-Gel Approach to Making Photochromic Xerogels and Glasses," Abstracts, 1984 American Ceramic Society Meeting, Am. Ceram. Soc. Bull. 63, 499 (1984).
6. R. Roy, L.J. Yang and S. Komarneni, "Controlled Microwave Sintering and Melting of Gels," Abstracts, 1984 American Ceramic Society Meeting, Am. Ceram. Soc. Bull. 63, 459 (1984).
7. S. Komarneni, L.J. Yang and R. Roy, "Hydrothermal Reaction Sintering of Single and Diphasic Xerogels," Abstracts, 1984 American Ceramic Society Meeting, Am. Ceram. Soc. Bull. 63, 459 (1984).
8. R. Roy, S. Komarneni and L.J. Yang, "Controlled Microwave Sintering and Melting of Gels," J. Am. Ceram. Soc. 68, 392 (1985).
9. S. Komarneni, R. Roy, E. Breval and Y. Suwa, "Hydrothermal Route to Ultrafine Powders Utilizing Single and Diphasic Gels," Abstracts of the Second International Symposium on Hydrothermal Reactions in University Park, p. 62.

10. S. Komarneni, R. Roy, E. Breval, M. Ollinen and Y. Suwa, "Hydrothermal Route to Ultrafine Powders Utilizing Single and Diphasic Gels," Adv. Ceramic Mats. 1, 87 (1986).

11. R. Roy, Y. Suwa and S. Komarneni, "Nucleation and Epitaxial Growth in Reactions of the Diphasic (Crystalline + Amorphous) Gels," presented at the Second International Conference on Ultrastructure Processing of Ceramics, Glasses and Composites in February 1985 (jointly supported by NSF).

12. T.C. Simonton and R. Roy, "Natural Gel Derived Ceramics: Chemistry, Microstructure and Properties of Opal, Chert, Agate, Etc.," Abstracts of the American Ceramic Society Meeting, Cincinnati, OH, 1985, p. 269.

13. R. Roy, "Seeding: A Special Approach to Diphasic Xerogels," Abstracts of the American Ceramic Society Meeting, Cincinnati, OH, 1985, p. 270.

14. R. Roy, "Microwave Melting of Ceramics and Gels," Patent applications filed via AFOSR.

15. C. Scherer and C. Pantano, "Ti-Si Glasses Using a Colloidal Sol-Gel Process," presented at the Third International Workshop on Glasses and Glass Ceramics from Gels, Montpellier, France, 1985.

16. S. Komarneni and R. Roy, "Microwave Processing of Zeolites," AF Invention 17310 (1985).

17. Y. Suwa, R. Roy and S. Komarneni, "Crystallographic Effects in Seeded (Diphasic Gels): II. Microstructural and Sintering Properties," Abstracts of the American Ceramic Society Meeting, Cincinnati, OH, 1985, p. 270.

18. Y. Suwa, R. Roy and S. Komarneni, "Enhancing Densification by Solid State Epitaxy in Structurally Diphasic Al_2O_3-MgO Xerogels," Abstracts, Materials Research Society, 1985 Fall Meeting, p. 468 (1985).

19. S. Komarneni and R. Roy, "Anomalous Microwave Sintering and Melting of Zeolites," Abstracts, Materials Research Society, 1985 Fall Meeting, p. 468 (1985).

20. R. Roy, Y. Suwa and S. Komarneni, "Nucleation and Epitaxial Growth in Reactions of Diphasic (Crystalline + Amorphous) Gels," in Ultrastructure Processing of Ceramics, Glasses and Composites (Eds. L.L. Hench and D.R. Ulrich), pp. 247-258 (1986).

21. Y. Suwa, R. Roy and S. Komarneni, "Lowering Sintering Temperature and Enhancing Densification by Epitaxy in Structurally Diphasic Al_2O_3 and Al_2O_3-MgO Xerogels," Mat. Sci. Eng. 83, 151 (1986).

22. S. Komarneni and R. Roy, "Anomalous Microwave Melting of Zeolites," Mat. Lett. 4, 107 (1986).

23. S. Komarneni, G. Vilmin, Y. Suwa and R. Roy, "Enhancing Densification of Al_2O_3-MgO Xerogels by Double Seeding with α-Al_2O_3 and $MgAl_2O_4$," Abstracts, The American Ceramic Society 88th Annual Meeting, p. 92 (1986).

24. S. Komarneni, A. Kijowski, T.C. Simonton and R. Roy, "Diphasic Glass Composites," Abstracts, The American Ceramic Society 88th Annual Meeting, p. 92 (1986).

25. T.C. Simonton, S. Komarneni and R. Roy, "Diphasic Composites of Natural Gel Derived Ceramics," Abstracts, The American Ceramic Society 88th Annual Meeting, p. 117 (1986).

26. T.C. Simonton, S. Komarneni and R. Roy, "Radiation Assisted Chemical Bonding of Natural and Synthetic Gel-Derived Ceramics," Abstracts, The American Ceramic Society 88th Annual Meeting, p. 122 (1986).

27. S. Komarneni, Y. Suwa and R. Roy, "Application of Compositionally Diphasic Xerogels for Enhanced Densification: The System Al_2O_3-SiO_2," J. Am. Ceram. Soc. 69, C-155 (1986).

28. T.C. Simonton, R. Roy, S. Komarneni and E. Breval, "Microstructure and Mechanical Properties of Synthetic Opal: A Chemically Bonded Ceramic," J. Mat. Res. 1, 667 (1986).

29. S. Komarneni, Y. Suwa and R. Roy, "Enhancing Densification of 93% Al_2O_3-7% MgO Triphasic Xerogels with Crystalline α-Al_2O_3 and $MgAl_2O_4$ Seeds," J. Mat. Sci. Lett. 6, 525 (1987).

30. T.C. Simonton, S. Komarneni and R. Roy, "Ultrafine Microstructure in Synthetic Opal, A Diphasic Composite," Abstracts, Materials Research Society, 1986 Fall Meeting, p. 747 (1986).

31. W.A. Yarbrough and R. Roy, "Extraordinary Effects of Mortar-and-Pestle Grinding on Microstructure of Sintered Alumina Gel," Nature 322, 347 (1986).

32. C.P. Scherer and C.G. Pantano, "Titania-Silica Glasses Using a Colloidal Sol-Gel Process," J. Non-Cryst. Solids 82, 246 (1986).

33. W.A. Yarbrough and R. Roy, "Microstructure Evolution in Sintering of AlOOH Gels," J. Mat. Res. (in press).

34. R. Roy, "Some New Advances with SSG Derived Nanocomposites," Abstracts, Third International Conference on Ultrastructure processing of Ceramics, Glasses and Composites, p. 44 (1987).

35. R. Roy, S. Komarneni and W.A. Yarbrough," Some New Advances with SSG Derived Nanocomposites," Third International Conference on Ultrastructure Processing of Ceramics, Glasses and Composites (Eds. J.D. MacKenzie and D.R. Ulrich) (submitted for publication).

36. D. Zaide, E. Breval and C.G. Pantano, "Colloidal Sol/Gel Processing of Ultra-low Expansion TiO_2/SiO_2 Glasses," presented at the Fourth International Workshop on Glasses-Ceramics from Gels, Kyoto, Japan, 1987.

37. Y. Suwa, S. Komarneni and R. Roy, "Effect of Seeding on Crystallization and Sintering of Diphasic Al_2O_3-MgO Monolithic Gels," Proceedings of the Japanese Ceramic Society, Vol. 3, pp. 735-736 (1987).

Reprint #1

Application of Compositionally Diphasic Xerogels for Enhanced Densification: The System Al_2O_3-SiO_2

J. Am. Ceram. Soc., 69 [7] C-155-C-156 (1986)

Application of Compositionally Diphasic Xerogels for Enhanced Densification: The System Al_2O_3-SiO_2

SRIDHAR KOMARNENI,* YOSHIKO SUWA,* AND RUSTUM ROY*,†

Materials Research Laboratory, The Pennsylvania State University, University Park, Pennsylvania 16802

Stoichiometric mullite (71.38 wt% Al_2O_3-28.17 wt% SiO_2) and 80 wt% Al_2O_3-20 wt% SiO_2 gels were prepared by the single-phase and/or diphasic routes. Dense sintered bodies were prepared from both sets of gels in the Al_2O_3-SiO_2 system. Apparent densities of 96% and 97% of theoretical density were measured for the diphasic (using two sols) mullite samples sintered at 1200° and 1300°C for 100 min, respectively; this compared with 85% and 94% for the single-phase xerogels under the same conditions, and to much lower values for mullite prepared from conventional mixed powders. The microstructure of the mullite pellets from diphasic xerogel precursors is also considerably finer.

THERE is enormous interest in the sol-gel method and especially the use of metal alkoxide precursors at present for making ultrahomogeneous glasses and ceramics for technological applications throughout the world. The above method was developed some 30 years ago at The Pennsylvania State University[1-4] and it utilized both organic and inorganic precursors. In those studies the products were utilized for phase equilibrium studies; the technological applications of this process were not pursued. Fifteen to twenty years later several groups exploited this process successfully for various technological applications from nuclear fuel to ceramic fibers, window coatings, and abrasive grain.[5-8]

This triggered the present enormous worldwide interest in the science of this process. The universal goal of all such research was in making ceramics and glasses from starting materials that are homogeneous on the "unit-cell" scale. A recent conceptual innovation in the sol-gel method is the use of *heterogeneity* on a "nano" scale for applications and processing of ceramics.[9-12] This conceptual innovation is based on the hypothesis[10] that diphasic or multiphasic xerogels which are heterogeneous must store more metastable energy than the single-phase gels since the heats of reaction of the different nanophases must also be added into the total stored metastable energy for the former. The objective of the present work was to demonstrate the value of compositional heterogeneity for enhanced densification using the system Al_2O_3-SiO_2 as an example.

EXPERIMENTAL PROCEDURE

Single-phase and diphasic gels of 28.17 wt% SiO_2 and 71.83 wt% Al_2O_3 (stoichiometric mullite composition) and 20 wt% SiO_2 and 80 wt% Al_2O_3 were prepared. Single-phase gels were prepared by first dissolving aluminum nitrate nonahydrate in absolute ethanol, adding and mixing with tetraethoxysilane, and then gelling the solution at 60°C in a water bath. Diphasic gels were prepared in two ways: (1) using one sol and one solution and (2) using two sols. Diphasic gels of the first type were made by initially peptizing boehmite,[‡] mixing with tetraethoxysilane, and gelling at room temperature. Diphasic gels of the second type were made by initially peptizing boehmite, mixing with Ludox,[§] and gelling at room temperature. The mole ratios of HNO_3 to AlOOH ranged between 0.05 to 0.09. The weight percent of water varied between 82 and 88.

The single-phase and diphasic gels which utilized tetraethoxysilane were heated at 500°C for 4 h to burn organics and the xerogels were pelletized for sintering. The diphasic gels made from two sols were formed into gel tablets and did not require a heat treatment since there were no organics involved. The various gel pellets or tablets were sintered by stepwise

CONTRIBUTING EDITOR — W. J. LACKEY

Received February 18, 1986, revised copy received March 21, 1986, approved March 24, 1986.
Supported by the Air Force Office of Scientific Research under Contract No. F49620-85-C-0069
*Member, the American Ceramic Society
†Also associated with the Department of Agronomy
‡Also associated with the Department of Geochemistry and Mineralogy

‡Dispural, Remet Chemical Corp., Chadwicks, NY.
§Ludox "AS", E. I. du Pont de Nemours and Co., Inc., Wilmington, DE.

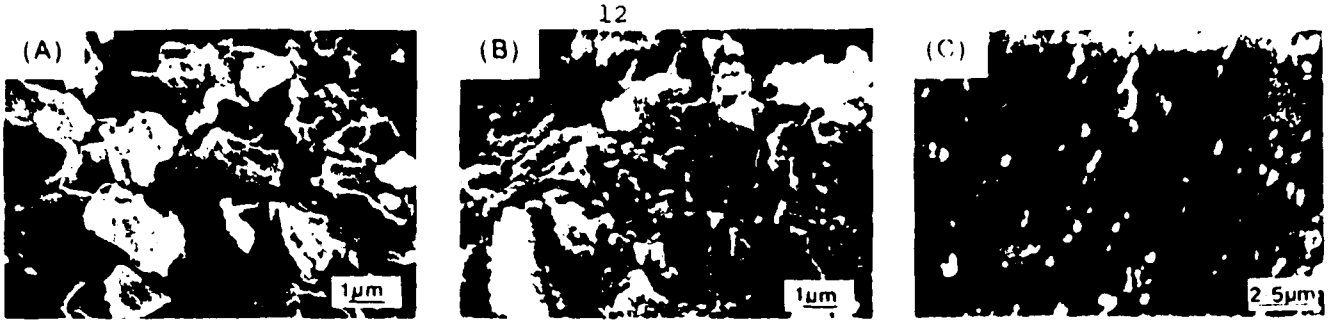

Fig. 1. (A) Fracture surface of single-phase mullite gel. (B) Fracture surface of boehmite tetraethoxysilane diphasic mullite gel. (C) Fracture surface of diphasic (boehmite + SiO_2) mullite gel.

Table I. Apparent Densities of Al_2O_3-SiO_2 Gels Sintered to Two Different Temperatures

Nature of gel	Gel composition		Density after sintering* (g/cm³)	
	Al_2O_3 (wt%)	SiO_2 (wt%)	1200°C	1300°C
Single-phase $Al(NO_3)_3 + Si(OC_2H_5)_4$	71.8	28.2	2.71 (85.4)	2.98 (94.0)
Diphasic $AlOOH + Si(OC_2H_5)_4$	71.8	28.2	2.92 (92.0)	2.92 (92.0)
Diphasic $AlOOH + SiO_2$[†]	71.8	28.2	3.03 (95.9)	3.06 (96.7)
Diphasic $AlOOH + SiO_2$[‡]	80.0	20.0	3.30 (97.1)	3.36 (98.8)

*Numbers in parentheses are percentages of theoretical density. †Average for eight different samples. ‡Cabot, E. I. du Pont de Nemours and Co., Inc., Wilmington, DE.

heating in air using a programmed furnace. The heating rates were 1°C/min up to 200°C (heated for 1 h at this temperature), 1.5°C/min between 200° and 500°C, 3°C/min between 500° and 800°C, and 10°C/min above 800°C. The samples were heated for 100 min at the final sintering temperatures of 1200° or 1300°C. Microstructures of the sintered materials were determined by scanning electron microscopy (SEM).[9] Densities of the sintered materials after evacuation were measured by the Archimedes technique. The reported densities are apparent densities as opposed to bulk densities because the open pores are evacuated before the density measurements.

Results and Discussion

The microstructures of single phase and diphasic mullite gels are shown in Fig. 1. The fractured surface of the single-phase gel shows nonuniform grain growth and much porosity (Fig. 1(A)) owing to poor sinterability. The pellet could be easily crumbled with the fingers, which suggests little or no sintering. The diphasic gel made from boehmite and tetraethoxysilane shows grains in the order of 0.1 to 0.25 μm with considerable porosity. On the other hand, fractured surfaces of diphasic gels made from boehmite and Ludox sols show no porosity, indicating a well-sintered body (Fig. 1(C)). These results demonstrate the enhancement of sintering behavior of the diphasic gels made from two sols as has been postulated.[10] The enhanced sintering behavior of the diphasic gels compared to the single phase gels results at least in part from the higher metastable energy of the former compared to the latter.[10] The sintering behavior of the single-phase and diphasic gels as measured by their densities is also presented in Table I. These results show that diphasic gels sinter to higher densities than single-phase gels (Table I). The diphasic gels of 80-20 and 71.8-28.2 wt% composition made from boehmite and Ludox sols exhibit the highest densities. The sintered diphasic pellets of both compositions (80-20 and 71.8-28.2 wt% Al_2O_3-SiO_2) appear translucent and are similar to the transparent mullites prepared by Prochazka and Klug[13] by hot-pressing and hot isostatically pressing starting materials derived from alkyl oxides.[13] Indeed careful reading of this paper shows that, in fact, the authors had prepared diphasic gels while possibly intending to make homogeneous single phase gels. The densities achieved by the diphasic route for the 80 wt% Al_2O_3 and 20 wt% SiO_2 compositions at 1200° and 1300°C are much higher than those reported by Debely *et al.*,[14] for the same composition prepared by heterocoagulation of narrow size dispersions of Al_2O_3 and SiO_2 powders. The densities achieved here by the diphasic route for the mullite composition at 1200° and 1300°C are also much higher than those reported by others[14-16] for mullite powder prepared by various more conventional techniques. Thus, the use of diphasic xerogels appears to be superior to the other methods[14-16] for obtaining dense sintered bodies in the system Al_2O_3-SiO_2.

Conclusions

The use of compositionally diphasic xerogels in the system Al_2O_3-SiO_2 leads to enhanced sintering. This enhanced sintering is achieved, we believe, by the higher metastable energy available in the diphasic gels compared to the single phase gels.

[9]Model DS-130, International Scientific Instruments, Santa Clara, CA.

References

[1] R. Roy and E. F. Osborn, "The System Al_2O_3-SiO_2-H_2O," *Am. Mineral.*, **39** [11-12] 853-85 (1954).

[2] V. C. Hill, R. Roy, and E. F. Osborn, "The System Alumina-Gallia-Water," *J. Am. Ceram. Soc.*, **35** [6] 135-42 (1952).

[3] D. M. Roy and R. Roy, "An Experimental Study of the Formation and Properties of Synthetic Serpentines and Related Layer Silicate Minerals," *Am. Mineral.*, **39** [11-12] 957-75 (1954).

[4] R. Roy, "Aids in Hydrothermal Experimentation: II. Methods of Making Mixtures for Both 'Dry' and 'Wet' Phase Equilibrium Studies," *J. Am. Ceram. Soc.*, **39** [4] 145-46 (1956).

[5] J. P. McBride, "Preparation of UO_2 Microspheres by Sol-Gel Techniques," Rept. No. ORNL-3823, Oak Ridge National Laboratory, Oak Ridge, TN, 1966.

[6] R. G. Sowman, "Alumina-Chromia-Metal(IV)-Oxide Refractory Fibers Having a Microcrystalline Phase," U.S. Pat. No. 4,125,406, 1978.

[7] H. Dislich and E. Hussmann, "Amorphous and Crystalline Dip Coatings Obtained from Organometallic Solutions: Procedures, Chemical Processes and Products," *Thin Solid Films*, **77** [1-3] 129-39 (1981).

[8] M. A. Leitheiser and R. G. Sowman, "Non-Fused Alumina Based Abrasive Material," U.S. Pat. No. 4,314,827, 1982.

[9] R. A. Roy and R. Roy, "Diphasic Xerogels: I. Ceramic-Metal Composites," *Mater. Res. Bull.*, **19** [2] 169-77 (1984).

[10] D. Hoffman, R. Roy, and S. Komarneni, "Diphasic Ceramic Composites via a Sol-Gel Method," *Mater. Lett.*, **2** [3] 235-37 (1984).

[11] D. Hoffman, S. Komarneni, and R. Roy, "Preparation of a Diphasic Photosensitive Xerogel," *J. Mater. Sci. Lett.*, **3** [6] 439-42 (1984).

[12] R. Roy, S. Komarneni, and D. M. Roy, "Multiphase Ceramic Composites Made by Sol-Gel Technique," pp. 347-59 in *Better Ceramics Through Chemistry*. Edited by C. J. Brinker. Elsevier North Holland, New York, 1984.

[13] S. Prochazka and F. J. Klug, "Infrared-Transparent Mullite Ceramic," *J. Am. Ceram. Soc.*, **66** [12] 874-80 (1983).

[14] P. E. Debely, E. A. Barringer, and H. K. Bowen, "Preparation and Sintering Behavior of Fine-Grained Al_2O_3-SiO_2 Composites," *J. Am. Ceram. Soc.*, **68** [3] C-76-C-78 (1985).

[15] S. Kanzaki, H. Tabata, T. Kumazawa, and S. Ohta, "Sintering and Mechanical Properties of Stoichiometric Mullite," *J. Am. Ceram. Soc.*, **68** [11] C-6-C-7 (1985).

[16] D. D. Rodrigo and P. Boch, "High Purity Mullite Ceramics by Reaction Sintering," *Int. J. High Tech. Ceram.*, **1** [1] 3-30 (1985).

Manuscript #1

Some New Advances with SSG-Derived Nanocomposites

SOME NEW ADVANCES WITH SSG-DERIVED NANOCOMPOSITES

Rustum Roy, S. Komarneni and W. Yarbrough
Materials Research Laboratory
The Pennsylvania State University
University Park, PA 16802

INTRODUCTION

In 1982 we turned our attention which, for over 30 years, had focussed on using the SSG route to making ultrahomogeneous materials (1) towards making ultraheterogeneous materials. The terms diphasic xerogels or SSG-derived nanocomposites both accurately describe the products we are concerned with. Basically, we utilize one of two SSG methods (2) to make a solid which is either or both, compositionally or crystallographically heterogeneous on a 10-100 nm scale. We have shown in several papers the profound effects that such diphasicity can have on formation temperature of phases (3-5), on sintering and on microstructure (6,7). Kumagai and Messing (8) and Messing et al. (9) have also reported in detail on the sintering effects in one system: Al_2O_3. In the present paper we report on three other applications of diphasic xerogels as novel ceramic materials.

I. We introduced the utilization of crystallographic diphasicity (=seeding) almost simultaneou [see Ervin, 1949 (10)] with the development of the SSG method itself. Thereafter we used it in dozens of studies not only in Al_2O_3 gel + corundum as in the first study but even with exceedingly complex ternary and quaternary compositions such as spodumene (11), scolecite, micas (12), etc. The mechanism envisaged here was the dissolution of the less stable phase and the deposition on the more stable seed-phase, via a solution phase. What was novel in our recent work was the fact that no solution was involved and the reaction proceeded basically in the solid state. This was done first on one-component systems such as Al_2O_3, TiO_2, etc.

The question naturally arises: Will complex compositions be able to respond to the nucleation advantage provided by the second phase; and growth by epitaxy actually occur in the

solid state. This problem has now been tackled in the systems ZrO_2-SiO_2, ThO_2-SiO_2 and MgO-Al_2O_3-SiO_2.

II. In the study of the cordierite composition it appeared that we had finally encountered a system where one could experimentally test the concept of metastable melting as the route whereby some gels may sinter at very low temperatures. This observation can only occur where the rate of the solid-state phase changes are slow enough that there is a chance for the relatively slow process of melting which is a reconstructive transition to occur first.

III. In our earliest reports on making diphasic xerogels (13,14) we reported on the post-gelation infiltration by solution and precipitation to cause exceedingly fine (1-2 nm) second phases of AgCl, $CrPO_4$, etc., to form inside SiO_2 and other networks.

In efforts to make low K-ceramic substrates we sought to make composite films of air + SiO_2, and to learn techniques of patterning the deposition of such layers by using a photoresist polymer as the second phase, via two stages of a polymer + ceramic nanocomposite.

EXPERIMENTAL

Preparation of $ZrSiO_4$ and $ThSiO_4$ Gel Precursors

Single phase zircon, $ZrSiO_4$ gels were made by mixing tetraethoxysilane (TEOS) and a zirconium oxychloride solution in ethanol and heating the mixture at 40°C. Structurally diphasic gels were obtained by adding zircon seeds to the above-mixed solution prior to gelation. The compositionally diphasic zircon gels were made by mixing a commercial silica sol (Ludox, E.I. DuPont de Nemours and Co., Inc., Wilmington, DE) and a hydrothermally prepared monoclinic zirconia sol and gently heating at 70°C. The zircon gels which are both compositionally and structurally diphasic were prepared by simply mixing the crystalline sols with the mixture of silica and zirconia sols prior to gelation as described above.

Single phase $ThSiO_4$ gels were prepared by mixing stoichiometric amounts of $Th(NO_3)_4.4H_2O$ and TEOS in ethanol (EtOH), and the subsequent addition of distilled water. The molar proportions of $Th(NO_3)_4$,$4H_2O$:TEOS:EtOH:H_2O components were 1:1:22:7, respectively. The resulting clear solution was stirred at room temperature and the gelation

occurred after a few hours. The mixing of thorite or huttonite (the α and β polymorphs of $ThSiO_4$, respectively) seeds in the above mixture prior to gelation led to the structurally diphasic gels. The amount of seeds added was calculated in order to obtain a nucleation frequency of about $3x10^{14}$ nuclei per cm^3 of precursor powder for the thorite-seeded gels, and $3x10^{13}$ nuclei per cm^3 for the huttonite-seeded gels. Compositionally diphasic $ThSiO_4$ gels were obtained by mixing the silica and a hydrothermally prepared thorianite sol and by heating the mixed sol suspension at 70°C under stirring. The both compositionally and structurally diphasic gels were obtained by mixing the crystalline thorite or huttonite seed sols with the silica and the thorianite sols and gelling as above. All the $ZrSiO_4$ and $ThSiO_4$ gels were dried at 110°C and the corresponding xerogels were ground in an agate mortar and pestle prior to the determination of their crystallization temperatures.

Determination of the Crystallization Temperature of $ZrSiO_4$ and $ThSiO_4$

Since the crystallizations of $ZrSiO_4$ and $ThSiO_4$ do not exhibit sharp exotherms by the differential thermal analysis, this technique could not be utilized to determine the effects of seeding on the crystallization of the phases. Instead, the amounts of $ZrSiO_4$ and $ThSiO_4$ phases crystallized at different temperatures in static experiments for fixed periods were determined semiquantitatively by powder x-ray diffraction (XRD) using the internal standard method (15). Anatase and quartz were used as internal standards for $ZrSiO_4$ and $ThSiO_4$ phases respectively. For determining the quantity of $ZrSiO_4$ crystallized, the relative intensity ratios of the (200) zircon peak to that of (101) anatase peak were used. For determining the quantity of $ThSiO_4$ crystallized, the relative intensity ratios of the (200) peak of thorite and the (120) peak of the huttonite to that of (101) peak of quartz were used. The absolute intensities were measured by determining the areas of the peaks and the relative intensities are expressed in arbitrary units. Powder XRD was carried out using a Picker Seimens diffractometer with graphite monochromated CuKα radiation.

Preparation of Cordierite, $Mg_2Al_4Si_5O_{18}$ by SSG Methods

Sol Preparation: Cordierite precursor sol was prepared by weighing tetraethoxysilane and aluminum sec-butoxide into a 1200 ml. polypropylene flask. Magnesium acetate tetrahydrate

was weighed into a 400 ml beaker, to which was added 200 ml absolute ethanol and 200 gms glacial acetic acid. The acetate was dissolved with stirring at room temperature, forming a slightly cloudy solution after one hour. While stirring the mixed alkoxides at room temperature, the acetate solution was added very slowly at first allowing time between additions for the thick white gel formed on each addition to break up. Additional absolute ethanol was now added (~300 ml) and the remaining acetate solution was slowly added to obtain a final volume of ~900 ml. Over the next 12 hours, substantial peptization of this suspension resulted in a much reduced viscosity and formed an essentially transparent liquid. This was diluted with absolute ethanol to 1000 ml in a volumetric flask which gave a stock sol, the composition being 0.25 M in Mg^{2+}, 0.50 M in Al^{3+}, and 0.625 M in Si^{4+}. This sol liquid was easily differentiated from a true solution by passing a laser beam through it. The beam was rendered visible by a relatively weak Tyndall effect, indicating the presence of peptized solids.

Gel Preparation: Gel solids were prepared from the above sol by two distinctly different methods. In the first of these, deionized water was added with incubation of the solution at 65°C. Gel times vary sharply with temperature and the amount of water added. Using 2 moles H_2O per equivalent total alkoxide resulted in gelation within 2 to 4 hours at room temperature, or 10 to 30 minutes at 65°C. The gel was initially transparent, but became increasingly transluscent to a cloudy white on continued reaction. These gels were incubated overnight at 65°C, and then were uncovered to evaporate alcohol. Drying at 65°C was continued for 48 hrs which resulted in colorless gel fragments, 1 to 5 mm in size. This method is designated as method 1 and is a slow, homogeneous gelation.

In the second method, 274 gms 28% aqueous NH_3 (~4.5 moles) was added to 1000 ml deionized water in a 2000 ml beaker. This was warmed on a hot plate to ~65°C and the sol was added while stirring at high speed with a high shear mixer. A white suspension is immediately formed and heating is discontinued. Temperature rose over the next 15 min to ~80°C. High speed/high shear mixing was continued for 4 hours with heating as needed to maintain at least 65°C. At this point, heating and mixing was discontinued and the mix was covered and left to stand overnight. Throughout the entire process pH was maintained at ~9 by excess NH_3. Solids

were recovered by centrifugation followed by successive washings with deionized water, absolute ethanol, and acetone. Solids were then dried at 65°C for 48 hrs. This resulted in the formation of an extremely fine white powder with minimal caking and agglomeration. This is designated as method 2 and is a relatively fast, heterogeneous gelation.

Spectrochemical analyses were performed on gels prepared by both methods, after an intermediate calcination at 500°C for 8 hrs. The results obtained for several preparations indicated no systematic loss of one cation with respect to any other.

Gels prepared by both methods were seeded with indialite, α-$Mg_2Al_4Si_5O_{18}$. This seed material was prepared from the homogeneous gel (method 1) by calcining at 1100°C for 12 hours and by grinding to a fine powder in a boron carbide mortar and pestle. To prepare a method 1 seeded gel, seed powder was added to the precursor sol so as to produce a gel containing 1 wt.% seed material in the total solids present as oxides. Gelation was then carried out as described earlier for method 1. To seed the heterogeneous gel of method 2, 25 mgs of the seed powder and 0.50 gms of gel powder were mixed by grinding in a boron carbide mortar and pestle using acetone.

Differential thermal analysis was carried out on different gel powders that passed through -270 mesh using a Dupont 1700 differential thermal analyzer.

Preparation of Thin Nanocomposite Layers of SiO_2 + Air

Sol Preparation: The source material was a relatively low surface area, high purity pyrogenic silica (Cab-O-Sil L90, Cabot Corp., Tuscola, IL). Silica sol was prepared using base (tetramethylammonium hydroxide at pH 9-11) stabilization. The silica was added to deionized water in portions while mixing in a high shear rate mixer. Base was added in portions as needed to adjust pH and inhibit gelation. Sols were prepared to be 15 to 25 wt.% in SiO_2 which were found to be stable indefinitely.

In this work, it was found possible to make thick, coherent SiO_2 films by using an acrylic latex which is used commercially as a paint base [Lucite 11018 (without post adduct), Rohm and Haas, Inc., Philadelphia, PA]. The latex is a copolymer formulation of methylmethacrylate and 2-ethylhexylacrylate containing two mole percent methacrylic acid. Hence the latex is stabilized

with ammonia at a pH of ~9 and is stable to higher concentrations of base, where a silica sol prepared with tetramethylammonium hydroxide or other suitable base is also stable. A coating formulation was found using the proportions given above and it was found that this could be cast and dried either as coatings on suitable substrates (e.g., silicon wafers) or as castings on a non-adherent surface (teflon) which would allow for tape or film formation. For thick layers it was found necessary to add humectants or plasticizers, polyethylene glycol proving satisfactory in the present case. Coatings were prepared by spin or dip coating Si wafers with a formulation consisting of 70% polymer and 30% silica, on a solids weight basis. These coatings were readily dried at temperatures ranging from ambient to 65°C. Polyethylene glycol (Carbowax™ 400, Fisher Scientific Co.) was used as a humectant and plasticizer for the thicker coatings. These coatings showed good adhesion to silicon and were fired at 900°C for 12 hours without cracking. Fired film thicknesses in the range of ~5 to 50 μm were prepared.

RESULTS AND DISCUSSION

I. Crystallization in Compositionally and/or Structurally Diphasic Gels in Binary Systems

$ZrSiO_4$ Gels

The lowest temperature at which zircon formed for the different kinds of gel precursors are reported in Table 1. The use of compositionally and/or structurally diphasic zircon gels resulted in a substantial lowering of the zircon crystallization temperature. For example, the single phase gels crystallized to zircon at approximately 1325°C while the structurally and compositionally diphasic gels crystallized at 1100°C and 1175°C respectively. However, the lowest crystallization temperatures for zircon were obtained by combining both the compositional and structural diphasicities (Table 1; Fig. 1). The data clearly show that isostructural seeding helps to control the thermodynamics of the reaction of formation of zircon, but one can notice that the compositional diphasicity also affects this reaction in the same positive way. As pointed out above and elsewhere, isostructural seeding works via epitaxial growth on the nuclei provided thereby lowering the crystallization temperature in the structurally diphasic gels. The lowering in compositionally diphasic gels may, at least in part, be attributed to the excess of metastable

energy that a diphasic gel stores (16). This additional energy (compared to a single phase gel) is derived from the exothermic heat of reaction of the two discrete phases, ZrO_2 and SiO_2, to yield the equilibrium phase, $ZrSiO_4$.

The effect of $ZrSiO_4$ seed concentration on the crystallization of zircon has also been studied and the results are plotted in Figure 2. The diphasic samples were all fired for 2 hours at 1120°C. The effect of seeding seems to level off at about 3 molar % addition, which corresponds to a nucleation frequency of $3x10^{14}$ seeds per cm^3 of equimolar mixture of silica and zirconia. The postulated mechanism for the lowering of zircon crystallization upon seeding is the heterogeneous nucleation and epitaxial growth. In order to test the validity of this mechanism (heterogeneous nucleation followed by epitaxial growth) the addition of a selected set of seed crystals was studied. Along with the results corresponding to the unseeded and the zircon-seeded precursors, data relating to rutile-seeded and thorite-seeded samples are presented in Figure 3. As expected, seeding with rutile (TiO_2), which is structurally different from zircon, has no effect at all. Thorite (α-$ThSiO_4$) is the most interesting case; its structure is the same as the zircon, but its lattice parameters are substantially larger. Seeding with the isostructural thorite, instead of catalyzing, completely inhibits the crystallization of zircon and thus the crystallization temperature is in effect raised. The reason for this counter-effect is not understood.

<u>$ThSiO_4$ Gels</u>

The amounts of huttonite crystallized from compositionally diphasic and single phase gels are shown as a function of temperature (Fig. 4). The β-polymorph of $ThSiO_4$ crystallized at a much lower temperature (by as much as 200°C) from the compositionally diphasic gels than from the single phase gels. The lower β-$ThSiO_4$ crystallization temperature from the compositionally diphasic gels is attributed, as pointed out above, to the excess free energy that a diphasic gel stores compared to a single phase gel (16). This excess energy is derived from the heat of reaction of the two discrete phases, ThO_2 and SiO_2 sols.

The amounts of thorite, α-$ThSiO_4$ crystallized from compositionally diphasic and single phase gels as a function of temperature are shown in Figure 5. Little or no α-$ThSiO_4$ crystallized

from the diphasic gel while a substantial amount of this α-phase resulted from the single phase gel. This may be due to the ease with which a single phase $ThSiO_4$ gel could crystallize into the least dense assemblage, thorite (the densities of thorite and huttonite are 6.7 and 7.2 respectively). A single phase $ThSiO_4$ gel is expected to have a statistically uniform distribution of thorium and silicon "ions" in an oxygen-hydroxyl-water matrix. It is therefore possible that the α-$ThSiO_4$ is produced as a metastable phase. This explanation assumes that huttonite is the stable form of $ThSiO_4$ in the temperature range studied, i.e. 1200-1450°C. When fired for 15 minutes at 1600°C both homogeneous and compositionally diphasic gel precursors led to huttonite only. This result is in agreement with the above assumption.

The relative intensity of huttonite (120) peak is plotted as a function of the firing temperature for 3 kinds of gel precursors: the unseeded single phase (homogeneous) gel, and the thorite- and huttonite-seeded gels (Fig. 6). The data show that seeding with β-$ThSiO_4$ nuclei lowers the crystallization temperature of this phase by about 100°C (compared to the unseeded gel) whereas the α-$ThSiO_4$ seeding seems to delay the formation of the β phase. These results are in agreement with the concept of "nucleation and epitaxial growth" which is believed to govern the reactions occurring in isostructurally seeded gels. The expected equilibrium phase (huttonite in the present case) can grow from the matrix onto the provided nuclei along certain crystallographic directions.

The relative intensity of thorite (200) peak versus the firing temperature for the three different gels is plotted in Figure 7. Seeding with thorite induces a slight lowering in the crystallization temperature of the thorite phase and a clear increase in the amount of thorite present in the fired powder. What is more interesting is that the addition of huttonite crystallites as a second phase to a noncrystalline $ThSiO_4$ gel allows one to completely avoid the formation of thorite.

If one assumes that huttonite is the stable polymorph of $ThSiO_4$ and that thorite is the metastable phase in the temperature range 1100-1600°C, two interesting observations can be made:

- seeding a $ThSiO_4$ single phase gel with thorite crystallites stabilizes this phase, i.e. the ratio of thorite to huttonite contents is significantly higher than in unseeded gels. But unfortunately, it is impossible to obtain only thorite, even when the samples were heated for a long time (6 days) at 1225°C.
- seeding a $ThSiO_4$ single phase gel with huttonite crystallites led only to the hypothetically stable huttonite. Unseeded single phase gels, however, crystallized to both thorite and huttonite in the temperature range of 1200-1450°C.

The content of thorite formed versus the firing temperature is plotted (Fig. 8) for three kinds of precursor gels: the compositionally (only) diphasic gel and the compositionally and structurally diphasic gel with crystalline thorite, and with crystalline huttonite as seeds. The gel seeded with thorite led to the formation of thorite (along with huttonite). The crystallization study of the huttonite content of these three precursors showed that in the unseeded gel the huttonite formation occurred at about 1075°C, in the thorite seeded gel at 1125°C and in the huttonite seeded gel it occurred below 1050°C (Fig. 8).

These results confirm the observations made with the $ZrSiO_4$ system and indicate that if one combines compositional and structural diphasicities one can further enhance the crystallization behavior of $ThSiO_4$ (e.g. the formation temperature of huttonite).

$Mg_2Al_4Si_5O_{18}$ Gels

Figure 9 shows the DTA results for the two types of cordierite gels. The gels prepared by method 1 show two crystallization exotherms. Powder XRD analysis was carried out on DTA samples just prior to the first exotherm, after the first but just before the second, and just after the second. These showed, respectively, little or no crystallinity, the pattern of the metastable stuffed β-quartz structure sometimes called μ-cordierite, and the pattern indexed as the disordered form of cordierite, properly known as indialite, but generically referred to by many ceramists as cordierite. Interestingly, the gel prepared by method 2 showed only a broad, ill-defined exotherm, and XRD pattern obtained of this material, even after heating at 1200°C for 6 hours showed only a poorly crystallized material, which appeared to consist primarily of a saphirine structure material with possibly some spinel and mullite. Hence, the gel prepared using method 1

gave results on calcination in agreement with the results reported by Zelinsky et al. for a similar gel prepared using a somewhat different technique (17); and, also in agreement with the crystallization behavior of glasses of this composition. However, the gel prepared using the high-speed precipitation process of method 2 showed a significantly different behavior.

It was suspected that this might be due to a segregation of the constituents in the precipitation process, forming in effect a di- or triphasic gel system having sufficient compositional heterogenity to resist crystallization to the stable phase. The material was studied using transmission electron microscopy, powder XRD and x-ray emission. The relative intensities of the x-ray emission agree qualitatively with the bulk chemical compositions determined earlier, and no evidence of compositional variation could be found. If compositional heterogeneity is the reason for the differences in crystallization behavior, such heterogeneity must be on a scale of ~50 nm or less. Given the fact that temperatures of ~900°C or less, the material effectively melts and forms a relatively low viscosity liquid, it appears unlikely that heterogeneity on this scale would persist. Alternatively, the high-speed precipitation method may have resulted in the formation of a more highly disorganized material, which does not possess the necessary precursor structures or nuclei which would lead to the formation of the more commonly seen phases. No seeding effects could be seen for both gels in the DTA results. However, a substantial microstructural refinement could be seen in the gel material of method 1. The seeded powder of method 2 gave μ-cordierite initially with indialite forming on calcination to higher temperatures while the unseeded gel gave poorly crystalline material as described above.

II. Metastable Melting

In 1982, one of us [Rustum Roy (18)] predicted that compositions having both chemically heterogeneous and structurally metastable configuration(s), such as those obtained in the formation of many diphasic gels, must have a metastable "melting point" well below temperatures at which stable liquidus behavior is encountered. The term "metastable melting" was coined at the time to differentiate this type of behavior from the common gradual relaxation of viscosity in more conventionally prepared noncrystalline, supercooled liquids or glasses. In the initial study of gels prepared using method 1, differential thermal analysis (DTA) was used to determine the

temperature(s) at which crystallization might be observed. At the end of the DTA run it was found that the relatively coarse powder (-270 mesh) had melted or "sintered" to a body only a fraction of the original volume of the sample cup. Examination of this with a low power stereomicroscope showed that the material has fused to a solid mass and the original powder fragments were no longer in evidence. Figure 10B shows the secondary electron image of the surface of such a sample. This behavior was surprising as the preparation of dense glass ceramics of stoichiometric composition by the sintering of glass powders was reported to be difficult even by hot pressing (19,20). This same behavior was observed to an even more marked degree with the fine powder which resulted from the use of method 2. Figure 11A shows the very fine structure of the powder from method 2 after calcination at 500°C for 8 hours; and, Figure 11B shows the same material after calcining at 900°C for 1 hour. It could even be seen that glassy filaments were drawn between differentially shrinking regions, an example of which is clearly seen in Figure 11B. This type of behavior has obvious potential for the preparation of a large number of composite materials and efforts to gain a further understanding, as well as to test possible applications, are continuing.

III. Nanocomposite Films of SiO_2 + Air and Their Patterning

Thick (50 μm), low-K SiO_2 coatings were obtained by using a mixture of a SiO_2 sol and an acrylic latex. In the case of the gel-derived materials of the present work we found it possible to impregnate the coating with a photoresist, expose, develop, etch the coating where the resist was removed in development, and remove the remaining resist to obtain a finished patterned piece. The photoresist and developer used are commercially available (Microposit S-1400 and developer CD-30, Shipley Co., Whitehall, PA) and are widely used in the preparation of integrated circuits. Etching of the silica was readily achieved using a 20% hydrofluoric acid solution. The remaining photoresist was then stripped with HPLC grade acetone. Figure 12 shows the pattern after exposure and development, but before etching of the silica and stripping of the photoresist. Exposure was accomplished in 15 minutes using water-filtered radiation from a 400-watt Hg arc lamp source. The photomask was prepared by photographing the pattern with a 35-mm camera loaded with black and white negative film.

CONCLUSIONS

We report herein several discrete studies establishing the potential of nanocomposites derived by solution-sol-gel (SSG) routes.

1. By using binary systems (ZrO_2-SiO_2 and ThO_2-SiO_2) and a phase which shows dimorphism ($ThSiO_4$-[huttonite] and $ThSiO_4$-[thorite]) we have adduced additional conclusive evidence for the solid-state epitaxy in the firing of such materials.
2. Using a ternary system (MgO-Al_2O_3-SiO_2) we have been able to demonstrate that even with such complex systems where movements of multiple atoms are involved, the effect of crystallographic diphasicity is profound.
3. In the same system at the cordierite composition ($2MgO.2Al_2O_3.5SiO_2$) we have been able to show the effects of metastable melting and consequent rapid sintering.
4. By using a diphasic organic-inorganic composite precursor we have been able to demonstrate the ability to make coherent low K (K = 3) films and process them in normal substrate applications.

ACKNOWLEDGEMENT

This work draws on the research supported by two sponsors: AFOSR Contract F496200-85-C-0069 and NSF Grant DMR-8119476.

REFERENCES

1. R. Roy, Aids in Hydrothermal Experimentation. II. Methods of Making Mixtures for Both "Dry" and "Wet" Phase Equilibrium Studies, J. Am. Ceram. Soc. 39, 145-146 (1956).

2a. R. Roy, Y. Suwa and S. Komarneni, Nucleation and Epitaxial Growth in Diphasic (Crystalline + Amorphous) Gels, Science of Ceramic Chemical Processing, L.L. Hench and D.R. Ulrich, Eds., Wiley, New York, 1986, pp. 247-258.

2b. R. Roy, New Ceramics Via the Solution-Sol-Gel Route: From Ultrahomogeneity to Ultraheterogeneous Nanocomposites, Science (in press).

3. Y. Suwa, R. Roy and S. Komarneni, Lowering Crystallization Temperatures by Seeding in Structurally Diphasic Al_2O_3-MgO Xerogels, J. Am. Ceram. Soc. 68, C-238–C-240 (1985).

4. Y. Suwa, S. Komarneni and R. Roy, Solid-State Epitaxy Demonstrated by Thermal Reactions of Structurally Diphasic Xerogels: The System Al_2O_3, J. Mat. Sci. Lett. 5, 21-24 (1986).

5. G. Vilmin, S. Komarneni and R. Roy, Lowering Crystallization Temperature of Zircon by Nanoheterogeneous Sol-Gel Processing, J. Mat. Sci. (in press).

6. S. Komarneni, Y. Suwa and R. Roy, Application of Compositionally Diphasic Xerogels for Enhanced Densification: The System Al_2O_3-SiO_2, J. Am. Ceram. Soc. 69, C-155–C-156 (1986).

7. Y. Suwa, R. Roy and S. Komarneni, Lowering Sintering Temperature and Enhancing Densification by Epitaxy in Structurally Diphasic Al_2O_3 and Al_2O_3-MgO Xerogels, Mat. Sci. Eng. 83, 151-159 (1986).

8. M. Kumagai and G.L. Messing, Enhanced Densification of Boehmite Sol-Gels by α-Al_2O_3 Seeding, J. Am. Ceram. Soc. Commun. 67, C230-C231 (1984).

9. G.L. Messing, M. Kumagai, R.A. Shelleman and J.L. McArdle, Seeded Transformations for Microstructural Control in Ceramics, Science of Ceramic Chemical Processing, L.L. Hench and D.R. Ulrich, Eds., Wiley, New York, 1986, pp. 259-271.

10. G. Ervin, The System Al_2O_3-H_2O, Ph.D. Thesis in Ceramic Technology, The Pennsylvania State University, 1949.

11. R. Roy, D.M. Roy and E.F. Osborn, Compositional and Stability Relationships Among the Lithium Aluminosilicates: Eucryptite, Spodumene and Petalite, J. Am. Ceram. Soc. 33, 152-159 (1950).

12. M. Koizumi and R. Roy, Synthesis and Stability of the Calcium Zeolites, J. Geol. 68, 41-53 (1959).

13. D. Hoffman, R. Roy and S. Komarneni, Diphasic Ceramic Composites Via a Sol-Gel Method, Mat. Lett. 2, 245-247 (1984).

14. D. Hoffman, S. Komarneni and R. Roy, Preparation of a Diphasic Photosensitive Xerogel, J. Mat. Sci. Lett. 3, 439-442 (1984).

15. B.D. Cullity, Elements of X-ray Diffraction, 2nd Ed., Addison-Wesley, Reading, MA, pp. 555 (1978).

16. D. Hoffman, R. Roy and S. Komarneni, Diphasic Xerogels, A New Class of Materials: Phases in the Al_2O_3-SiO_2 System, J. Am. Ceram. Soc. 67, 468-471 (1984).

17. B.J.J. Zelinski, B.D. Fakes and D.R. Uhlmann, Crystallization Behavior of Sol-Gel Derived Glasses, J. Non-Cryst. Solids 82, 307-313 (1986).

18. R. Roy, Ceramics From Solutions: Retrospect and Prospect, Abstracts, The Materials Research Society Annual Meeting, Boston, MA, p. 370 (1982).

19. J.M. Bind, Low Thermal Expansion Modified Cordierites, U.S. Patent 4,403,017 (1983).

20. Y. Hirose, H. Doi and D. Kamigaito, Thermal Expansion of Hot-Pressed Cordierite Glass Ceramics, J. Mat. Sci. Lett. 3, 153-155 (1984).

TABLE 1

Lowest temperature at which zircon crystallized from different types of gel precursors.

Type of Gel	Zircon crystallization temperature (°C)
Single phase gel	1325
Compositionally diphasic gel	1175
Structurally* diphasic (single phase gel seeded with $ZrSiO_4$) gel	1100
Both compositionally and structurally* diphasic gel	1075

*2 molar % crystalline zircon seeds were added.

FIGURE CAPTIONS

Figure 1. Relative intensity of zircon (200) peak as a function of the firing temperature for gels prepared with Ludox and the monoclinic zirconia sol.

Figure 2. Relative intensity of zircon (200) peak as affected by varying concentrations of $ZrSiO_4$ seeds.

Figure 3. Relative intensity of zircon (200) peak versus firing temperature for unseeded gels and gels seeded with zircon, thorite and rutile crystals.

Figure 4. Relative intensity of huttonite (120) peak as a function of the firing temperature for an unseeded diphasic gel and an unseeded single phase gel.

Figure 5. Relative intensity of thorite (200) peak as a function of the firing temperature for an unseeded diphasic gel and an unseeded single phase gel.

Figure 6. Relative intensity of huttonite (120) peak as a function of the firing temperature for an unseeded single phase gel and for the same gel seeded with thorite or huttonite.

Figure 7. Relative intensity of thorite (200) peak as a function of the firing temperature for an unseeded single phase gel and for the same gel seeded with thorite or huttonite.

Figure 8. Relative intensity of thorite (200) peak as a function of the firing temperature for an unseeded compositionally diphasic gel and for the same gel seeded with thorite or huttonite.

Figure 9. Differential thermal analysis of cordierite gels: Top three curves are unseeded and seeded homogeneous gels (method 1) and the bottom curve is unseeded heterogeneous gel (method 2).

Figure 10. Scanning electron micrographs of homogeneous gel (method 1): A. untreated powder; B. fused sample after DTA runs.

Figure 11. Scanning electron micrographs of heterogeneous gel (method 2): A. untreated powder; B. fused sample with filaments after heating to 900°C.

Figure 12. Exposed and developed photoresist impregnated silica film showing pattern used to test via formation. Scale is in cm.

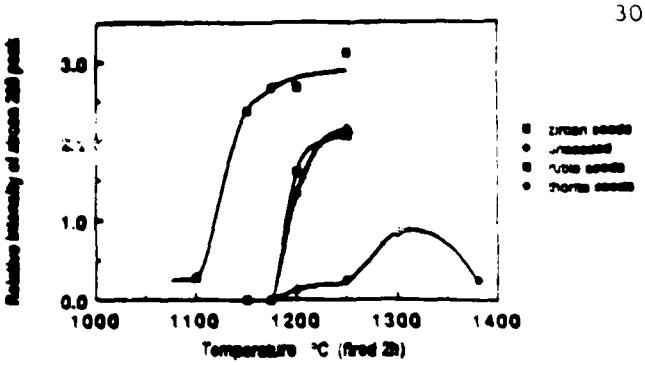

Fig. 1

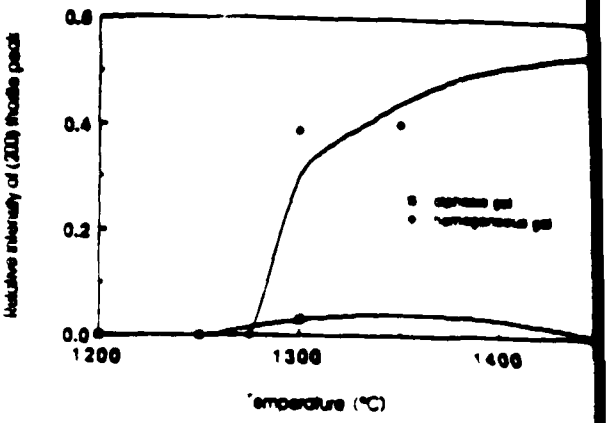

Fig. 5

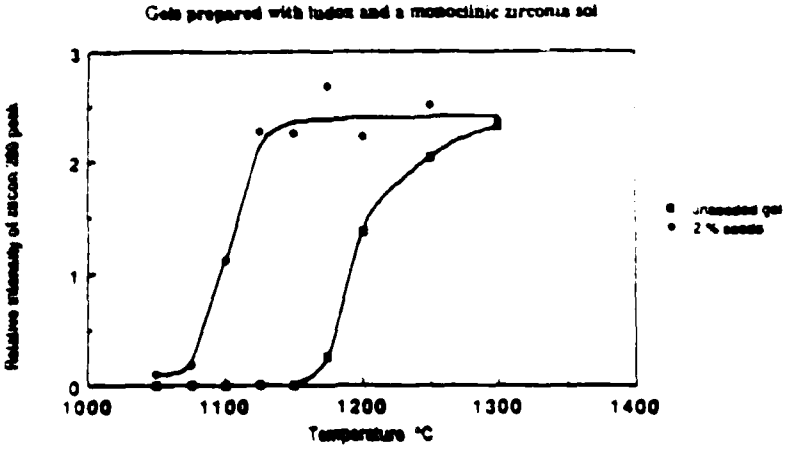

Fig. 2

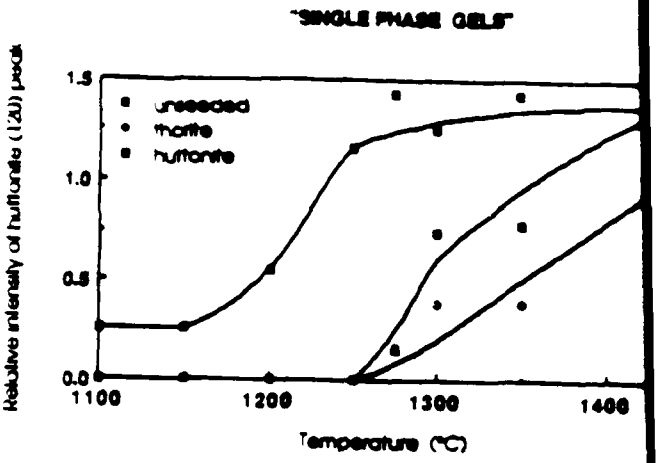

Fig. 6

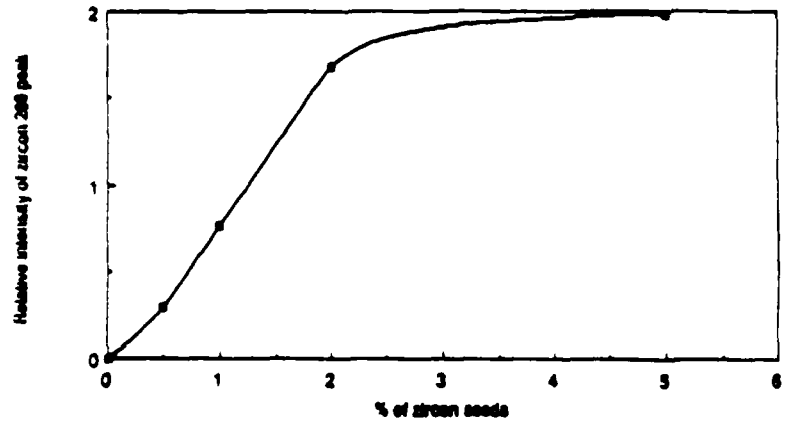

Fig. 3

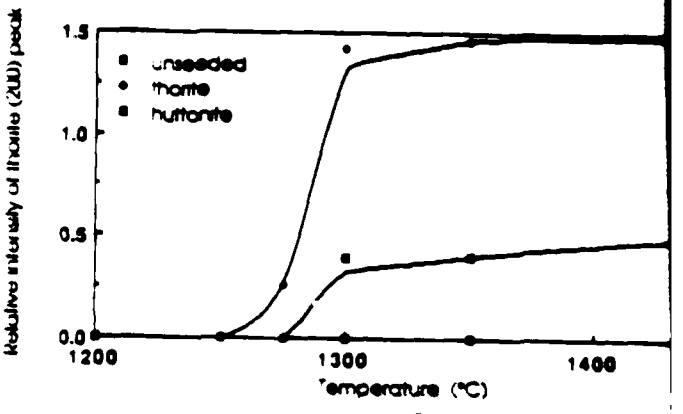

Fig. 7

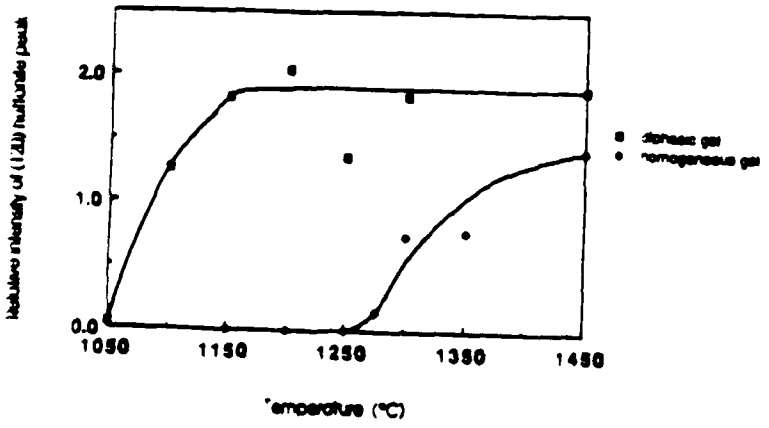

Fig. 4

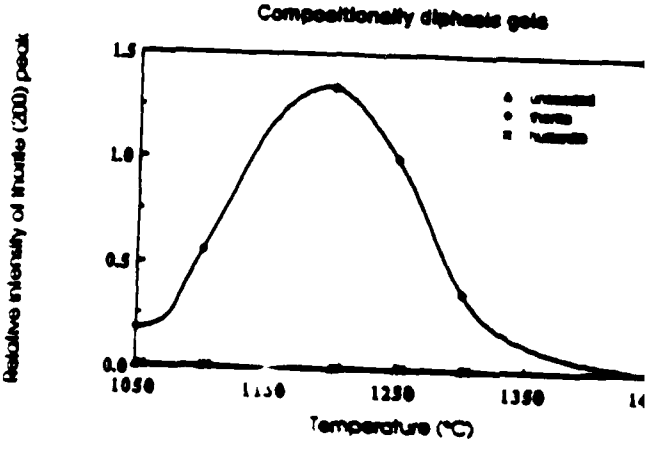

Fig. 8

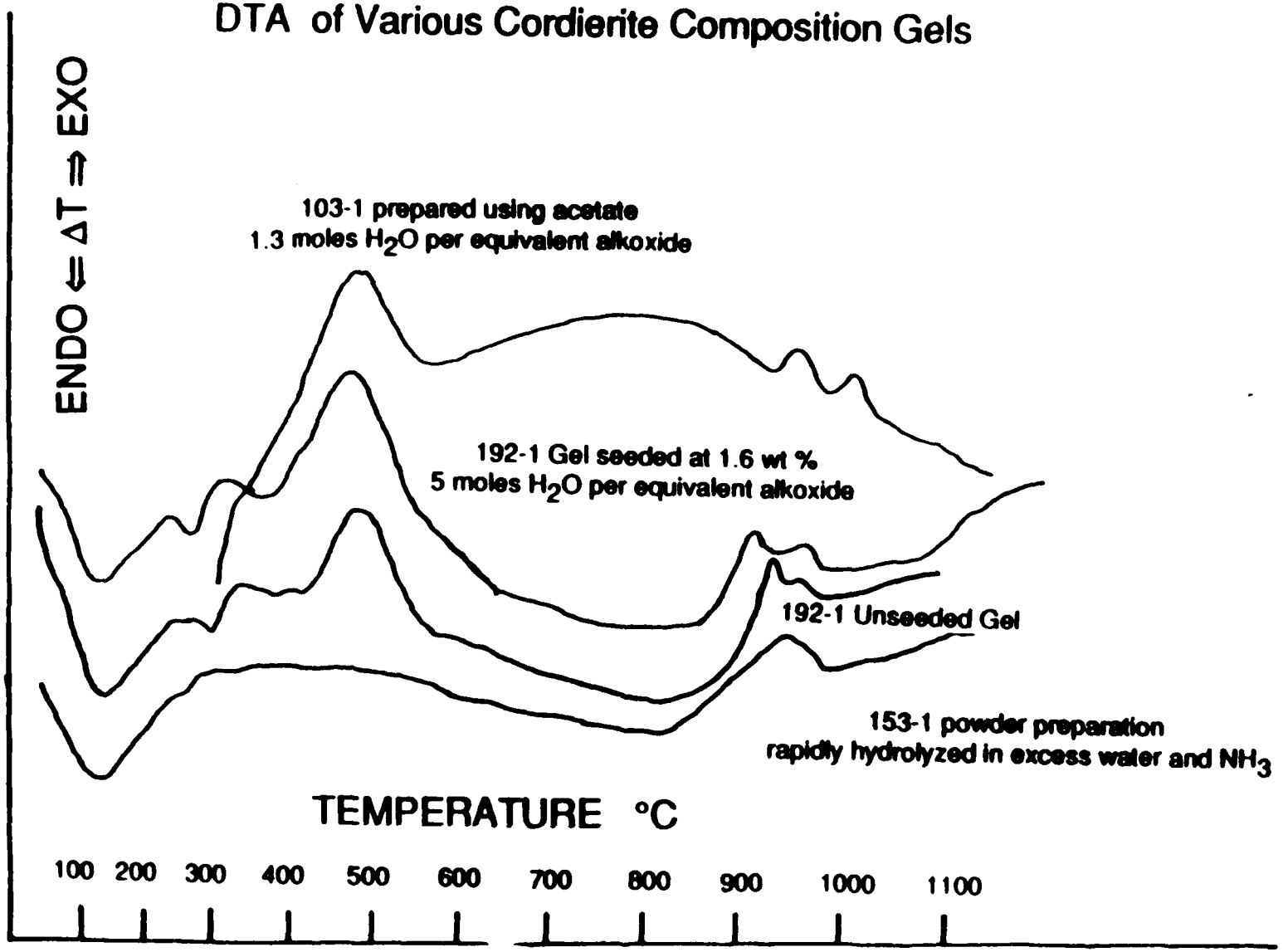
DTA of Various Cordierite Composition Gels
ENDO ⇐ ΔT ⇒ EXO
103-1 prepared using acetate
1.3 moles H_2O per equivalent alkoxide
192-1 Gel seeded at 1.6 wt %
5 moles H_2O per equivalent alkoxide
192-1 Unseeded Gel
153-1 powder preparation
rapidly hydrolyzed in excess water and NH_3
TEMPERATURE °C
100 200 300 400 500 600 700 800 900 1000 1100

Fig. 9

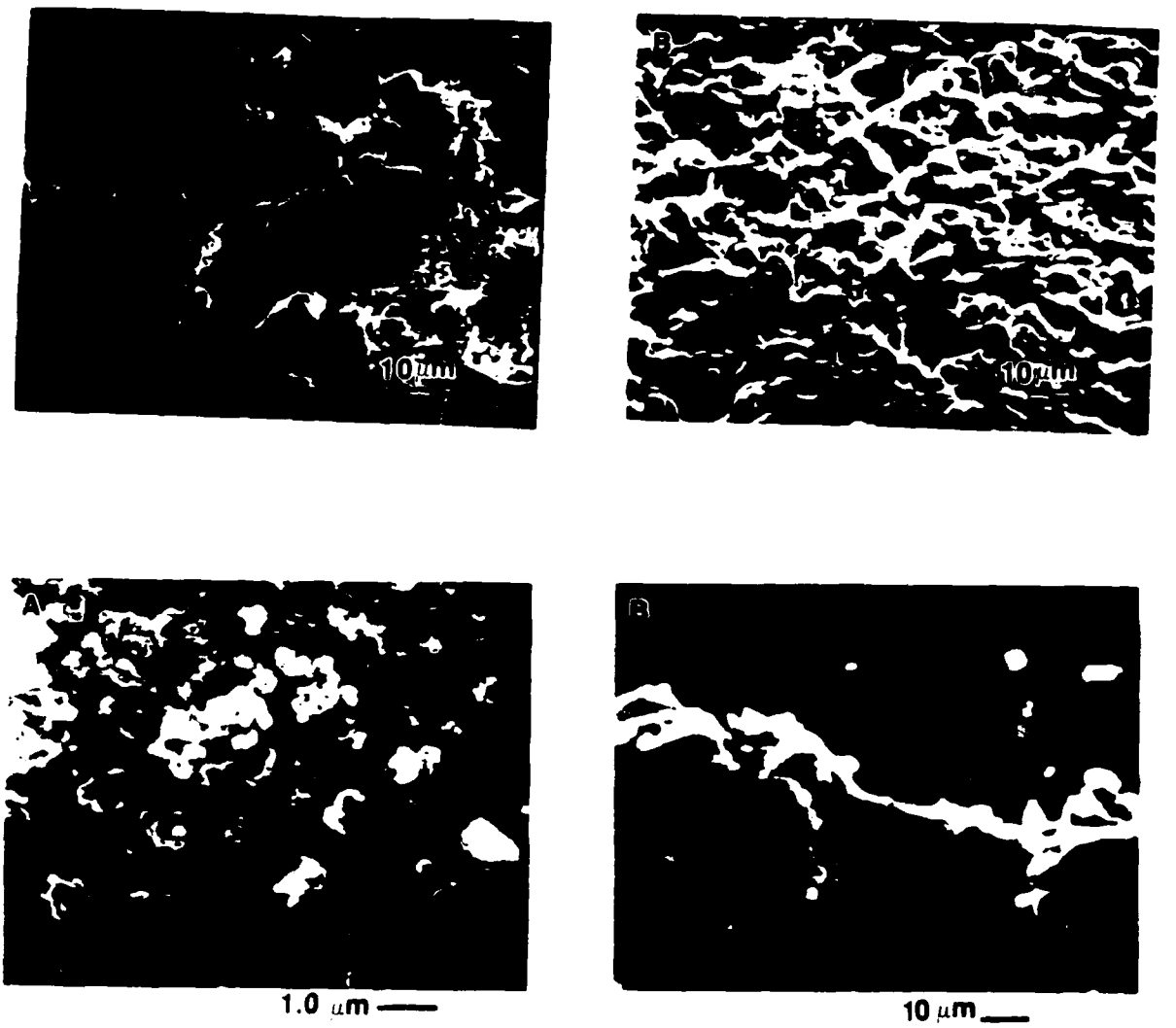
10μm
10μm
A
1.0 μm
B
10 μm

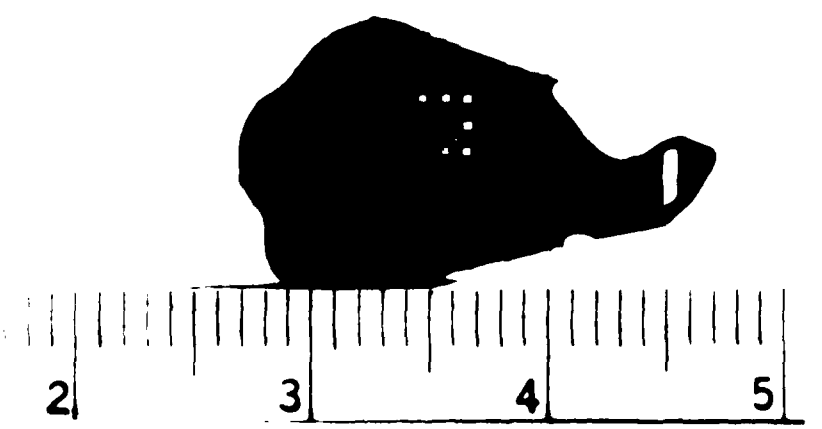
2
3
4
5

Reprint #2

Lowering the Sintering Temperature and Enhancing
Densification by Epitaxy in Structurally Diphasic Al_2O_3 and Al_2O_3-MgO Xerogels

Materials Science and Engineering, 83 (1986) 151-159

Lowering the Sintering Temperature and Enhancing Densification by Epitaxy in Structurally Diphasic Al_2O_3 and Al_2O_3–MgO Xerogels

YOSHIKO SUWA and RUSTUM ROY

Materials Research Laboratory, The Pennsylvania State University, University Park, PA 16802 (U.S.A.)

SRIDHAR KOMARNENI

Materials Research Laboratory, and Department of Agronomy, The Pennsylvania State University, University Park, PA 16802 (U.S.A.)

(Received November 25, 1985; in revised form February 10, 1986)

ABSTRACT

The densification and sintering behavior of diphasic xerogels derived from boehmite and Al_2O_3-MgO compositions seeded with α-Al_2O_3, spinel ($MgAl_2O_4$), α-Fe_2O_3, Cr_2O_3, kaolinite and Ludox was studied by measuring densities and by microstructural characterization of sintered materials. Isostructural seeding with the final equilibrium phase, i.e. α-Al_2O_3 in boehmite and α-Al_2O_3 and spinel in Al_2O_3-MgO gels, resulted in enhanced densification as well as sintering at lower temperatures. Solid state epitaxy appears to be the mechanism by which isostructural seeding affects the densification and sintering behavior. Microstructural characterization revealed uniform grain growth with little or no porosity in the gels with isostructural seeds, while non-uniform grain growth and porosity were seen in unseeded gels as well as in gels with non-isostructural seeds. Isostructural seeding may become a generalizable process for enhancing densification and sintering in sol-gel ceramic processing.

1. INTRODUCTION

The thrust of our "second-generation" sol-gel work has been to make diphasic gels which are heterogeneous on a nanometer (1-10 nm) scale, as distinct from our past, and present, worldwide utilization of the sol-gel method as a means to make ultrahomogeneous glasses and ceramics [1-4]. The methods that we have developed include one which involves the post-formation of a non-crystalline or crystalline phase within a preformed host gel structure of different composition and another which basically makes a gel from two pre-existing sols. The success of the method and its generalizable nature have been demonstrated elsewhere [5-8]. A second subset of our diphasic xerogels consists of those which have phases which are only structurally different, made for example by mixing crystalline and non-crystalline gels of the same compositions. "Seeding" of colloids dates back at least to the work of Zsigmondy [9, 10] between 1905 and 1920, but he was not concerned with such structurally diphasic cases. This approach of crystallographic seeding (*i.e.* creating a specific diphasic heterogeneity) was our own first attempt at utilizing diphasic xerogels and dates back to our very earliest work, starting in 1948, on Al_2O_3-H_2O [11, 12] and MgO-Al_2O_3-H_2O [13].

While we showed that diaspore seeding was critically important in this low temperature regime in forming that phase at much lower pressures in both Al_2O_3-H_2O and MgO-Al_2O_3-H_2O systems than was otherwise attainable, Ervin [11] also found that α-Al_2O_3-seeded boehmite gels did not lower the boehmite-to-corundum transition temperature in that hydrothermal study. Ervin wrote: "Seed crystals were ordinarily added to the raw materials in making equilibrium runs, the most important of these being diaspore.... Two mixtures served for the majority of the runs, one of α-Al_2O_3 plus seeds and one of alumina gel plus seeds.... The alumina gel usually was electrodialyzed and used wet. The seeds were mixed with the wet gel by long stirring with a micro-spatula. Other mixtures

0025-5416/86/$3.50

were often made up for special purposes. Actually, diaspore is the only substance which was ever observed to grow from seed."

Since 1982 when we first reported the diphasic xerogel materials [14], we began to examine the effect of potential epitaxial seeding on transformation temperatures in the higher temperature regime. A wide range of diphasic xerogels was found to show a lowering in reaction temperatures by solid state epitaxial growth on seed crystals [15-17].

Much of the recent revival of interest in sol-gel science has derived from the patent by Leitheiser and Sowman [18] of the rapid and low temperature densification of sol-gel-derived abrasive grains with compositions in the system Al_2O_3-MgO. Detailed X-ray and electron microscopy examination by Breval *et al.* [19] in our laboratory showed an extraordinarily fine microstructure, especially of the spinel phase, reminiscent of our own materials obtained from diphasic xerogels. Parallel work by Yarbrough and Roy [20] illustrates these effects on unique structure quite dramatically.

Because of the unexpected solid state epitaxy effects found by differential thermal analysis [15-17] in our above-referenced work, including the possibility of epitaxy of spinel on corundum and vice versa, it was deemed important to study the mechanisms and effects of such seeding on the identically significant process of densification of ceramics in the system MgO-Al_2O_3. Our colleagues Kumagai and Messing [21] have already noted such effects of the seeding of α-Al_2O_3 on densification of the boehmite-derived xerogels.

2. EXPERIMENTAL DETAILS

2.1. Preparation of xerogels in the Al_2O_3 system

All the diphasic xerogels of the Al_2O_3 system were made using boehmite (Dispural, Remet Chemical Corporation, Chadwicks, NY) as one gel with different seeds such as α-Al_2O_3 (A-16 SG, Aluminum Co. of America Inc., Pittsburgh, PA), spinel ($MgAl_2O_4$) (Baikalox SG, Baikowski International Corporation, Charlotte, NC), quartz (Alfa Products, Danvers, MA), Cr_2O_3 (J. T. Baker Chemical Co., Phillipsburg, NJ) and α-Fe_2O_3. The latter were synthesized by the method of Matijevic [22].

In each case, boehmite (particle size, about 70 Å) was initially dispersed in water and peptized by the dropwise addition of 1 N HNO_3 with constant stirring until a clear hydrosol was obtained. The seed crystals, α-Al_2O_3 (particle size, about 0.2-0.4 μm), spinel (about 0.05-0.1 μm), quartz (about 0.5 μm), Cr_2O_3 (about 0.5 μm) and α-Fe_2O_3 (about 0.5 μm), were peptized with 1 N HNO_3 prior to their addition to boehmite hydrosol. The two sols were mixed thoroughly and the diphasic sol gelled in 0.5-8 h. The weight ratios of boehmite to water varied between 20 to 80 and 15 to 85. The mole ratios of HNO_3 to boehmite ranged between 0.05 and 0.07. In each series, gels and thence xerogels were prepared with varying concentrations of seeds, *e.g.* α-Al_2O_3 (0-2.7 wt.%) and spinel (0-7.3 wt.%). Colloidal boehmite precursor is helpful in uniformly dispersing the α-Al_2O_3 seed crystals by peptization and gelling. Precursors such as γ-Al_2O_3 do not gel and hence seed crystals have to be mixed by peptization and drying followed by gentle grinding to obtain a uniform powder.

2.2. Preparation of xerogels in the Al_2O_3-MgO system

Diphasic xerogels of different compositions in the Al_2O_3-MgO system were prepared from boehmite (Dispural) and $Mg(NO_3)_2 \cdot 6H_2O$. The $Mg(NO_3)_2$ solution was added dropwise to clear boehmite hydrosol, which was prepared by initially dispersing boehmite in water and subsequently adding 1 N HNO_3 dropwise while stirring. The seed crystals, α-Al_2O_3 (particle size, 0.2-0.4 μm) and spinel (about 0.05-0.1 μm), were peptized by HNO_3 and added to the boehmite hydrosol prior to the addition of $Mg(NO_3)_2$ solution. The boehmite hydrosol rapidly flocculated and gelled on the addition of $Mg(NO_3)_2$ solution. The gels were dried at room temperature for 10 days prior to characterization by different methods. The amount of water as well as the concentration of HNO_3 were critical for obtaining homogeneous gels. For gels with a ratio of 95.8 wt.% Al_2O_3 to 4.2 wt.% MgO (or 90 mol.% Al_2O_3 to 10 mol.% MgO) which corresponds to the eutectic composition, a ratio for boehmite to water of 12 wt.% to 88 wt.% was used. For gels with a ratio of 93 wt.% Al_2O_3 to 7 wt.%

MgO which corresponds to the 3 M composition, a ratio for boehmite to water of 10 mol.% Al_2O_3 to 90 mol.% MgO was used. A mole ratio of 0.07 HNO_3 to boehmite was found to give the best results. α-Fe_2O_3 and quartz were also used as seeds in addition to α-Al_2O_3 and spinel ($MgAl_2O_4$). The effect of varying concentrations of α-Al_2O_3 (0.045–0.9 wt.%) and spinel seeds (0.09–1.16 wt.%) on the two gel compositions was also investigated.

2.3. *Characterization of materials*

The gel tablets or pieces were sintered by stepwise heating in air using a programmed furnace. The heating rates were 1 °C min^{-1} up to 200 °C (heated for 1 h at this temperature), 1.5 °C min^{-1} between 200 and 500 °C, 3 °C min^{-1} between 500 and 800 °C, and 10 °C min^{-1} above 800 °C. The samples were heated for 100 min at the final sintering temperature. Microstructures of the sintered-and-annealed materials were determined by scanning electron microscopy using an ISI DS-130 instrument. The morphology and particle size of the seed crystals were determined by transmission electron microscopy using Philips EM 300 and 420 instruments. X-ray powder diffraction was carried out on samples heated to various temperatures with a Philips diffractometer using nickel-filtered Cu Kα radiation. The densities of the sintered materials after evacuation were measured by the Archimedes technique. These densities are apparent densities as opposed to bulk densities because the open pores are evacuated prior to the density measurements.

3. RESULTS AND DISCUSSION

3.1. *Densification of boehmite gels by seeding*

The effects of varying concentrations of different seeds such as α-Al_2O_3, spinel ($MgAl_2O_4$), Cr_2O_3, Fe_2O_3, kaolinite ($Al_2Si_2O_5(OH)_4$) and Ludox (amorphous SiO_2 sol) on densification of boehmite gels are presented in Table 1. The densification and sintering behavior is measured by the apparent densities of the sintered materials. These apparent densities are measured by eliminating the open pores by evacuation and, therefore, they are different from their bulk densities. The unseeded boehmite gels sintered to 98% of their theoretical density whereas both the Al_2O_3- and the spinel-seeded (0.5%) gels sintered to 99.6% of their theoretical density at 1200 °C (Table 1). The Cr_2O_3- and Fe_2O_3-

TABLE 1

Apparent densities of unseeded and seeded boehmite gels sintered (100 min) at different temperatures

Seed	*Amount* (wt.%)	*Apparent density* (g cm^{-3}) *at the following temperatures*				
		800 °C	*1000 °C*	*1200 °C*	*1300 °C*	*1450 °C*
No seed		3.29 (82.5)	3.30 (82.8)	3.91 (98.0)	3.912 (98.1)	13.90 (98.0)
α-Al_2O_3	0.08			3.94 (98.8)	3.94 (98.8)	3.96 (99.3)
α-Al_2O_3	0.16			3.95 (99.1)	3.93 (98.6)	3.96 (99.3)
α-Al_2O_3	0.40			3.97 (99.6)	3.94 (98.8)	3.94 (98.8)
α-Al_2O_3	0.5	3.27 (82.0)	3.37 (84.5)	3.97 (99.6)		
α-Al_2O_3	0.8			3.97 (99.6)	3.97 (99.6)	
α-Al_2O_3	2.7			3.94 (98.8)	3.81 (95.6)	
Spinel	0.1			3.94 (98.8)	3.74 (93.8)	3.89 (97.6)
Spinel	0.2			3.97 (99.6)	3.95 (99.1)	3.96 (99.3)
Spinel	0.5	3.27 (82.0)	3.34 (83.8)	3.97 (99.6)		
Spinel	1.0			3.95 (99.1)	3.95 (99.1)	
Spinel	7.3			3.91 (98.0)	3.91 (98.0)	
Cr_2O_3	0.5	3.23 (81.0)	3.39 (85.0)	3.49 (87.5)	3.92 (98.3)	
Ludox	0.15	3.23 (81.0)	3.30 (82.8)	3.47 (87.0)	3.88 (97.3)	
Ludox	0.35			3.50 (87.8)	3.91 (98.1	
Hematite	0.5	3.25 (81.5)	3.33 (83.5)	3.75 (94.1)	3.95 (99.1)	
Hematite	1.0			3.96 (99.3	3.97 (99.6)	
Kaolinite	0.5	3.34 (83.8)	3.34 (83.8)	3.84 (96.3)	3.93 (98.6)	

The numerals in parentheses are densities relative to the theoretical density of 3.986 for α-Al_2O_3.

seeded gels (where both Cr_2O_3 and Fe_2O_3 are isostructural with corundum) as well as the gels seeded with kaolinite and Ludox resulted in lower densities. All the densities reported here are high because of the elimination of open pores during the measurement. These measured densities do not clearly indicate the densification because the open pores are eliminated. Microstructural characterization is the best method of determining densification. The effect of seeding on densification is clearly seen from the microstructural studies. Microstructures of the unseeded gels show non-uniform grain growth and open porosity (Fig. 1(a)). Although the grain growth appears to be uniform (0.1–0.2 μm) in the spinel- and Fe_2O_3-seeded gels, they show considerable porosity (Figs. 1(b) and 1(c)). The α-Al_2O_3-seeded gels, however, show uniform grain growth with little porosity (Fig. 1(d)). The above results with different seeds clearly show that α-Al_2O_3 seeds are the most effective for enhanced densification and sintering with little or no porosity. The enhanced densification of α-Al_2O_3-seeded boehmite gels has been observed earlier [21] and here we show that the mechanism is epitaxial growth on isostructural seed crystals as has been postulated by us [15–17]. The fact that solid state epitaxy and not the colloidal phenomenon is the mechanism for enhanced densification and sintering is clearly shown by the studies on gels with different seeds [16]. Even though α-Fe_2O_3 and Cr_2O_3 are isostructural with α-Al_2O_3, they were not as effective as α-Al_2O_3 because of the lattice mismatch of about 5.5%. Thus it appears to be important to match the lattices exactly.

X-ray diffraction analyses of isothermally heated boehmite gels, both seeded and unseeded, show that α-Al_2O_3 crystallization was enhanced in seeded gels at 1050 °C while unseeded gels transformed to δ-Al_2O_3 and θ-Al_2O_3 but not to α-Al_2O_3 (Fig. 2). These

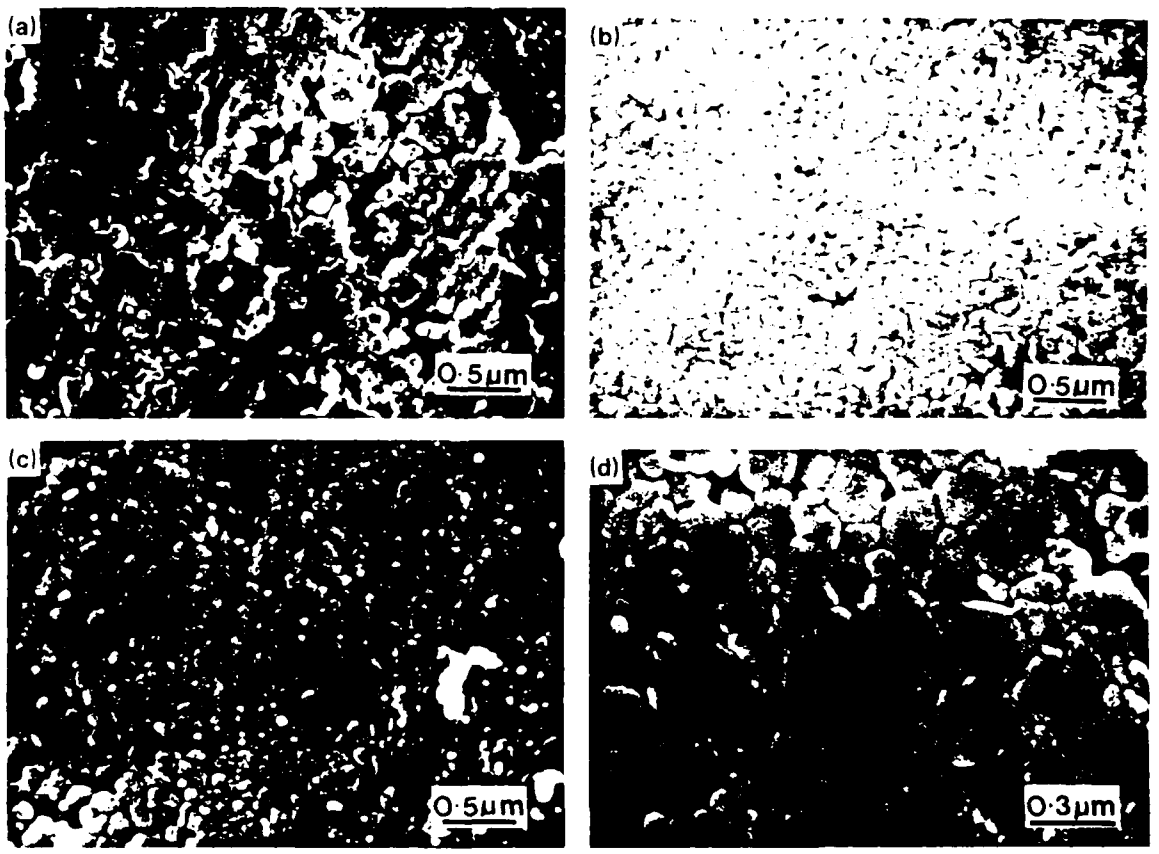

Fig. 1. Microstructures (polished surfaces) of boehmite gels sintered at 1200 °C: (a) unseeded gel; (b) spinel-seeded gel, (c) hematite-seeded gel; (d) α-Al_2O_3-seeded gel.

results clearly show the effect of 0.5 wt.% α-Al_2O_3 seeds in lowering the crystallization temperature of α-Al_2O_3 from that of boehmite.

3.2. Densification of two component gels by seeding: the system Al_2O_3-MgO

3.2.1. 93 wt.% Al_2O_3-7 wt.% MgO gels

These gels (of 3 M composition) seeded with α-Al_2O_3 and spinel show higher densities than the unseeded and Ludox-seeded gels (Table 2). Seeding with hematite which is isostructural with α-Al_2O_3 appears to enhance densification as well. The results with α-Al_2O_3 and spinel which are isostructural with the equilibrium phase assemblage of the sintered samples suggests that solid state epitaxy may be the cause of enhanced densification. The fact that colloidal effects are not the cause of enhanced densification is shown by the lack of effect on the Ludox-seeded gels (Table 2). The apparent densities measured here do not take the open porosity into consideration and that is why the densities achieved are quite high even for unseeded gels. The bulk densities of unseeded gels will be lower, however. Microstructural characterization of the sintered gels bears this out. Fractured surfaces of unseeded gels show much porosity and non-uniform grain growth (Fig. 3(a)). Spinel seeding resulted in uniform grain growth (Fig. 3(b)) and shows grains of the order of 1 μm. The α-Al_2O_3-seeded gels show dense microstructure with submicrometer-sized grains (Fig. 3(c)). These results show that isostructural seeding results in en-

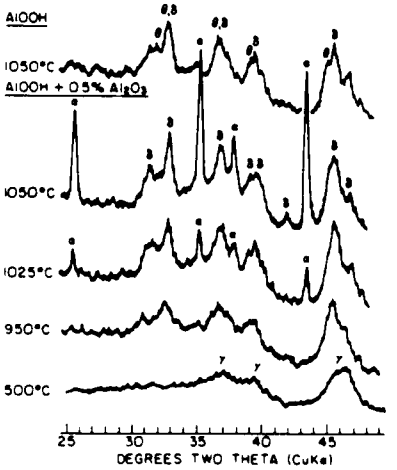

Fig. 2. X-ray powder diffraction patterns of boehmite and boehmite seeded with 0.5 wt.% α-Al_2O_3 heated at various temperatures.

TABLE 2

Apparent densities of unseeded and seeded gels of 93 wt.% Al_2O_3-7 wt.% MgO sintered (100 min) at different temperatures

Seed	*Amount* (wt.%)	*Apparent density* (g cm^{-3}) *at the following temperatures*				
		800 °C	*1000 °C*	*1200 °C*	*1300 °C*	*1450 °C*
No seed		3.25 (83.8)	3.35 (86.4)	3.44 (88.7)	3.62 (93.4)	3.63 (93.6)
α-Al_2O_3	0.07			3.44 (88.7)	3.44 (88.7)	3.72 (95.9)
α-Al_2O_3	0.14				3.54 (91.3)	3.81 (98.3)
α-Al_2O_3	0.1			3.81 (98.3)	3.81 (98.3)	
α-Al_2O_3	0.2			3.86 (99.6)		
α-Al_2O_3	0.5	3.21 (82.8)	3.53 (91.0)	3.78 (97.5)	3.71 (95.7)	
α-Al_2O_3	1.0			3.75 (96.7)	3.77 (97.2)	
α-Al_2O_3	2.0			3.76 (96.9)	3.83 (98.8)	
Spinel	0.09				3.70 (95.4)	3.43 (88.4)
Spinel	0.18			3.70 (95.4)	3.66 (94.4)	
Spinel	0.46			3.72 (95.9)	3.68 (94.9)	
Spinel	0.20			3.74 (96.5)	3.70 (95.4)	
Spinel	0.50	3.26 (84.1)	3.36 (86.7)	3.78 (97.5)	3.77 (97.2)	
Ludox	0.5	3.26 (84.1)	3.33 (85.9)	3.55 (91.6)	3.77 (97.2)	
Hematite	0.24			3.71 (95.7)	3.66 (95.4)	
Hematite	0.50			3.71 (95.7)	3.76 (97.0)	

The numerals in parentheses are densities relative to the theoretical density of 3.877 for the 93 wt.% Al_2O_3 - 7 wt.% MgO composition.

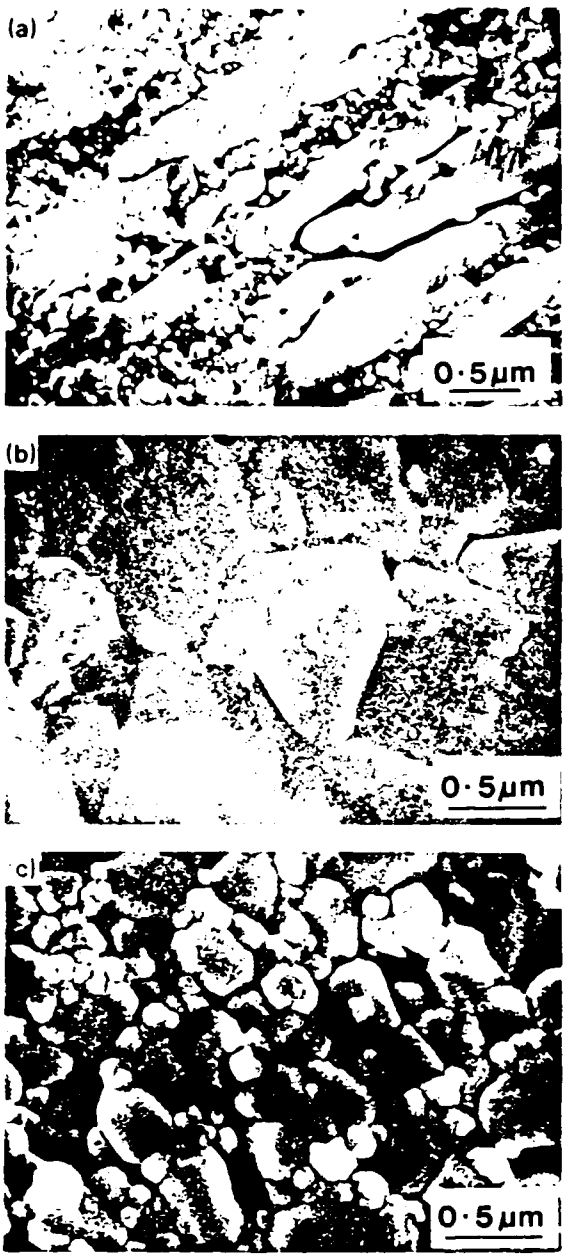

Fig. 3. Microstructures (fractured surfaces) of 93 wt.% Al_2O_3-7 wt.% MgO gels sintered at 1300 °C: (a) unseeded gel; (b) spinel-seeded gel; (c) α-Al_2O_3-seeded gel.

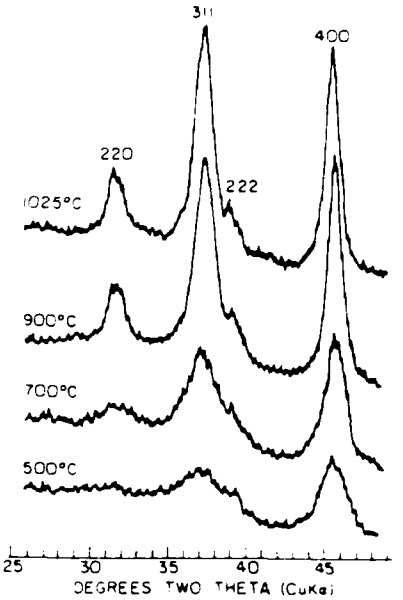

Fig. 4. X-ray powder diffraction patterns of spinel-seeded 93 wt.% Al_2O_3-7 wt.% MgO gels heated to different temperatures showing only γ-Al_2O_3.

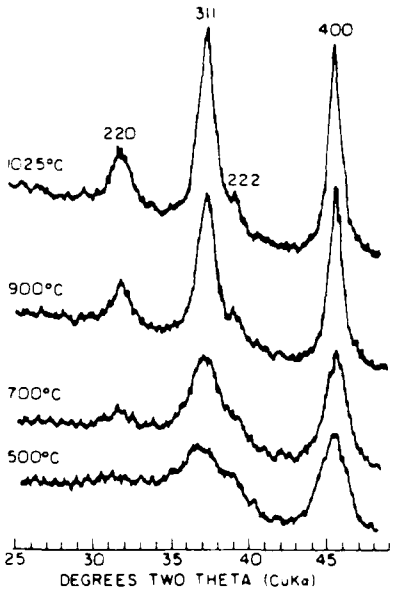

Fig. 5. X-ray powder diffraction patterns of unseeded 93 wt.% Al_2O_3-7 wt.% MgO gels heated to different temperatures showing only γ-Al_2O_3.

hanced densification and sintering by solid state epitaxy.

X-ray diffraction analyses of the unseeded and spinel-seeded gels show that the γ-Al_2O_3-$MgAl_2O_4$ solid solution phase was stabilized by the presence of MgO in this system (Figs. 4 and 5) unlike the Al_2O_3 system where the θ (clearly detected at larger angles) and α polymorphs formed (Fig. 2). The γ-Al_2O_3-$MgAl_2O_4$ solid solution was identified by lattice parameter a_0 calculations (Table 3)

TABLE 3

Identification of phases by X-ray diffraction in Al_2O_3-MgO xerogels after heat treatment

Sample	*Heat treatment temperature* (°C)	*Lattice parameter* a_0 *of the spinel phase* (Å)	*Phases identified by X-ray diffraction*
$MgAl_2O_4$ (PDF 21-1152)	None	8.083	Spinel ($MgAl_2O_4$)
Commercial γ-Al_2O_3	None	7.908	γ-Al_2O_3
Boehmite (Dispural)	500	7.892	γ-Al_2O_3
93 wt.% Al_2O_3-7 wt.% MgO, no seeds	500	7.976	γ-Al_2O_3-$MgAl_2O_4$ solid solution
93 wt.% Al_2O_3-7 wt.% MgO, no seeds	700	7.974	γ-Al_2O_3-$MgAl_2O_4$ solid solution
93 wt.% Al_2O_3-7 wt.% MgO, no seeds	1025	7.974	γ-Al_2O_3-$MgAl_2O_4$ solid solution
93 wt.% Al_2O_3-7 wt.% MgO, no seeds	1100	≈8.04-8.08	α-Al_2O_3 and γ-Al_2O_3-$MgAl_2O_4$ phase separation
93 wt.% Al_2O_3-7 wt.% MgO, 0.5 wt.% α-Al_2O_3 seeds	500	7.974	γ-Al_2O_3-$MgAl_2O_4$ solid solution
93 wt.% Al_2O_3-7 wt.% MgO, 0.5 wt.% α-Al_2O_3 seeds	700	7.974	γ-Al_2O_3-$MgAl_2O_4$ solid solution
93 wt.% Al_2O_3-7 wt.% MgO, 0.5 wt.% α-Al_2O_3 seeds	900	7.974	γ-Al_2O_3-$MgAl_2O_4$ solid solution + trace α-Al_2O_3
93 wt.% Al_2O_3-7 wt.% MgO, 0.5 wt.% α-Al_2O_3 seeds	1025	7.980	γ-Al_2O_3-$MgAl_2O_4$ solid solution + α-Al_2O_3
93 wt.% Al_2O_3-7 wt.% MgO, 0.5 wt.% α-Al_2O_3 seeds	1100	8.083	α-Al_2O_3 and $MgAl_2O_4$
93 wt.% Al_2O_3-7 wt.% MgO, 0.5 wt.% $MgAl_2O_4$ seeds	500	7.974	γ-Al_2O_3-$MgAl_2O_4$ solid solution
93 wt.% Al_2O_3-7 wt.% MgO, 0.5 wt.% $MgAl_2O_4$ seeds	700	7.974	γ-Al_2O_3-$MgAl_2O_4$ solid solution
93 wt.% Al_2O_3-7 wt.% MgO, 0.5 wt.% $MgAl_2O_4$ seeds	900	7.974	γ-Al_2O_3-$MgAl_2O_4$ solid solution
93 wt.% Al_2O_3-7 wt.% MgO, 0.5 wt.% $MgAl_2O_4$ seeds	1025	7.974	γ-Al_2O_3-$MgAl_2O_4$ solid solution
93 wt.% Al_2O_3-7 wt.% MgO, 0.5 wt.% $MgAl_2O_4$ seeds	1100	8.083	α-Al_2O_3 and $MgAl_2O_4$

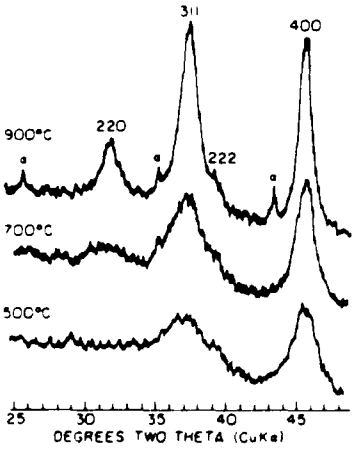

Fig. 6. X-ray powder diffraction patterns of α-Al_2O_3(0.5 wt.%)-seeded 93 wt.% Al_2O_3-7 wt.% MgO gels heated to different temperatures.

from the 400 and 440 *hkl* reflections. The solid solution showed a_0 parameters intermediate to those of $MgAl_2O_4$ and γ-Al_2O_3 (Table 3). The crystallization of 93 wt.% Al_2O_3-7 wt.% MgO gels with α-Al_2O_3 seeds as a function of temperature is shown in Fig. 6. The α-Al_2O_3-seeded gels show enhanced crystallization of α-Al_2O_3 at 900 °C (Fig. 6) but the unseeded or spinel-seeded gels (Figs. 4 and 5) do not. Both α-Al_2O_3- and spinel-seeded gels were effective in the complete transformation of γ-Al_2O_3-$MgAl_2O_4$ solid solution to α-Al_2O_3 and spinel (Fig. 7) at 1100 °C. The unseeded gels, however, do not completely transform to α-Al_2O_3 and spinel and show γ-Al_2O_3 as a shoulder on the spinel peak (Fig. 7).

3.2.2. 95.2 wt.% Al_2O_3-4.8 wt.% MgO gels

These gels seeded with α-Al_2O_3 and spinel show enhanced densification as measured by densities compared with those of the unseeded gels (Table 4). Here also solid state epitaxy is clearly the mechanism of enhanced densification as discussed above. This composition showed a decrease in density as the sintering temperature was increased; this may be attributed to closed porosity at higher temperatures.

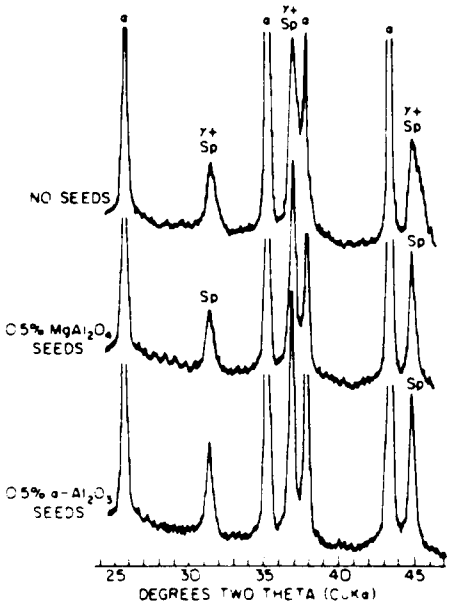

Fig. 7. X-ray powder diffraction patterns of unseeded and spinel or α-Al_2O_3-seeded 93 wt.% Al_2O_3-7 wt.% MgO gels at 1100 °C showing the complete transformation of γ-Al_2O_3 to α-Al_2O_3 in seeded gels and the presence of γ-Al_2O_3 in unseeded gel.

4. CONCLUSIONS

We have presented here sufficient data to show that diphasic seeding affects the densification and sintering behavior of MgO-Al_2O_3. Isostructural seeding utilizing the principle of solid state epitaxy appears to be the mechanism of action in enhancing densification and sintering at lower temperatures. While the work of Messier *et al.* [23] on the propagation of a crystalline wave through amorphous germanium films at room temperature has been attributed to epitaxy also, in that case a liquid phase is postulated to crystallize on the substrate. In this case the isostructural seeds appear to cause reorganization of a non-crystalline but energetically excited metastable xerogel state [16]. If this proves to be true, the lowering of ceramic processing temperatures in a wide variety of systems may be possible with isostructural seeding.

ACKNOWLEDGMENT

This research was supported by the U.S. Air Force Office of Scientific Research under Contract F49620-85-C-0069.

TABLE 4

Apparent densities of unseeded and seeded gels of 95.8 wt.% Al_2O_3-4.2 wt.% MgO sintered (100 min) to different temperatures

Seed	*Amount* (wt.%)	*Apparent density* (g cm^{-3}) *at the following temperatures*			
		1000 °C	*1200 °C*	*1300 °C*	*1400 °C*
No seed		3.36 (85.7)	3.38 (86.2)	3.34 (85.2)	3.45 (88.0
α-Al_2O_3	0.09		3.82 (97.4)	3.47 (88.5)	
α-Al_2O_3	0.18		3.85 (98.2)	3.51 (89.5)	
α-Al_2O_3	0.45	3.42 (87.2)	3.82 (97.4)	3.59 (91.6)	
α-Al_2O_3	0.90		3.63 (92.6)	3.67 (93.6)	
Spinel	0.12		3.30 (84.2)	3.61 (92.1)	
Spinel	0.23		3.75 (95.7)	3.48 (88.8)	
Spinel	0.58	3.36 (85.7)	3.71 (94.6)	3.50 (89.3)	
Spinel	1.16		3.63 (92.6)	3.57 (91.1)	

The numerals in parentheses are densities relative to the theoretical density of 3.920 for the 95.8 wt.% Al_2O_3-4.2 wt.% MgO composition.

REFERENCES

1 R. Roy, *J. Am. Ceram. Soc.*, *52* (6) (1969) 344.
2 G. J. McCarthy and R. Roy, *J. Am. Ceram. Soc.*, *54* (12) (1971) 639.
3 B. E. Yoldas, *J. Mater. Sci.*, *12* (1977) 1203.
4 L. L. Hench and D. R. Ulrich (eds.), *Ultra Structure Processing of Ceramics, Glasses, and Composites*, Wiley, New York, 1984.
5 R. A. Roy and R. Roy, *Mater. Res. Bull.*, *19* (2) (1984) 169.
6 D. Hoffman, R. Roy and S. Komarneni, *Mater. Lett.*, *2* (3) (1984) 245.
7 D. Hoffman, S. Komarneni and R. Roy, *J. Mater. Lett.*, *3* (6) (1984) 439.
8 R. Roy, S. Komarneni and D. M. Roy, Multiphase ceramic composites made by sol-gel technique, in C. J. Brinker (ed.), *Better Ceramics Through Chemistry*, North-Holland, Amsterdam, 1984, pp. 347-359.
9 R. Zsigmondy, *Zur Erkenntnis der Kolloide*, Fischer, Jena, 1905.
10 R. Zsigmondy and P. A. Thiessen, *Das Kolloide Gold*, Akademie, Leipzig, 1925, p. 229.
11 G. Ervin, Jr., Alumina and its hydrates, *Ph.D. Thesis*, The Pennsylvania State University, 1949.
12 G. Ervin and E. F. Osborn, *J. Geol.*, *59* (1951) 381.
13 D. M. Roy, R. Roy and E. F. Osborn, *Am. J. Sci.*, *251* (5) (1953) 337.
14 R. A. Roy and R. Roy, New metal-ceramic hybrid xerogels, *Abstracts, Materials Research Society Annu. Meet., Boston, MA*, 1982, p. 377.
15 R. Roy, Y. Suwa and S. Komarneni, Nucleation and epitaxial growth in diphasic (crystalline + amorphous) gels, in L. L. Hench and D. R. Ulrich (eds.), *Science of Ceramic Chemical Processing*, Wiley, New York, 1986, pp. 247-258.
16 Y. Suwa, S. Komarneni and R. Roy, *J. Mater. Sci. Lett.*, *5* (1986) 21.
17 Y. Suwa, R. Roy and S. Komarneni, *Commun. Am. Ceram. Soc.*, *68* (1985) C238.
18 M. A. Leitheiser and H. G. Sowman, *U.S. Patent 4,314,827*, 1982.
19 E. Breval, G. C. Dodds and N. H. Macmillan, *Mater. Res. Bull.*, *20* (4) (1985) 413.
20 W. A. Yarbrough and R. Roy, Microstructural evolution in sintering of AlOOH gels, *Extended Abstracts, 87th Annu. Meet. of the American Ceramic Society*, American Ceramic Society, Columbus, OH, 1985, p. 269.
21 M. Kumagai and G. L. Messing, *Commun. Am. Ceram. Soc.*, *67* (1984) C230.
22 E. Matijevic. Monodispersed colloidal metal oxides, sulfides, and phosphates, in L. L. Hench and D. R. Ulrich (eds.), *Ultrastructure Processing of Ceramics, Glasses, and Composites*, Wiley, New York, 1984, pp. 334-352.
23 R. Messier, T. Takamori and R. Roy, *Solid State Commun.*, *16* (1975) 311.

Reprint #3

Extraordinary Effects of Mortar-and-Pestle Grinding
on Microstructure of Sintered Alumina Gel

Reprinted from Nature, Vol. 322, No. 6077, pp. 347-349, 24 July 1986
Macmillan Journals Ltd., 1986

Extraordinary effects of mortar-and-pestle grinding on microstructure of sintered alumina gel

W. A. Yarbrough & Rustum Roy

Materials Research Laboratory, The Pennsylvania State University, University Park, Pennsylvania, USA

The use of the mortar and pestle in the laboratory dates back to the earliest attempts to understand and use the materials around us. Even now, it is difficult to imagine an alternative to crushing and grinding for the preparation of many samples. Traditionally, mortar-and-pestle mixing or grinding has been held to be a relatively mild and controlled process, although it was recognized that the grinding of materials harder than the material of the mortar and pestle would result in some contamination. Thus, good practice forbade grinding of, for example, mullite and alumina in agate mortars. That this technique is not so innocuous was demonstrated by Dachille and Roy[1] with respect to the stresses generated. They showed that phases usually obtained only at 10–20 kbar can be obtained metastably by simple grinding in a laboratory mortar. There are numerous examples of solid-state phase transformations being produced by prolonged or intense comminution[2], two of the best-documented cases of stress/shear-induced transformation being the conversion of calcite to aragonite[1], and of quartz to amorphous silica[3,4], both by prolonged grinding in a laboratory mortar and pestle. Here we show that the very small amounts of material generated by the wear of mortar and pestle surfaces by even mild grinding can also have substantial effects on the microstructure and transformation kinetics of certain ceramic systems so treated.

Materials prepared by the sol-gel method are typically obtained as non-crystalline or poorly crystallized metastable solids which may then be calcined for densification and/or transformation to a more stable crystalline phase. In the preparation of dense non-crystalline solids (glasses), uncontrolled crystallization or devitrification is undesirable, as this usually leads to a loss of mechanical integrity and other desired properties, such as transparency. In other materials, where a given stable crystalline phase may be the desired product, the kinetics of transformation and the microstructure of the material obtained can be controlled by 'seeding' with the desired phase or with chemically dissimilar materials having, or readily transforming to, the desired structure.

Seeding with crystals of the expected or desired phase has long been used as an aid in the study of phase equilibria, and the importance of even minor amounts of a second phase, isostructural with a stable phase of the composition under study, has already been noted[5,6]. In particular, we have reported the remarkably enhanced transformation kinetics obtained by seeding sol-gel-derived materials[7-10]. This may well turn out to be a route to a new class of crystalline solids: nanocomposites (di- or multiphasic solid aggregates), where the size range of the monophasic regions is ~1-100 nm. One of the striking properties of a structurally diphasic xerogel (for example, boehmite sol mixed with an α-alumina sol) is the solid-state epitaxy which occurs on heating, with considerably accelerated kinetics. Thus, Fig. 1 (taken from ref. 9) compares the differential thermal analysis (DTA) of a monophasic boehmite sol with that of a diphasic sol of boehmite and various amounts of α-alumina. Seeding with amounts as small as 0.08 wt % results in a marked lowering of the transformation temperature. Moreover, there is a marked change in the microstructure of the alumina formed. In the unseeded material, monocrystalline cells ~10 μm across are formed, whereas in the seeded material, the grain size is <1 μm (ref. 10).

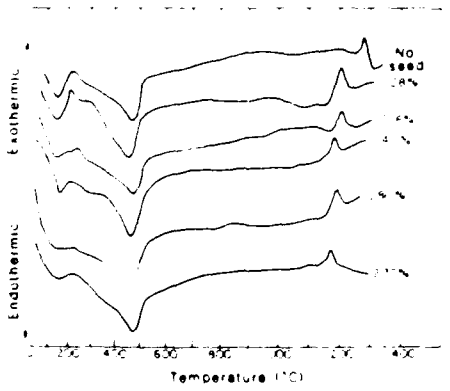

Fig. 1 DTA results showing the effect of seeding with various amounts of α-alumina on the transformation temperature of boehmite gel

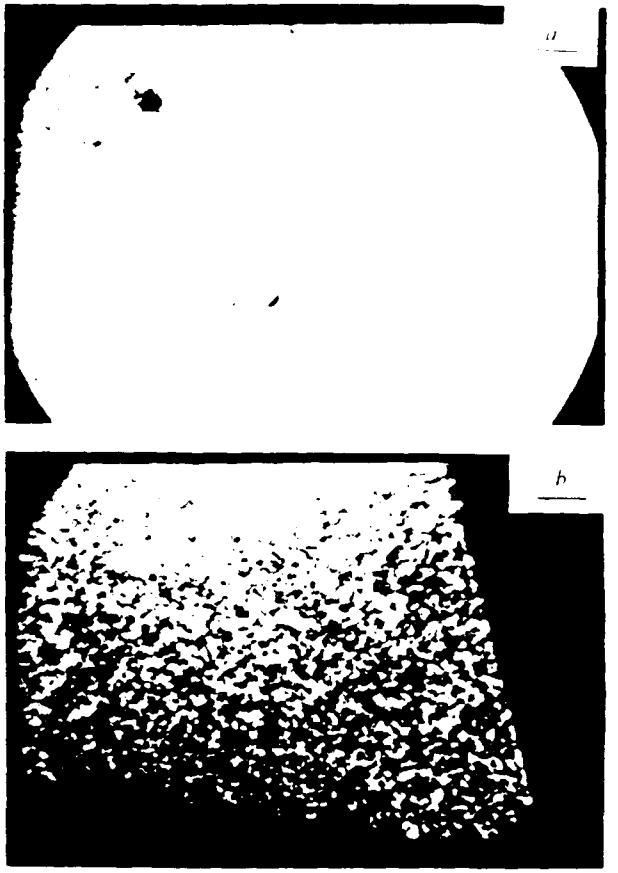

Fig. 2 Boehmite gel fragment prepared from water 'ground' in Diamonite mortar and pestle as seen after calcination at 1,200 °C for 2 h: *a*, Bright-field transmitted light, *b*, crossed polars. Scale bars, 10 μm

The mortar and pestle experiment was conducted using a Fisher Scientific Co. 'Diamonite' (corundum) mortar and pestle. After thoroughly cleaning the mortar and pestle, 200 ml of deionized water was added to the mortar. The water was slowly 'ground' in the mortar using only light to moderate pressure for 5 min. This water, slightly turbid with suspended detritus from the wear of the mortar and pestle surfaces, was then used to prepare a boehmite (aluminium oxide monohydrate) sol using 13.90 g of a commercially available microcrystalline boehmite (Dispereal, Remet Chemical Co.) The boehmite was peptized using 15.0 ml of 1.00 M HNO_3; the sol was then dried at 90-95 °C to produce a boehmite xerogel. A second batch of xerogel was prepared in precisely the same manner using the same lots of

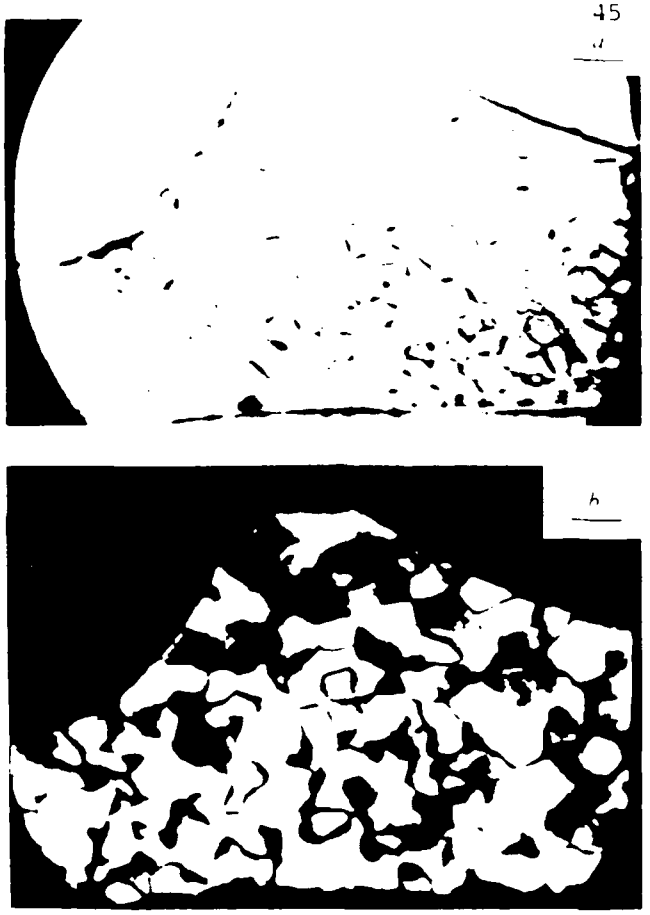

Fig. 3 Boehmite gel fragment prepared from water 'ground' in agate mortar and pestle as seen after calcination at 1,200 °C for 2 h. *a*, Bright-field transmitted light, *b*, crossed polars. Scale bars, 10 μm

material (water, acid and boehmite), the only modification being the use of a mortar and pestle of agate instead of Diamonite. Fragments of these xerogels were lightly crushed in an agate mortar and pestle. Calcination was performed in air using a Lindberg model 51524 furnace equipped with a model 59258-E1 controller (Lindberg Co.). This furnace uses exposed $MoSi_2$ elements and had been modified by installing a type S thermocouple positioned just above the sample for accurate temperature measurement. The maximum calcination temperature was 1,200 °C for a period of 2 h, which is sufficient to convert all of the material to α-alumina. The powders were dispersed in immersion oil and examined with a polarizing microscope.

Alpha aluminium oxide (α-alumina) is anisotropic and uniaxial negative. Assuming that a sufficient crystallite size is attained on transformation, its birefringence makes observation in a polarizing microscope relatively easy. Figures 2 and 3 show transmitted-light photomicrographs (Figs 2*a* and 3*a* in bright field transmitted light, Figs 2*b* and 3*b* using crossed polars) of the calcined powders. Transformation occurs by the nucleation and growth of the α phase in a matrix of very finely divided and poorly crystallized transitional aluminas (δ and θ). The microstructure exhibited in Fig. 2 is identical to that obtained in a xerogel seeded with α-alumina or with materials having the corundum crystal structure, that seen in Fig. 3 is identical to that seen with unseeded or non-isostructurally seeded gels.

Scientists almost universally use milling or grinding in a mortar and pestle as a means of preparing powdered materials, in industry as well as in the laboratory. It is so routine that in many cases no report is made of the materials and methods used[11]. Enhanced transformation kinetics and nucleation frequency in milled materials have been variously attributed to particle size effects[12] and possibly lattice strain[13]. Dynys and Halloran[13], in fact, considered and rejected the possibility that detritus from milling was responsible for these effects. In their experiment, α-alumina milling debris was collected, dried and dry-mixed (at 1 wt%) with powders obtained from the calcination of ammonium alum. Pressed pellets were prepared and fired in air. No effect could be seen either by transmission electron microscopy or by comparison of the transformation kinetics of doped and undoped material. Assuming that the nature of the interface between seed and bulk phase, and the uniformity of seed distribution, are of controlling importance, it is not surprising to find that the efficacy of seeding depends on how the seed phase is produced and introduced to the bulk material. Effects due to the method of seed introduction have been observed previously[14]. This demonstration of the power of trace contaminants introduced by grinding has led us to question our common laboratory and commercial practice.

This work was supported by a grant from the Air Force Office of Scientific Research, AFOSR grant no. 83-0212.

Received 7 March; accepted 24 April ...

1. Dachille, F. & Roy, R. *Nature* **186**, ... (1960).
2. Lee, J. ... *J. Mater. Sci. Engng* ... (...).
3. Ray, R. ... *J. Am. Ceram. Soc.* **A102**, ... (...).
4. Dale, A. ... *Trans. Br. Ceram. Soc.* **23**, ... (...).
5. Ervin, G. & Osborn, E. F. ... *Geol.* **59**, ... (...).
6. Ross, D. M. *Am. Miner.* **39**, ... (...).
7. Suwa, Y., Ross, R. & Komarneni, S. *J. Am. Ceram. Soc.* (in the press).
8. Ross, R., Suwa, Y. & Komarneni, S. in *Ultrastructure Processing of Ceramics, Glasses and Composites* (eds Hench, L. L. & Ulrich, D. R.) (Wiley, New York, ...).
9. Suwa, Y., Komarneni, S. & Ross, R. *J. Mater. Sci. Lett.* **5**, ... (...).
10. Yarbrough, W. A. & Ross, R. *J. Mater. Res.* (submitted).
11. Gugliotta, M. & Principi, G. *J. Non-Cryst. Solids* **48**, ... (...).
12. Gregorio, A. G. & Veasey, T. J. *Mater. Sci.* ... (...).
13. Dynys, F. W. & Halloran, J. W. *J. Am. Ceram. Soc.* **65**, ... (...).
14. Bokhonov, A. I. *Solid State Transformations*, ed. Strata, N. N. (Gorkii, E. K. & Karpash, V. M., Institute of Solid State Physics and Semiconductors, Academy of Sciences of the Byelorussian SSR, Minsk, Trans. ... Williams Bureau, New York, ...).

Reprint #4

Enhancing Densification of 93% Al_2O_3-7% MgO
Triphasic Xerogels with Crystalline α-Al_2O_3 and $MgAl_2O_4$ Seeds

Enhancing densification of 93% Al_2O_3–7% MgO triphasic xerogels with crystalline α-Al_2O_3 and $MgAl_2O_4$ seeds

S. KOMARNENI, Y. SUWA, R. ROY
Materials Research Laboratory, The Pennsylvania State University, University Park, Pennsylvania 16802, USA

The scientific development of using solution sol gel (SSG) approaches to making ultrahomogeneous ceramics and glasses in our laboratories in the early fifties was first reviewed in 1956 [1]. Starting in the mid-sixties to early seventies many technologies entered the production phase, making nuclear fuel pellets, window glass coatings, fibres, and abrasive grains. Since the late seventies the strong revival of interest has again focused on the science of the process in order to obtain ultrafine, ultrahomogeneous ceramics. In 1982 [2] a radical change in the direction of our SSG work towards making maximally heterogeneous di- (or more) phasic materials was announced. Since then this laboratory has exploited the basic concept to make a variety of *nanoheterogeneous* materials [3–6] which exhibit remarkable lowerings of the sintering temperature and control of the microstructure [7, 8]. The nanoheterogeneous materials can be of three types: (1) compositionally heterogeneous, (2) structurally heterogeneous, and (3) both compositionally and structurally heterogeneous. The first type of material is made up of nanometre size regions of amorphous or semicrystalline sols which differ in composition. For example, amorphous SiO_2 sol and semicrystalline AlOOH (boehmite) sol can be mixed to yield the $Al_2Si_2O_5$ (mullite) composition [6]. The second type of material is made up of amorphous or semicrystalline gels containing a small amount of crystalline seeds as a sol, the crystalline seeds being the same as the final equilibrium phase [7]. The structurally di-phasic materials are extensions of our very earliest work on the SSG process in 1949, 1951, 1952 [9–11] where we seeded a gel with the expected equilibrium phase in order to accelerate the formation of that phase especially at lower temperatures. As an example, exactly the same AlOOH gel with a dispersion of α-Al_2O_3 (corundum) seed crystals which we used in 1949 can be used to control the microstructure of the ceramics [12] and lower the sintering temperature [13, 14]. The third type of di-phasicity is a combination of the first and second types. For example, mullite seed crystals can be used in a mullite composition gel which is itself made up of a di-phasic mixture of SiO_2 and AlOOH sols. The densification and sintering of mullite takes advantage of the heat of reaction of the compositional heterogeneity in the compositionally di-phasic xerogels. Similar effects caused by solid-state epitaxy on lowering the crystallization temperature and enhancing densification in structurally heterogeneous gels have been reported earlier by us [7, 8, 12, 15]. The use of heterogeneous gels for reaction in the solid-state is new, although, as noted above, the same "seeding" was extensively practiced by us [9–11] in the hydrothermal p-t regime. All the above studies show that significant effects can be achieved in the processing of ceramics by the use of nanoheterogeneous materials.

The objective of the present study was to show the effects of providing competing epitaxial bases in a binary system. Thus we could study the effect of α-Al_2O_3 and $MgAl_2O_4$ on the densification of a composition such as 93% Al_2O_3, 7% MgO xerogels. This, of course, represents the composition of 3M's new abrasive grain [16]. The effects of α-Al_2O_3 and $MgAl_2O_4$ seed crystals used separately on densification of 93% Al_2O_3, 7% MgO xerogels have already been reported by us in an earlier paper [12].

Four types of nanoheterogeneous 93% Al_2O_3, 7% MgO gels were prepared. Unseeded Al_2O_3–MgO gels were made by first dispersing boehmite in water, subsequently peptizing with 1 N HNO_3 to obtain a clear boehmite hydrosol and by adding $Mg(NO_3)_2$ solution drop-wise while stirring. Gelling occurred immediately upon the addition of $Mg(NO_3)_2$ solution and the gels were dried at room temperature for about 10 days. Gels with 0.5% $MgAl_2O_4$ (spinel) or α-Al_2O_3, or both seed crystals were made using the above procedure, except that the peptized seed crystals were added to the boehmite hydrosol prior to the $Mg(NO_3)_2$ addition. The particle size of α-Al_2O_3 seed crystals ranged between ~0.2 and 0.4 μm while that of the $MgAl_2O_4$ seed crystals ranged between ~0.04 and 0.1 μm. Both the concentration of HNO_3 and the amount of water were found to be critical in obtaining homogeneous gels. A weight ratio of 10:90 boehmite to water and a mole ratio of 0.07:1 HNO_3 to boehmite gave the best gels.

The different gel tablets or pieces were sintered in air by stepwise heating in a programmed furnace. At least two replicates of each type of gel were sintered. The heating rates were 1 °C min^{-1} up to 200 °C (soaked for 1 h at this temperature), 1.5 °C min^{-1}

TABLE I Apparent densities (g cm^{-3}) and per cent theoretical of unseeded and seeded gels

Seed	Sintering temperature (°C)	
	1200	1300
No seed	3.44 (88.7)	3.62 (93.4)
α-Al_2O_3	3.81 (98.3)	3.81 (98.3)
$MgAl_2O_4$	3.70 (95.4)	3.66 (94.4)
α-Al_2O_3 + $MgAl_2O_4$	3.79 (97.8)	3.74 (96.6)

0261–8028/87 $03.00 + .12

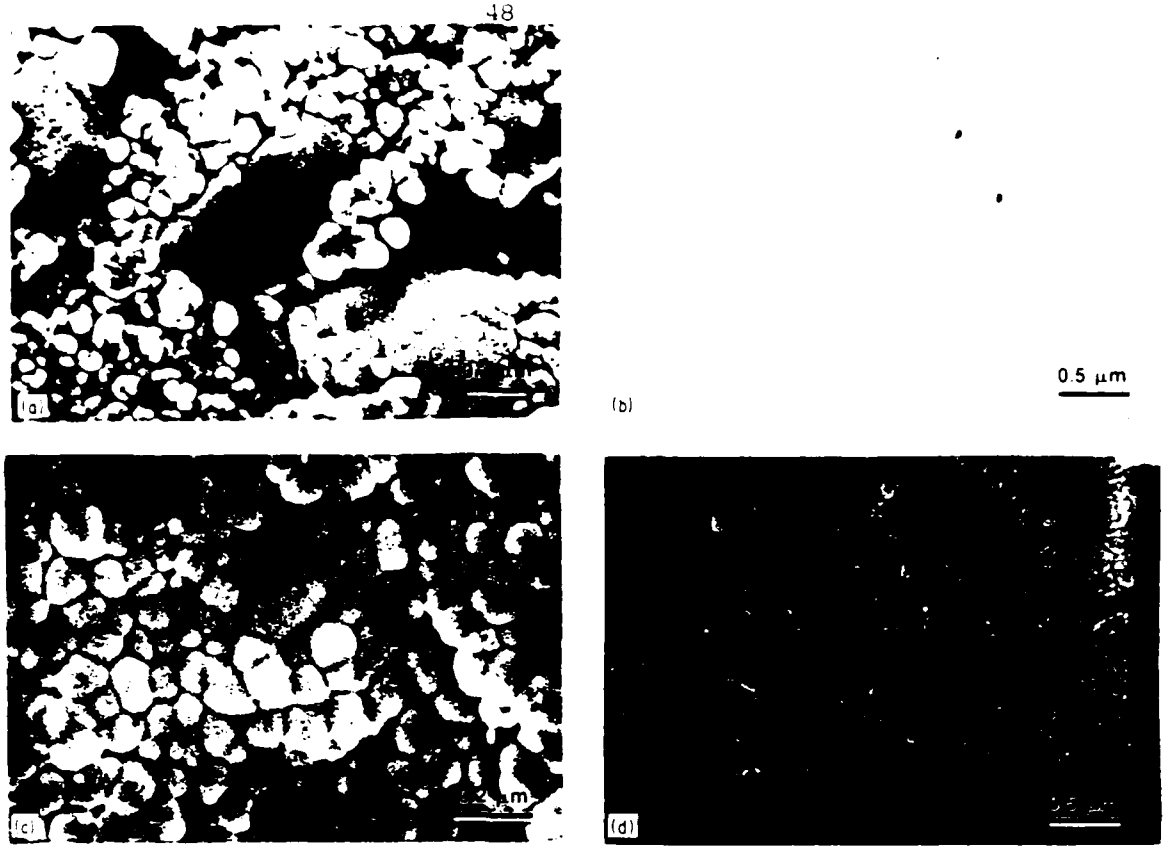

Figure 1 Microstructures of 93% Al_2O_3–7% MgO gels sintered at 1300 C (a) Fractured surface of unseeded gel, (b) polished and etched surface of spinel seeded gel, (c) polished and etched surface of α-Al_2O_3 seeded gel, and (d) polished and etched surface of α-Al_2O_3 and spinel seeded gel

between 200 and 500 C, 3 C min^{-1} between 500 and 800 C, and 10 C min^{-1} above 800 C. The samples were heated for 100 min at the final sintering temperature of 1200 or 1300 C. The densities of the sintered tablets after evacuation were measured by the Archimedes' technique and reported as apparent densities. Microstructural characterization of the fractured or polished samples were carried out by scanning electron microscopy using an ISI DS-130 microscope. The particle size of the seed crystals was determined by transmission electron microscopy using Philips EM 300 and 420 microscopes.

The apparent densities of the sintered gel tablets are given in Table 1. These data show that seeded gels have higher densities than the unseeded gels at both temperatures. The gels seeded with α-Al_2O_3 or double seeded with α-Al_2O_3 + $MgAl_2O_4$ exhibit the highest densities. The major phase in the equilibrium assemblage of these gels is α-Al_2O_3 while the minor phase is spinel. Earlier studies have shown that α-Al_2O_3 seeding in Al_2O_3 gels increased densification [12–14] by nucleation and epitaxial growth process. The use of spinel seeds to affect the densification of spinel phase also resulted in a 6% enhanced densification. When both α-Al_2O_3 and spinel seeds were used, the densities attained were comparable to the α-Al_2O_3 seeded gels and 98% theoretical density was achieved. The densities reported here are apparent densities which are measured after evacuation of the open pores and hence do not give a clear indication of the extent of porosity. Microstructural characterization, however, reveals the porosity clearly and the extent of densification can be gauged. The microstructural development in the sintered gels is shown in Fig. 1. Fractured surfaces of the unseeded gel show large corundum crystals surrounded by small spinel crystals (Fig. 1a). The crystals appear more like a loose powder than a sintered body. The use of spinel seeds appears to result in better densification but shows large corundum crystals and some pores (Fig. 1b). The α-Al_2O_3 seeded gel shows good densification. However, some intergranular pores remain (Fig. 1c). The gel seeded with α-Al_2O_3 and $MgAl_2O_4$ shows cellular structure with virtually no porosity. These results clearly demonstrate the effect of isostructural seeding in enhancing densification of 93% Al_2O_3–7% MgO sol–gel materials by nucleation and epitaxial growth as has been shown for the Al_2O_3 system [12–14]. Isostructural seeding with the crystalline phases that result in the final equilibrium assemblage may be a generalizable process for enhancing densification. The generalizable nature of this process is being evaluated at present in other compositional systems.

Acknowledgement

This work was supported by the Air Force Office of Scientific Research under Contract F49620-85-C-0069.

References

1 R ROY *J Am Ceram Soc* **39** (1956) 145
2 R A ROY and R ROY Abstracts, Annual Meeting of Materials Research Society, Boston, Massachusetts (1982) p 377
3 *Idem, Mater Res Bull* **19** (1984) 169
4 D HOFFMAN, R ROY and S KOMARNENI *Mater Lett* **2** (1984) 245
5 D HOFFMAN, S KOMARNENI and R ROY, *J Mater Sci Lett* **3** (1984) 439
6 D HOFFMAN, R ROY and S KOMARNENI *J Am Ceram Soc* **67** (1984) 468
7 Y SUWA, R ROY and S KOMARNENI *ibid* **68** (1985) C-238
8 R ROY, Y SUWA and S KOMARNENI "Ultrastructure Processing of Ceramics, Glasses and Composites", edited by L L Hench and D R Ulrich (Wiley, New York, 1986)
9 G ERVIN Jr PhD thesis, Pennsylvania State University (1949)
10 G ERVIN Jr and E F OSBORN *J Geol* **59** (1951) 381
11 V G HILL, R ROY and E F OSBORN *J Am Ceram Soc* **35** (1952) 135
12 Y SUWA, R ROY and S KOMARNENI *Mat Sci Engng*, in press
13 M KUMAGAI and G L MESSING *J Am Ceram Soc* **67** (1984) C-230
14 *Idem, ibid* **68** (1985) 500
15 Y SUWA, S KOMARNENI and R ROY *J Mater Sci Lett* **5** (1986) 21
16 M A LEITHEISER and H G SOWMAN US Pat 4 314 827 (1982)

Received 30 September
and accepted 10 November 1986

Reprint #5

Anomalous Microwave Melting of Zeolites

Volume 4, number 2 MATERIALS LETTERS February 1986

ANOMALOUS MICROWAVE MELTING OF ZEOLITES

Sridhar KOMARNENI [1] and Rustum ROY

Materials Research Laboratory, The Pennsylvania State University, University Park, PA 16802, USA

Received 18 October 1985

Microwave absorption in transparent ceramics or minerals containing no transition metals may be due to losses caused by ionic "rattling" in a rigid cage. Evidence for this appears in the fact that some zeolites can be melted in a matter of seconds in a standard kitchen-type microwave oven with a frequency of 2.45 GHz. This dielectric heating behavior is controlled in part by the topology of the anionic framework, location and nature of the exchange ions within the framework. Faujasite (Linde 13X) and Linde type A saturated with Na^+ are the strongest absorbers. This rapid heating behavior of zeolites by microwaves opens up a new method for the processing of these important materials, and of ceramic bodies containing them in general.

1. Introduction

During the very recent past it has become clear that direct coupling of microwave energy into ceramic materials can be used to heat and even melt them. Krage [1] summarizes this use for ferrimagnetic phases where the loss, and hence heating, mechanism is the eddy current loss. The melting of UO_{3-x} phases by Haas [2] was linked to possible mixed-valence energy-level transitions. But neither of these could explain the absorption of 2.45 GHz radiation by calcium silicates and aluminates [3], nor by the mixture of phases dominated by $NaAlSiO_4$-nepheline [4]. Our own earlier work [5] was even more striking in that even pure SiO_2 and Al_2O_3 when presented in gels could be heated to very high temperatures, even the melting points, in an ordinary 600 W 2.45 GHz home oven.

Almost all the work to date has been conducted under relatively crude conditions of observation of heating/melting in home ovens. Due to the extreme difficulty of obtaining absorption spectra in these frequency ranges only a very few point-by-point measurements of such spectra are available as in β-Al_2O_3 [6].

The present work is an attempt to build up a body of empirical data on the crystal *structural* control of the absorption of 2.45 GHz radiation in non-magnetic high band gap phases. Using the model that the 2.45 GHz loss mechanism is the tail of the absorption usually peaking in the megahertz region due to ionic motion in a "cage" (as in most glasses and a few rather special crystalline structures) we chose to study the family of minerals, the zeolites, where we could study the influence of both the size (and shape) of such a cage, and the ions lodged within it. It was soon found that some of these phases are the most powerful absorbers of such microwave absorption yet reported and that there was a strong structural dependence of such absorption.

2. Phases studied

Zeolites are tectosilicates, that is they are formed by the linking together of SiO_4 and AlO_4 tetrahedra at all the corners to give three-dimensional anionic networks [7], which are articulated in one of several ways to create large holes or cages. For every Si^{IV} which is replaced in the framework by Al^{3+} a negative charge is created which is neutralized by an electrochemical equivalent of cations located in the cages. The zeolite framework is sufficiently open to accommodate water or other molecules along with cations. The open nature of the framework imparts commercially important properties such as gas adsorption,

[1] Also associated with the Department of Agronomy.

0 167-577x/86/$ 03.50

Volume 4, number 2 MATERIALS LETTERS February 1986

cation exchange, catalysis, molecular sieving and ion sieving [8].

The framework of each particular zeolite creates cages with openings which range from 10 Å down to 3 Å and this hole or opening size and shape is the structural parameter which controls its use in the technologies cited. Many excellent reviews summarize the structures of zeolites [7,8].

A selection of zeolites, together with a few feldspathoids, feldspars and clay minerals for comparison purposes were selected for the present work. Linde Molecular Sieves types 3A, 4A, 5A and 13X and Ionsiv IE-95 were the synthetic zeolites used in this investigation. Natural zeolites used were: clinoptilolite, Castle Creek, Idaho; chabazite, Christmas, Arizona; erionite, Pine Valley, Nevada; mordenite, Union Pass, Arizona; phillipsite, Pine Valley, Nevada; analcime, Wikieup, Arizona. Feldspathoids such as pollucite (Manitoba, Canada) and sodalite (Bancroft, Ontario) and feldspars such as albite and K-orthoclase (Barstow, California) and clay minerals including Na-montmorillonite (Wyoming) and Ca-montmorillonite (Texas) were used in this study. In order to study the influence of the exchanged cation, Linde 4A was treated with CsCl and Linde 13X was treated with CsCl, KCl and $CaCl_2$ repeatedly and finally washed free of excess salt in order to exchange saturate the zeolites with the respective cations. Since our earlier work [5] had shown the importance of size of sample, ≈10 g of each sample was pelletized in the same molds.

3. Microwave heating: results

A 4″ × 4″ × 4″ cavity was created out of fiberfrax insulation inside a 600 W kitchen-type microwave oven (2.45 GHz frequency). Proper insulation is essential for attaining the highest temperatures and for melting to occur although the relative absorptions reported are not affected. The temperature attained *near* the sample in the cavity was measured by inserting a sheathed Pt–Rh thermocouple. The striking microwave heating behavior of Linde Molecular Sieve types 3A, 4A and 5A is presented in fig. 1. Type 4A which is the Na^+ form of A, heated up very rapidly and started melting after 1 min whereas the mixed K + Na cation form (3A) (table 1) heated up

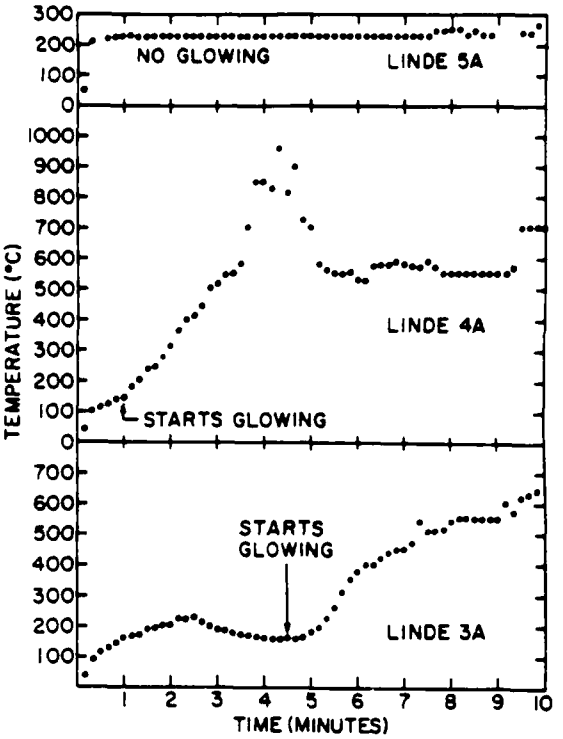

Fig. 1. Temperature (*near* sample) versus time for the microwave heating of zeolite A.

slowly and started melting only after about 5 min. By contrast, type 5A (a mixed Ca + Na form) (table 1) could not be melted at all. Similarly, a Cs treated 4A heated up much more slowly and did not melt under similar conditions (table 2). Melting can be seen both visually and using a microscope. The glassy-looking melted material was found to be amorphous by X-ray powder diffraction. The mea-

Table 1
Chemical analyses (in %) of synthetic Linde zeolites, type A

Oxide	Linde 3A	Linde 4A	Linde 5A
SiO_2	32.2	34.0	35.1
Al_2O_3	28.3	28.5	28.5
CaO	0.10	<0.05	12.1
Na_2O	6.52	17.6	4.40
K_2O	16.7	<0.05	0.30
H_2O total	16.70	20.12	19.03
total	100.52	100.2	99.4

Table 2
Microwave heating behavior of zeolites and other aluminosilicates

Sample	Time for melting [a] (minutes)
Linde 3A (K-form)	4.79 ± 0.47 [b]
Linde 4A (Na-form)	1.30 ± 0.19
Linde 5A (Ca-form)	no melting
Linde 4A, Cs exchanged [c]	no melting
Linde 13X (Na-form)	1.01 ± 0.40
Linde 13X, K exchanged [c]	2.99 ± 1.89
Linde 13X, Ca exchanged [c]	no melting
Linde 13X, Cs exchanged [c]	1.30 ± 0.86
Ionsiv IE-95 (chabazite + erionite)	1.15 ± 0.32
clinoptilolite, Idaho [d]	1.35 ± 0.20
phillipsite, Nevada [d]	1.34 ± 0.62
erionite, Nevada [d]	2.49 ± 1.44
chabazite, Arizona [d]	no melting
mordenite, Arizona [d]	no melting
analcime, Arizona	no melting [e]
sodalite, Bancroft, Ontario	no melting
pollucite, Canada	no melting
albite, Brazil	no melting
K-feldspar, California	no melting
Na-montmorillonite, Wyoming	no melting
Ca-montmorillonite, Texas	no melting

[a] Melting was indicated by glowing of the sample while heating in the microwave cavity and confirmed by visual, microscopic and X-ray observations of the sample after heating was stopped.
[b] Plus or minus sign denotes standard deviation based on four or more replicas.
[c] Extent of exchange was not determined.
[d] Mixed cation forms as they occur in nature.
[e] Melting occurred in two out of eight samples by treatment after more than five minutes.

sured temperatures presented in fig. 1 are *near* the sample and not from within the sample. Therefore, they are lower than the melting points. However, from the phase diagrams for these systems we note that the melting points (lowest eutectic) range from 1200 to 1500°C. Thus there appear to be clear differences caused by cation content and probably also more importantly their location in the framework topology.

In the typical case we noted that heating started at a "point" (2–3 mm across) within the 1" pellet and spread gradually throughout the pellet.

Commercial Linde 13X (also a Na cation form) heated up very rapidly and started to melt after 1 min. However, as in the 4A case, ion exchange of K^+ into 13X decreased the heat-up rate and ion exchange with Ca^{2+} made it essentially unsusceptible for melting. On the other hand, the Cs form behaved very similarly to the Na^+ form (see table 2 for details). The sodalite sample which consists of sodalite or β-cages just like the Linde A and Linde 13X did not heat up (table 1), and this can be attributed to a lack of large channels in sodalite unlike in the zeolites A and X. The structures of zeolite A and 13X are formed by linking of sodalite cages through double four-membered rings and double six-membered rings respectively, while the sodalite structure is formed by direct face-sharing of four-membered rings in the neighboring sodalite cages [7]. Thus framework topology plays an important role in the direct coupling of microwave energy.

The type 4A and 13X phases were also reacted at 150, 300 and 450 W power levels. These synthetic zeolites which started to melt after a minute at 600 W did not melt by prolonged treatment at 300 W or less. At 450 W, however, these zeolites again melted in a matter of a minute and no difference in heat-up rate could be detected between the 450 and 600 W power levels. Studies are now in progress to determine the effect of power on melting these two zeolites using a 1 kW microwave c en.

Several other synthetic zeolites such as Ionsiv IE-95 and natural zeolites such as clinoptilolite, phillipsite and erionite which have quite different structures and contain mixed cation also heated up rapidly and melted within a matter of minutes (table 2). However, chabazite and mordenite zeolites which are predominantly Ca forms (in nature) did not melt under the present conditions.

Analcime, $NaAlSi_2O_6 \cdot H_2O$, which is one of the least hydrated and least open zeolites did not heat-up rapidly at all. Pollucite, $CsAlSi_2O_6$, which is the anhydrous Cs form of analcime likewise did not heat rapidly or melt (table 2) because the Cs^+ ion in pollucite is almost immobile within the tight mesh of the framework [7]. Albite and K-feldspars which have no channels or cavities and where the Na and K cations are locked-in did not melt (table 2). Clay minerals such as montmorillonites which have no channels or cavities did not melt (table 2) even though these layer silicates exhibit cation exchange behavior. These results lend credence to the hypothesis given above

that the microwave absorption behavior of zeolites is a function of the location as well as the mobility of the cations within the zeolite framework. However, our earlier results show that alumina, silica and aluminosilicate gels which are non-crystalline can also be melted when more thoroughly insulated [5] with zirconia.

4. Discussion

Measurements of the dielectric properties in the high-frequency (>100 MHz) region are really rare [9,10]. Glazun et al. [10], however, showed that in zeolite A with Na^+ ions, one has a loss peaking at about 2.45 GHz (see fig. 5.16 in ref. [8]). Glazun and Zhilenkov attributed this loss to the "rattling" of the Na^+ in the 6-rings of that structure [11]. From our preliminary data several additional considerations may be added. First, the model of the loss mechanism at 2.45 GHz is probably the tail of an ionic motion which peaks in the MHz region. The absence of any substantial absorption in the clays, which have laterally mobile Na^+ suggest that we need a well defined (?) three-dimensional cage. The differences between widely different frameworks appears to be secondary above a certain threshold (i.e. larger than in analcite) but whether 4 Å or 10 Å seems to be secondary. Electrostatic forces holding divalent ions in the cages appear to be sufficient to require energies for relaxation which push the peaks into the shorter-wavelength regions. The fact that Cs^+ heats rapidly in 13X shows that the mass of the ion is not overriding, whereas the steric fit into the 6–12 membered oxygen cage may be (see K^+ in 3A). These empirical studies are being pursued in parallel with the setting up of a 10 MHz–100 GHz spectrometer for absorption spectra measurements.

The novel microwave sintering and melting of zeolites reported here is useful in a wide variety of technologies: the pelletizing of catalysts; the processing of zeolites which have been used in decontamination of wastes; ceramic processing in general by using zeolites as "thermal seeds".

Acknowledgement

This work has been supported by the AFOSR Grant #83-0212.

References

[1] M.M. Krage, Am. Ceram. Soc. Bull. 60 (1981) 1232.
[2] P.A. Haas, Am. Ceram. Soc. Bull. 58 (1979) 873.
[3] L. Quemeneur, J. Choisnet, B. Raveau, J.M. Thiebaut and G. Roussy, J. Am. Ceram. Soc. 66 (1983) 855.
[4] J.F. MacDowell, Am. Ceram. Soc. Bull. 63 (1984) 282.
[5] R. Roy, L.J. Yang and S. Komarneni, Am. Ceram. Soc. Bull. 63 (1984) 459.
[6] P. Barker, J. Ditzenberger and J. Remeika, Phys. Rev. B14 (1976) 4254.
[7] R.M. Barrer, Zeolites and clay minerals as sorbents and molecular sieves (Academic Press, New York, 1978).
[8] D.W. Breck, Zeolite molecular sieves, structure, chemistry and use (Wiley, New York, 1974).
[9] B. Morris, J. Phys. Chem. Solids 30 (1969) 73.
[10] B.A. Glazun, V.M. Federov, M.M. Dubinin and I.V. Zhilenkov, Izv. Akad. Nauk SSSR Ser. Khim. (1966) 393.
[11] B.A. Glazun and I.V. Zhilenkov, Russian J. Phys. Chem. 40 (1966) 734.

Reprint #6

Microstructure and Mechanical Properties of
Synthetic Opal: A Chemically Bonded Ceramic

Microstructure and mechanical properties of synthetic opal: A chemically bonded ceramic

Thomas C. Simonton, Rustum Roy, Sridhar Komarneni,[a] and Else Breval
Materials Research Laboratory, The Pennsylvania State University, University Park, Pennsylvania 16802

(Received 13 November 1985; accepted 17 July 1986)

Among chemically bonded ceramics (i.e., those not utilizing thermally activated diffusion for bonding) the French synthetic opal gilsonite provides an excellent existence theorem. By using optical, scanning, and electron microscopy techniques and x-ray, chemical, and differential thermal analyses, it is shown for the first time that the synthetic opal is composed of two separate phases: noncrystalline silica and crystalline (tetragonal) zirconia balls. The zirconia balls with sizes ranging from 7–50 nm appear to be present in an extraordinary regular "lattice" in the void spaces of the silica "balls" of mean size 200 nm. A comparison of the fracture toughness, K_{IC}, data for the gilsonite and natural opal shows that the former is significantly tougher than the latter. The K_{IC} values for gilsonite fall between those of the Corning 0337 Glass Ceramic and Wesgo Al-500 alumina, showing that surprisingly tough ceramics can be made near room temperature by resorting to chemical bonding.

I. INTRODUCTION

One of us (R. R.) has coined the term Chemically Bonded Ceramics (CBC) to describe polycrystalline inorganic bodies or monoliths that are bonded or held together without the use of thermally activated solid-state diffusion. Ordinary concrete or cement paste is the prototypical CBC, and dental cements and phosphate-bonded refractories are other examples. The importance of CBC as a class of materials of commendable significance in the future has been pointed out by Birchall and Kelly.[1] The energy content for manufacture of equivalent volumes of CBC is roughly one-third of that for typical polymers and one-tenth or less of metals like steel and aluminum. That the hope for making novel, high-performance ceramics, via processing innovations, is real has been shown by the Imperial Chemical Industries (ICI) development of macro-defect-free (MDF) cements (see Birchall[2]), which when reinforced with nylon fibers develops toughnesses near that of alumina.

Nature also provides us with many examples of *ceramics* made at low temperatures—indeed, most sedimentary rocks constitute a fine set of such CBC. In such cases the bonding between preexisting particles is not achieved by thermally activated diffusion at high temperatures, but rather by low-temperature chemical reactions of various kinds. Among the sedimentary rocks and minerals, the high silica solution sol-derived phases such as opal, chalcedony, jasper, agate, etc., are obvious models of CBC. The argument that nature required millions of years to make CBC and that time is of the essence in making such materials was effectively destroyed by the preparation of "synthetic opal" by P. Gilson. This material, which is available commercially now from Nakazumi Chemicals,[3] therefore presented itself as an excellent example of what has been achieved in respect to mechanical properties and how the microstructure is related to these properties.

II. EXPERIMENTAL PROCEDURE

A. Materials

Three varieties of Gilson synthetic opal (designated hereafter as gilsonite) and a natural white opal-A from Australia (courtesy of D. K. Smith) were investigated. The gilsonites were purchased from Kashan, Inc., P. O. Box 3318, Austin, Texas; although, they are now manufactured exclusively by Nakazumi Crystal Laboratory, 3-1-304 Sugahara-cho, Ikeda-shi, Osaka-fu 563, Japan. The gilsonite varieties, milky white, crystal, and black, were named for the body color displayed, and each variety exhibited intense "fire" that extended throughout the entire sample. The colors observed ranged from red to violet hues, and the overall appearance of the gilsonite was similar to natural precious opal except the fire was more intense and continuous throughout the sample. The natural white opal-A exhibited very little fire, but was uniform and free from macroscopic flaws.

B. Characterization

The x-ray diffraction (XRD) analysis was carried out on powdered samples as well as on some bulk pieces to determine the crystalline phases present. A Philips Norelco diffractometer with Ni-filtered Cu$K\alpha$ radiation, which was operated at 1°2θ per minute with 1° entrance and ev · slits, was used.

An ISI D 130 scanning electron microscope (SEM) and Philips 420 transmission electron microscope (TEM), each with an x-ray spectrometer, were

[a] Also affiliated with the Department of Agronomy.

 0003-6951/86/050667-08$01.75

used for microstructure characterization and major element identification. Polished samples for SEM microstructure characterization were etched in 10% HF for 15 or 30 s and then Au coated. Polished samples for SEM elemental identification were unetched and C coated. The TEM samples were untreated powders.

Differential thermal analysis (DTA) curves were obtained using a DuPont 900 thermal analyzer. The sample was heated in air from room temperature to 1400 °C at a rate of 10 °C/min using a Pt vs Pt–13% Rh thermocouple. In addition, thermal stability was studied by heating bulk samples for 4 h at temperatures ranging from 240°–900 °C. The furnace temperature was increased 50 °C/h from room temperature to the desired temperature, and the sample was allowed to slowly cool in the furnace when heating was finished.

Vickers hardness, H_V, and fracture toughness, K_{IC}, were determined by microindentation. Indents were made by applying a load of 19.6 N to a flat, polished sample for 10 s. Data for each sample were collected from 8–10 indents and averaged, and K_{IC} was calculated using the equation reported by Lawn and Fuller,[4] which is strictly valid for conical indentors. However, reasonable data can be obtained for lower toughness materials with a Vickers indentor if the half-angle between indentor faces is taken to be 68°.[5]

Additional characterization included chemical analysis, density determination, and optical photography. Direct current arc emission spectrography was employed to determine the major, minor, and trace elements present, and quantitative analysis was performed using a dc plasma spectrophotometer (DCP). Carbon content was estimated by CO_2 coulometry where the sample was heated to ~1000 °C in a Pt crucible. More reliable values were obtained using a Carlo ERBA model 1106 elemental analyzer where the sample was combusted in a tin capsule at 1500°–1600 °C in a flow of O_2 and He. Density measurements were performed on bulk samples based on the Archimedes principle using the equation reported by Mason and Berry.[6] Photographs were taken using a Nikon SMZ-10 stereoscopic microscope of water-immersed samples to illustrate macroscopically observable features of the gilsonite.

III. RESULTS

A. Optical microscopy

Figures 1(a) and 1(b) are photographs taken at low magnifications showing the macroscopically observable features of the gilsonite. Figure 1(a) is a typical view of the top surface (that surface where the grain pattern resembles that of natural precious opal and which is perpendicular to the columnar structure) and Fig. 1(b) is a view of the surface perpendicular to the top.

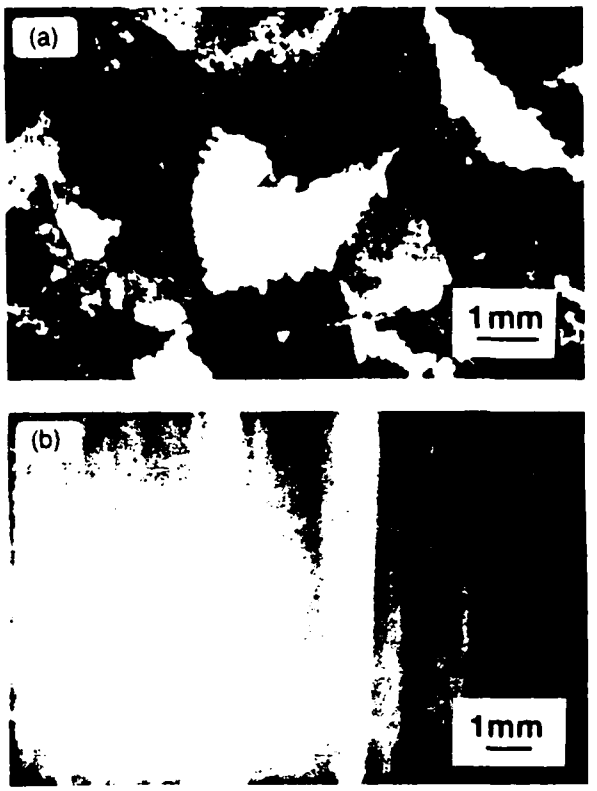

FIG. 1. Optical photographs of gilsonite: (a) top surface showing jagged grain contacts; (b) view of the surface perpendicular to the top showing columnar structure.

One of the characteristics of the gilsonite was the jagged grain contacts that were observed on the top surface in each variety, particularly the black. In some cases the grain contacts resembled the teeth on a saw blade [Fig. 1(a)]. The grains were irregularly shaped but generally tended to be equant rather than greatly distorted in any one direction. The size of grains for the black and crystal varieties was roughly 1–2 mm across, and for the milky white the size was generally < 1 mm. The grain size at the top surface for a given sample was observed to vary with the thickness of the sample.

Another interesting feature of the gilsonite is the marked columnar structure [Fig. 1(b)] that was best seen in the milky white variety. The columns were not physically separable, but a given column diffracted light of the same color over its entire length, making it easy to observe individual columns.

B. Powder x-ray diffraction

The diffraction patterns of all the synthetic opals provided the first unexpected result in that the material was clearly diphasic. There was a large diffuse band centered around 21.4°2θ corresponding to a d value of ~4.1 Å indicating *very* poorly crystalline cristobalite or

noncrystalline SiO_2. The diffuse band was also seen in all XRD patterns of opal-A and is indicative of this near amorphous variety of naturally occurring opal.[7] The second phase proved to be well-crystallized tetragonal zirconia.

Powdered gilsonite samples examined by XRD after heating to 1400 °C during DTA runs exhibited crystallization of the disordered SiO_2 to low cristobalite with some minor evidence of tridymitic stacking. The tetragonal zirconia phase reflections remained unchanged within the limits of experimental error upon heating to 1400 °C, and no $ZrSiO_4$ could be detected.

C. Chemical analysis

Emission spectrographic analysis of gilsonite powders showed only the presence of Si and Zr at levels in appreciable quantities. Quantitative DCP results for SiO_2 and ZrO_2 are summarized in Table I and show the gilsonite to be dominantly SiO_2 with 3.3%–5.4% ZrO_2 by weight. Finely divided graphite was thought to be a possible additive for controlling body color of the black gilsonite and, therefore, C analysis was performed. The C-analysis results (Table I) indicate that small amounts of carbon, 0.15%, were contained in the milky and black varieties in a form that was released very slowly even at high temperatures. It is doubtful that such a small amount of carbon could adequately color the black gilsonite. Moreover, the milky variety released an amount of carbon equal to the black gilsonite. The carbon released is more likely due to organic residues trapped in the sample during preparation (assuming an alkoxide

TABLE I. Chemical analysis of gilsonite samples.

Gilsonite	SiO_2%	ZrO_2%	C[a] %	C[b] %
Crystal	95.8	3.27	0.015	0.02
Milky	93.5	5.25	...	0.15
Black	93.8	5.43	0.031	0.15

[a] Determined coulometrically at 1000 °C.
[b] Determined by combustion at 1500°–1600 °C.

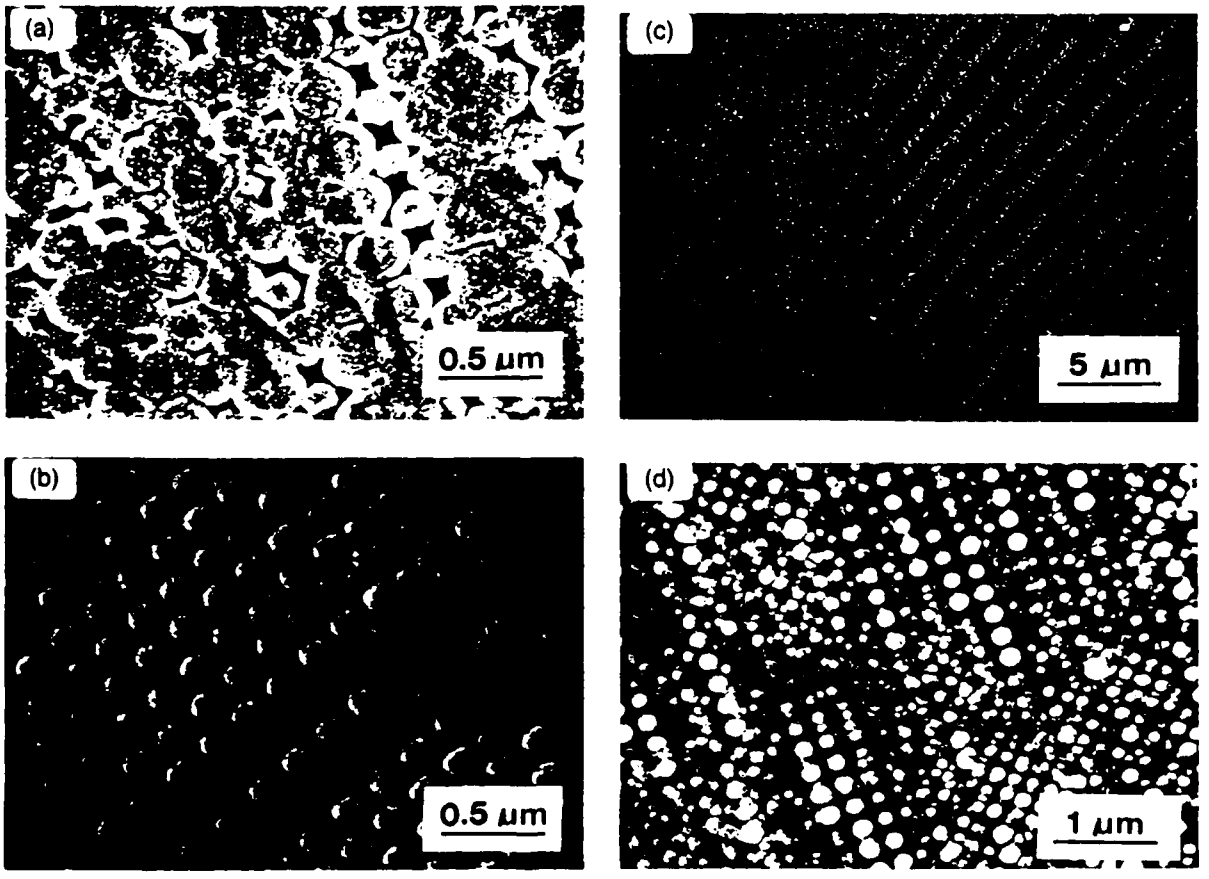

FIG. 2. Scanning electron micrographs of natural and synthetic opals: (a) microstructure of white opal from Australia; (b) microstructure of gilsonite shows striking similarity to natural opal; (c) same as (b) but taken at lower magnification showing two regions with different packing orientations; (d) microstructure of gilsonite parallel to the columnar structure [see Fig. 1(b)].

route for the preparation of the silica balls), organics absorbed during the cutting and polishing of the samples, residual binder, or dispersant.

D. Scanning electron microscopy

Micrographs of polished and etched natural opal and gilsonite samples are presented in Fig. 2. Figure 2(a) depicts the microstructure of an area of the natural white opal that shows weak fire. The color play is produced by diffraction of light from an orderly packing of uniformly sized silica balls and associated voids or low-density regions.[8] The balls shown in Fig. 2(a) averaged between 300–350 nm in diameter and exhibit in the SEM a fine structure suggesting that the larger particles were agglomerates of smaller ones, perhaps 30 nm across. Corresponding micrographs of the gilsonite, Fig. 2(b), shows a striking similarity to its natural counterpart, except that no void areas were observed in the gilsonite. The silica balls of the gilsonite were approximately 200 nm in diameter and formed a hexagonal-close-packed layer analogous to a {111} plane in a fcc crystal structure. Figure 2(c) was taken at a lower magnification showing two regions in which the packing orientation was markedly different. The fcc packing observed in the gilsonite was not unusual. Sanders[9] reported work on light diffraction by natural opal-A and observed that domains of orderly packing were commonly fcc with only occasional hcp sequences.

Figure 2(d) is a micrograph of a sample cut parallel to the macroscopically observable columnar structure [or perpendicular to the surface of Figs. 2(a)–2(c)]. The lineations observed in Fig. 2(d) trend in the same direction as the columnar structure. The packing of the balls observed here was not hexagonal as seen before in Fig. 2(b), but tended to be a square packing, which corresponds to a {100} plane in a fcc structure. The x-ray mapping shows a homogeneous Zr distribution in the gilsonite and no Zr in the natural opal-A.

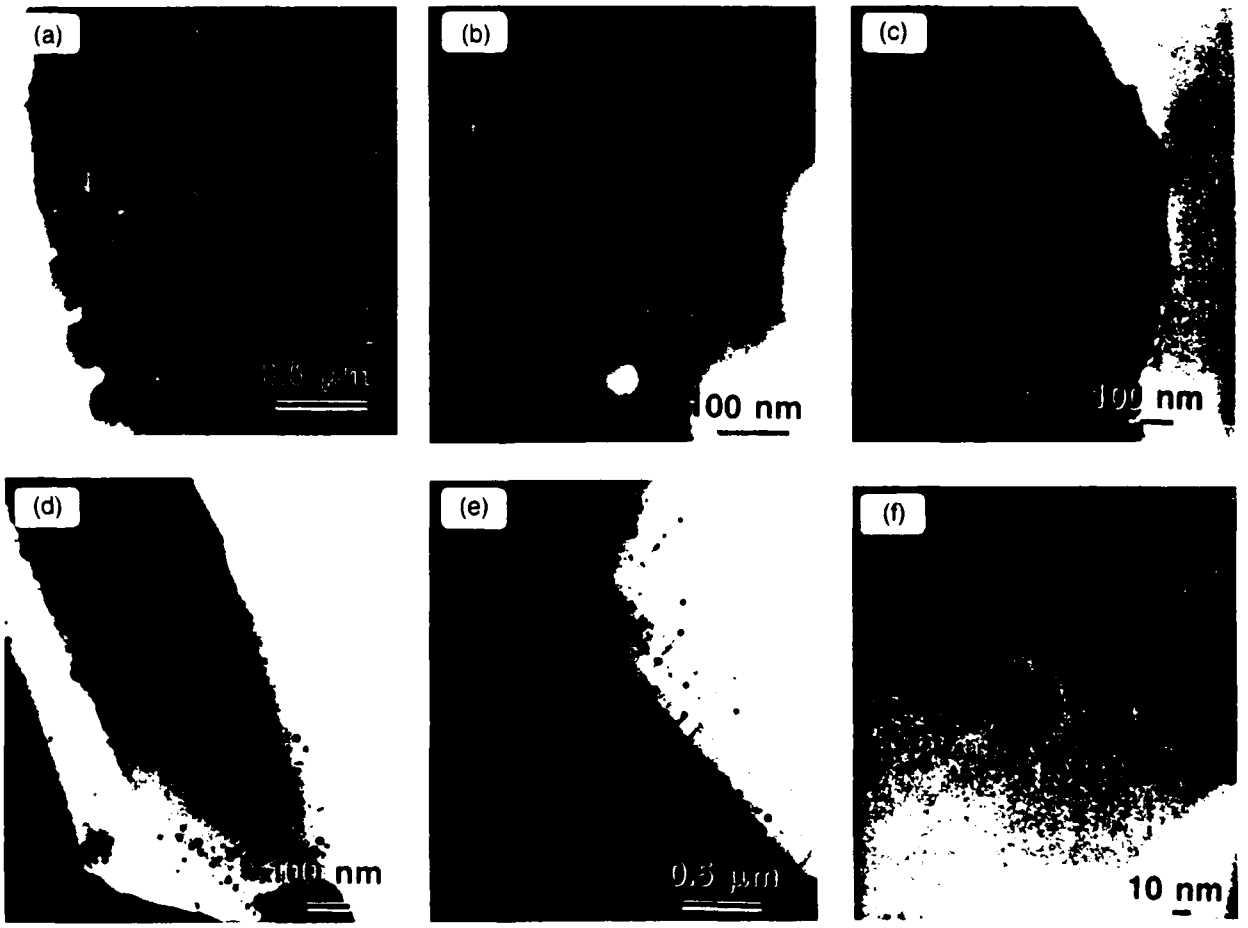

FIG. 3. Transmission electron micrographs of natural and synthetic opals. (a) and (b) microstructure of white opal from Australia at two magnifications showing silica balls and void spaces. (c)–(f) microstructure of gilsonite showing different arrays of ZrO_2 balls from 7–50 nm.

E. Transmission electron microscopy

Figure 3 shows the micrographs of untreated natural opal and gilsonite. The natural opal [Figs. 3(a) and 3(b)] shows outlines of balls averaging 300–350 nm in diameter, and associated interstitial voids, just as in the SEM micrographs [Fig. 2(a)]. No fine structure within the balls could be observed in the TEM except for triangularly arranged ovals clearly seen on several of the balls. Sanders and Darragh[10] also observed similar features on natural opals they investigated and concluded that these features were contact points between successive layers of balls. The SEM and TEM investigations both revealed the same features of the gross morphology except for the fine structure of the 300–350 nm silica balls, which was observed only in the SEM.

Unlike the natural opal, the gilsonite TEM results [Figs. 3(c)–3(f)] revealed the presence of separate crystalline ZrO_2 balls that were nearly spherical and ranged in diameter from 7–50 nm. Some fine structure was observed within a few of the ZrO_2 balls, but most appeared homogeneous throughout. A few balls showed a core or even concentric banding, but this was probably produced by the superposition of balls from two or more layers. Last, some ZrO_2 balls showed banding [Fig. 3(f)], which may have been the result of twinning. The striking feature of the microstructure was the relative arrangements of the 200 nm NCS-SiO_2 balls and the 7–50 nm ZrO_2 balls.

The ZrO_2 balls were arranged in basically two types of patterns: hexagonal rings and nearly square grids. The hexagonal rings averaged between 210 and 230 nm in diameter and formed a hcp array [Fig. 3(C)]. The grids were of two spacings, the larger was approximately 220–230 nm apart and the smaller on the order of 110 nm. The smaller grids were thought to be due to the superposition of two layers of the larger grids shifted with respect to each other by $\frac{1}{2}$ the grid spacing. Moreover, overlapping of the hexagonal rings was observed and was clearly the result of the superposition of two or more layers of silica and zirconia balls.

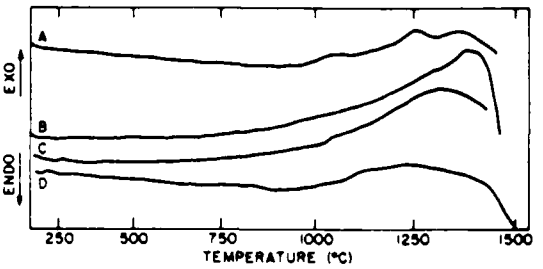

FIG. 4. Differential thermal analysis curves for natural and synthetic opals. A white opal, Australia, B crystal white gilsonite, C black gilsonite, D milky gilsonite.

Microdiffraction patterns of gilsonite taken on the TEM showed that the matrix SiO_2 was noncrystalline on the 2–3 nm scale and that the ZrO_2 balls were very well crystallized. The XRD data had clearly shown the ZrO_2 phase to be mainly tetragonal, but in the TEM layer spacings greater than 3 Å were observed indicating that some monoclinic phase was probably also present. Elemental analysis in the TEM showed that the Zr in the gilsonite samples was confined to the dark balls and the matrix contained only Si. No reaction rims of $ZrSiO_4$ composition or structure could be found.

F. Differential thermal analysis

The similarity of the effect of heating upon the gilsonite and natural white opal are illustrated by the DTA curves of Fig. 4. The prominent feature for each was the broad exotherm that reached a maximum between 1220° and 1370 °C. The maxima appear approximately at 1370°, 1310°, and 1220 °C for the crystal, black, and milky gilsonite, respectively. The natural opal exhibited two maxima at 1250° and 1350 °C, which was the approximate range of maxima observed for the synthetic opals. Jones and Segnit[7] reported data on DTA runs for natural opal-A and observed one strong exotherm at

TABLE II. Mechanical property data for opal and other selected materials.

Sample	ρ (g/cm^3)	H_v (GPa)	K_{IC} (MPa$\sqrt{m}$)	K_{IC}^a (MPa$\sqrt{m}$)
Natural white opal	2.143	4.13	0.81	...
Crystal gilsonite	2.264	5.05	3.00	2.58
Milky gilsonite	2.292	5.33	2.55	2.18
Black gilsonite	2.281	5.48	2.68	2.24
Fused silica	2.198	5.20	2.47	2.13
Corning 0337 glass ceramic[b]	...	12.7	1.6	...
Wesgo Al-500[b]	...	14.2	3.5	...

[a] Niihara *et al.*[11]
[b] Marion.[4]

approximately 1350 °C, which they attributed to the rapid crystallization of the disordered SiO_2 to cristobalite. The variability of the position and sharpness of the exothermic effect of cristobalite crystallization for such disordered samples, both natural and synthetic, was not considered unusual. All of the high-temperature exothermic effects reported here were likely due to cristobalite crystallization over a range of temperatures. Powder XRD data confirmed that well-crystallized cristobalite had formed after the exotherm in the DTA runs.

G. Mechanical properties

Vickers hardness (H_v), fracture toughness (K_{IC}), and density (ρ) data obtained from study samples and for other selected materials are summarized in Table II. A comparison of the data for the natural opal and gilsonite highlights the significantly larger K_{IC} values obtained for the gilsonite. These values may be compared with those reported for a typical Corning 0337 glass ceramic and Wesgo's commercial Al-500 alumina and show that the gilsonite is a reasonably tough ceramic. The differences in hardness for the opals was less pronounced with the synthetic phase harder than the natural opal. The densities were similar except for the slight increase in the gilsonite due to the presence of small quantities of zirconia.

Another interesting feature of the data was the strong similarity between the gilsonite and fused silica. The similarity was not only reflected in the numbers obtained, but also in the nature of the indent and associated cracks. Instead of forming well-defined indents and well-developed cracks as the natural opal did, the gilsonite and fused silica formed indents that had a tendency to fracture conchoidally, and the associated cracks were shorter ($c/a \sim 1.5$). Corrections were made for the low crack-to-indent ratio using the empirical formula reported by Niihara and colleagues.[11] The corrections lowered the observed K_{IC} values by approximately 15%, indicating that even with poor crack development the uncorrected estimates of K_{IC} reflect the true fracture toughness of the gilsonite and fused silica.

H. Thermal stability

Vickers hardness and fracture toughness data for the milky gilsonite and natural white opal heated to 900 °C are summarized in Table III. These data clearly show a striking difference in the change of hardness and fracture toughness with heating between the gilsonite and opal. The hardness of the gilsonite decreased only ~3% after heating to 900 °C, while the natural opal hardness decreased ~41%. The fracture toughness of the gilsonite decreased only ~7% after heating to 900 °C, but by comparison, the natural opal exhibited a 16% decrease in K_{IC} after heating to only 240 °C and was macroscopically fractured throughout the body of the sample. After heating to 400 °C, small chips spalled off the natural opal leaving very lustrous fracture surfaces, and crazing was so pronounced that indent cracks could not be distinguished from ones produced by heating. In sharp contrast to the natural opal, the gilsonite developed no fractures of any kind, either macro- or microscopic, and the appearance was unchanged by heating to 900 °C with no loss of fire. The XRD traces revealed no changes in the number, shape, or relative intensities of the reflections for either the gilsonite or natural opal with heating to 900 °C.

TABLE III H_v and K_{IC} for heat-treated samples

	Natural white opal		Milky gilsonite	
T (°C)	H_v (GPa)	K_{IC} (MPa$\sqrt{m}$)	H_v (GPa)	K_{IC} (MPa$\sqrt{m}$)
22	3.95	0.98	5.30	2.55
240	3.66	0.68	5.32	2.46
400	3.40	crazed	4.91	2.41
590	3.36	crazed	5.55	2.38
900	2.90	crazed	5.17	2.40

IV. DISCUSSION

A. Preparation of gilsonite

Virtually nothing has been reported in the open literature about the preparation of gilsonite except a general speculation proposed by Nassau[12]. The authors have the latest descriptive literature from the Nakazumi Company and no data are provided. Nassau proposed three basic steps: the production of uniform silica balls, probably from alkoxide hydrolysis; gravitational settling of the coloidal particles in the sol; and production of a monolith, possibly involving heating, deposition of silica in voids, and hydrostatic pressing. The present studies showing the presence of zirconia balls along with silica balls clearly indicate that Nassau's speculation omits a significant factor.

B. Role of ZrO_2

The intended purpose of the ZrO_2 in gilsonite is not clear, but two possibilities are considered here. The first possible role of the ZrO_2 may have been to improve the packing density of the monolith, and thereby enhance the optical and mechanical properties. Iler[13] reported that a hard film of silica composed of uniformly sized particles was difficult to prepare because the film cracked upon drying. He observed that by the addition of finer particles a hard and uniform film could be prepared without cracking. The packing density increased

TABLE IV. Theoretical porosities for the black gilsonite system.

vol % of 250 nm spheres	vol % of 50 nm spheres	vol % of 10 nm spheres	vol % of porosity
97.7	2.3	0.0	24.2
97.7	0.0	2.3	24.2
97.7	1.15	1.15	22.9
vol % of 200 nm spheres			
97.7	2.3	0.0	24.2
97.7	0.0	2.3	24.2
97.7	1.15	1.15	24.5

from 70% to approximately 80% with the addition of finer particles. The explanation was that the finer particles filled void spaces between larger particles so that there would be less void space to be compressed upon drying and, therefore, less shrinkage and cracking.

The packing of differently sized spheres has been considered theoretically,[14–16] and a program based on the equations reported by Ouchlyama and Tanaka[16] has been written by M. Silsbee of our laboratory for application to cement systems. The program was used to calculate the minimum porosity for gilsonite assuming a ternary system of close-packed spheres 200, 50, and 10 nm and 250, 50, and 10 nm in diameter. For the 200 nm system the minimum porosity was 9.9% by volume for a combination of 80% (200 nm) and 20% (10 nm) spheres by volume. A minimum porosity of 8.4% was obtained for the 250 nm system containing 80 % (250 nm), 10% (50 nm), and 10% (10 nm) spheres. Porosities of 8.4% and 9.9% represent significant reductions over a system of monosized particles where the porosity would be 25.9%. A rough estimate for the black gilsonite of the volume percent of all sizes of ZrO_2 balls was estimated using the results from the chemical analysis. The densities of the SiO_2 and ZrO_2 balls were assumed to be 2.1 and 5.1 g/cm^3, respectively.[17,18] The vol % SiO_2 was calculated to be 97.7 and for ZrO_2 was 2.3. The volume fraction of ZrO_2 calculated was much less than was required to obtain the minimum porosity as calculated above. Table IV lists calculated porosities for selected volume percent combinations of SiO_2 and ZrO_2 present in black gilsonite. The calculated porosities range from 22.9%–24.5% and represent only a minor porosity decrease over a monosized system. It was clear from the calculations performed that the ZrO_2 played at best a minor role in enhancing the mechanical properties of the gilsonite from a packing viewpoint.

Another possible role of the ZrO_2 in gilsonite was to improve the optical properties of the monolith. Studies by Sanders[8] and Sanders and Darragh[10] revealed that the diffraction of light by natural precious opal was caused by a change in the refractive index between the SiO_2 balls and their corresponding interstitial void regions when a regular packing of uniformly sized balls was achieved. It is essential to their model that a refractive index difference exist between the balls and voids. If there were no refractive index differences, the necessary light scattering could not take place. In natural precious opal the interstices formed by the close packing of SiO_2 balls were either true void spaces or low-density regions of silica where the refractive index difference was sufficient to cause light scattering. It is proposed for the gilsonite that the ZrO_2 balls, which were located in the tetrahedral interstices formed by the SiO_2 balls (as well as around them), provide the required refractive index difference for scattering of light. The TEM micrographs of natural white opal clearly showed regular interstitial void or low-density regions [Figs. 3(a), 3(b)], but none of the TEM micrographs of the gilsonite obtained in the study showed any clear indication of void space. The lack of void space in gilsonite suggests that the diffraction of light is caused by the average refractive index discontinuities caused by regular "layers" of ZrO_2.

C. Ring and grid formation

One of the most striking findings in this study was the extraordinarily regular arrangements of the ZrO_2 balls. A simple explanation for the development of such uniform structures of hexagonal rings and square grids is proposed based on the idea that the SiO_2 balls act as a

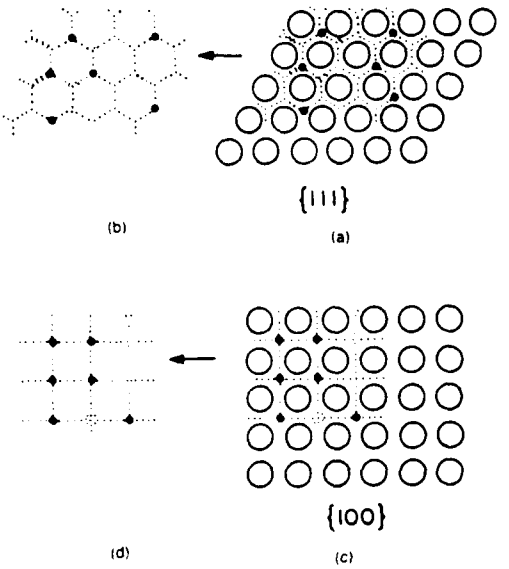

FIG. 5. Schematic drawings for ring and grid formation of spheres (a) and (b) fcc arrangement for {111} plane; (c) and (d) fcc arrangement {100} plane

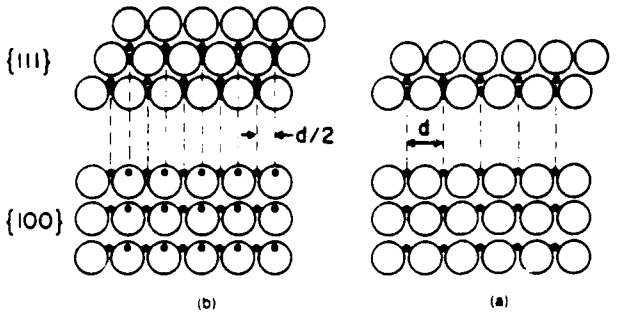

FIG. 6 Schematic drawings for ring and grid formation: (a) depiction for a thin particle with only one row of ZrO_2 spheres showing larger spacing; (b) depiction for a thicker particle with several rows of ZrO_2 spheres showing smaller grid spacing.

controlling superstructure. It was clear from the SEM micrographs of this study and from work on natural opal by previous investigators[8–10,19] that the SiO_2 balls exhibited a strong tendency to arrange themselves in a close-packed array. For the samples examined in this study a fcc structure was observed for the SiO_2 balls. Figures 5(a) and 5(c) represent a fcc arrangement of balls for {111} and {100} planes, respectively, produced by gravitational settling. Calculations showed that the interstices formed from 200 nm balls would have a diameter of 31 nm and that SiO_2 balls 323 nm in diameter would produce interstices of 50 nm in diameter. Therefore, the largest ZrO_2 balls could be accommodated only in the interstices, but the smaller ZrO_2 balls could fit around the SiO_2 balls as well. Figures 5(b) and 5(d) illustrate the arrangements of ZrO_2 balls obtained for the fcc {111} and {100} planes by simply drawing in ZrO_2 balls where they would best fit into the SiO_2 close-packed layer. The formation of complex patterns of hexagonal rings and grids is readily explained by the proposed model.

The grids observed produced two distinct spacings. One was approximately the diameter of the SiO_2 balls and the other was approximately one-half the SiO_2 ball diameter. The two spacings can be explained by Fig. 6, which illustrates the relationship between the {111} and {100} planes of a fcc arrangement of SiO_2 balls. The top view is the close-packed layer and the bottom diagram is a view perpendicular to it. If the top view were filled in with ZrO_2 balls the hexagonal ring pattern would develop as seen in Fig. 5(b), and the bottom view if filled in with ZrO_2 balls would produce the grid pattern of Fig. 5(d). The only difference between the rings and grids is the viewing orientation; no physical movement of the ZrO_2 balls is required. The two-layer spacings observed were simply a function of the number of rows of ZrO_2 balls in the particle. A thin particle with only one row of ZrO_2 balls [Fig. 6(a)] would show the larger spacing when viewed with the TEM. A thicker particle with more than one row of ZrO_2 balls would produce the smaller grid spacing [Fig. 6(b)].

The actual laying down of this intricate pattern of small ZrO_2 balls in the larger SiO_2 ball matrix is not understood, since one can only speculate whether the effect was achieved by the heterocoagulation of a diphasic sol or by the infiltration of a preexisting silicate sol. The regularity would seem to suggest a colloidal charge effect causing both the ordering of the ZrO_2 balls and their codeposition with the silica.

ACKNOWLEDGMENTS

The senior author gratefully acknowledges extensive discussions with Dr. B. E. Scheetz, Dr. D. K. Smith, and M. Silsbee. This research was supported by the Chemical and Atmospheric Sciences Program, U. S. Air Force Office of Scientific Research, under Contract No. F49620-85-C-0069.

REFERENCES

[1] J. D. Birchall and A. Kelly, Sci. Am. **249**(5), 104 (1983).
[2] J. D. Birchall, Philos. Trans. R. Soc. Lond. Ser. A **310**, 31 (1983).
[3] Y. Nakazumi, in the 27th Symposium on Synthetic Minerals, 1982, Paper No. S-2.
[4] B. R. Lawn and E. R. Fuller, J. Mater. Sci. **10**, 2016 (1975).
[5] R. H. Marion, in *Fracture Mechanics Applied to Brittle Materials, ASTM STP* 678, Edited by S. W. Freiman (American Society for Testing and Materials, Philadelphia, PA, 1979), pp 103–111.
[6] B. Mason and L. G. Berry, *Elements of Minerology* (Freeman, San Francisco, 1968), Chap. 4, p. 102.
[7] J. B. Jones and E. R. Segnit, J. Geol. Soc. Aust. **18**, 57 (1971).
[8] J. V. Sanders, Nature **204**, 1151 (1964).
[9] J. V. Sanders, Acta Crystallogr. A **24**, 427 (1968).
[10] J. V. Sanders and P. J. Darragh, Mineral Rec. **2**, 261 (1971).
[11] K. Niihara, R. Morena, and D. P. H. Hasselman, J. Mater. Sci. Lett. **1**, 13 (1982).
[12] K. Nassau, *Gems Made by Man* (Chilton, Radnor, PA, 1980), pp. 257–267.
[13] R. K. Iler, *The Chemistry of Silica: Solubility, Polymerization, Colloid and Surface Properties, and Biochemistry* (Wiley, New York, 1979), pp. 370–372, 671–676.
[14] A. R. Dexter and D. W. Tanner, Nature (London) Phys. Sci. **230**, 177 (1971).
[15] J. D. Dewar, *Computerized Simulation of Aggregate, Mortar and Concrete Mixtures*, British Ready Mixed Concrete Association, United Kingdom, 1983 (unpublished).
[16] N. Ouchlyama and T. Tanaka, Ind. Eng. Chem. Fundam. **23**, 490 (1984).
[17] B. Fegley and E. A. Barringer, Mater. Res. Soc. Proc. **32**, 187 (1984).
[18] B. Fegley, P. White, and K. Bowen, Ceram. Bull. **64**, 1115 (1985).
[19] E. A. Monroe, D. B. Sass, and S. H. Cole, Acta Crystallogr. A **25**, 578 (1969).

Manuscript #2

Natural Gel-Derived Ceramics: Mechanical Properties of Opal, Chert, Agate, Etc.

NATURAL GEL-DERIVED CERAMICS: MECHANICAL PROPERTIES OF OPAL, CHERT, AGATE, ETC.

T.C. Simonton, Rustum Roy, and S. Komarneni
Materials Research Laboratory, The Pennsylvania State University
University Park, PA 16802

Introduction

Nature has provided us with some of the best low-temperature ceramics such as opals, cherts, agates, etc., all derived from gels. Our intent in this area is to undertand the natural process and mimic it in the laboratory. The microstructure and mechanical properties of the above natural gel-derived ceramics have been studied to understand the mechanism of their formation. The microstructural characterization of the natural gel-derived ceramics has been reported earlier and the mechanical properties of these materials is reported here.

Materials

Samples were selected from five types of naturally occurring low-temperature-forming varieties of SiO_2. The materials were obtained in bulk when possible, but many samples were only available in lesser quantities. The locality, quantity available (B=bulk, L=limited), and a description is given below for each group.

Opals

Three types of opals were selected for study. Two were naturally occurring varieties of Opal-A and Opal-CT and the other was Gilson synthetic opal. Only one sample of Opal-A was available in quantity. Table 1 gives details.

Jasper

Jaspers are fine-grained silicates that characteristically contain significant amounts of iron as an impurity as well as other impurities. They are typically shades of brown and dark reds (Dana, 1962). Table 2 contains information for the jaspers used in the study.

Table 1. Selected Opal Types.

#	Sample	Quantity	Locality	Comments
1	Opal-A	B	Australia	white
2	Opal-A (1)	L	Andamooka, S. Aust.	white, some fire
3	Opal-A	L	Australia	white
4	Opal-CT (1)	L	Salt Creek, NSW	yellow-brown concretion
5	Opal-CT (1)	L	Lake Eyre, S. Aust.	porous, bulk wood replacement
6	Opal-CT (1)	L	Sunbury Victoria	yellow-brown
7	Opal-CT	L	Unknown	wood replacement retaining cellular structure
8	Gilson	L	Synthetic	milky white variety
9	Gilson	L	Synthetic	crystal white variety
10	Gilson	L	Synthetic	black variety

Table 2. Selected Jaspers.

#	Sample	Quantity	Locality	Comments
11	Bald Eagle	B	State College, PA	yellow
12	Bald Eagle	L	State College, PA	red
13	Omyhee	B		tan and light brown
14	Vera Cruiz	B	Vera Cruiz	dark brown
15	Green	B		dark green

Table 3. Selected Agates.

#	Sample	Quantity	Locality	Comments
16	Bloodstone	B		green with red spots
17	Brazil	B	Brazil	banded, light blues
18	Fire	B		poor fire
19	Montana	B	Montana	translucent, white
20	Moss	B		clear with green dendrites
21	Petrified Wood	B	Arizona	red, yellow, purple
22	Botswana	B		banded, dark
23	Blackskin	B		transparent

Table 4. Selected Flints.

#	Sample	Quantity	Locality	Comments
24	Black	B	Oak Hall, PA	black and uniform
25	England	B	England	gray, contains carbonate

Table 5. Cherts Selected for Study.

#	Sample	Quantity	Locality	Comments
26	Burlington	B	Burlington, IL	cream color
27	Oolitic	B	State College, PA	gray, well silicified
28	novaculite	B	Arkansas	white

Agate

Agates are pure forms of fine-grained chalcedony (a fibrous variety of quartz) that commonly exhibit banding, pleasing coloration, and translucency. Table 3 gives information for the agates used.

Flint

Dana (1962) defines flint as a term used to describe siliceous nodules found in chalk and limestone. Flint is fine-grained and it typically shades of gray, brown, and black. Table 4 lists those flints used in the study.

Chert

Chert is very similar to flint but there is no snarp mineralogical distinction between them. However, cherts tend to be lighter in color than flints (Dana, 1962). Table 5 lists the cherts studied. It should be noted that novaculite may be considered a slightly metamorphosed chert.

Methods

Static Bend Test

Samples 1 1/2 x 1/2 x 1/5 inches were cut to have a rectangular cross section and finished with 600 alumina powder. A strain gauge was glued to the center of the sample bottom. The sample was loaded using a three-point arrangement and the strain gauge was attached to a meter. At intervals of approximately 2 1/2, 5, 7 1/2, and 10 Kg the exact load was recorded and the corresponding strain was read from the strain gauge meter. Therefore, four measurements of Young's modulus, E, per sample were obtained.

Young's modulus was calculated using the following equations:

1. $E = m/\varepsilon\ [(h/2)/I]$
2. $M = P\ell/4$
3. $I = (1/12)bh^3$

m = bending moment
I = area moment of inertia
ε = strain
h = thickness (m)
P = load (Kg)
ℓ = length (m)
b = width (m).

The final result is given in giga Pascals (GPa) and is the average of

four measurements.

Vickers Hardness and Fracture Toughness

The samples were prepared to have parallel top and bottom surfaces with the top surface polished. Five to eight indents were made per sample at a load of 2 Kg for a loadtime of 10s. The size of the indent and the length of the radiating cracks were measured for each indent and then averaged for the entire sample. Vickers hardness, VH, and the fracture toughness, K_c, were then calculated from the data using the following formulae:

1. $VH(GN/m^2) = 1.8544Pg/D^2 10^9$

   P = load (Kg)
   D = length of indent diagonal (m)
   $g = 9.81\ m/s^2$

2. $K_c(MN/m^{3/2}) = Pg/\pi^{3/2}\tan\ a^{3/2}10^6$

   P = load (Kg)
   $g = 9.81\ m/s^2$
   $= 68°$
   a = crack length (m)

Density

Sample density was determined by finding the ratio or the weight in air and weight in water as given below. To enhance penetration of water into the sample a few drops of soap solution were added to 1 pint of deionized water as a lubricant. Also, the samples were evacuated while in the soap solution to remove any remaining gases.

1. $\rho = (Wa/Wa-Ww)\rho$

   Wa = weight in air
   Ww = weight in water
   ρw = density of water

Mechanical Properties and Density

Table 6 lists he Vickers hardness, fracture toughness, Young's modulus, and the density of the samples. The samples for which Young's modulus was determined are those from which uniform bars of sufficient size could be cut.

Table 6. Mechanical Properties and Density Results.

#	Sample	Vickers Hardness (GN/m^2)	Fracture Toughness ($MN/m^{3/2}$)	Young's Modulus (GPa)	Density (gm/cm^3)
1	Opal-A	4.1	0.81	59.6±0.02	2.143
2	Opal-A	3.6	0.74	—	2.127
3	Opal-A	3.9	0.76	—	2.128
4	Opal-CT	2.8	0.90	—	2.124
5	Opal-CT	2.5	1.1*	—	2.204
6	Opal-CT	1.4	0.66	—	2.089
7	Opal-CT	2.3	0.84	39.4±0.1	2.202
8	Gilson	5.2	2.5*	—	2.292
9	Gilson	5.1	3.0*	—	2.264
10	Gilson	5.5	2.7*	—	2.281
11	Bald Eagle Jasper	5.4	2.0	—	2.707
12	Bald Eagle Jasper	6.2	2.0	—	2.653
13	Owyhee Jasper	6.0	1.8	80.0±0.8	2.598
14	Vera Cruiz Jasper	6.6	1.6	—	2.626
15	Green Jasper	7.5	1.7	104±5	2.681
16	Bloodstone Agate	8.3	1.8	86.9±3.1	2.619
17	Brazil Agate	7.9	2.1	⊥ 75.2±2.0	2.622
				∥ 81.6±1.0	
18	Fire Agate	8.4	1.7	142±7	2.629
19	Montana Agate	8.4	1.9	82.2±0.6	2.648
20	Moss Agate	8.2	1.8	—	2.630
21	Petrified Wood	8.7	1.8	⊥ 91.6±2.5	2.649
				∥ 95.5±2.4	
22	Botswana Agate	9.1	2.3	102.5±1.3	2.650
23	Blackskin Agate	9.5	2.0	88.3±1.2	2.627
24	Black Flint	9.3	1.4	—	2.658
25	Flint	8.4	1.9	86.8±0.7	2.620
26	Chert	9.5	2.2	—	2.596
27	Oolitic Chert	8.5	1.4	92.8±6.9	2.648
28	Novaculite	6.6	1.2	96.5±4.8	2.676

* = poorly developed cracks
⊥ = perpendicular to grain or banding
∥ = parallel to grain or banding

Discussion

Hardness and Fracture Toughness

Various plots using the information presented in Tables 6 and 7 were constructed and examined to determine what factors influenced the observed mechanical properties. Of these plots, three exhibited useful information and are presented in Figures 1-3.

Figure 1 is a plot of Vickers hardness and fracture toughness. For the natural silicate materials there is a separation of the types (Opal-CT, Opal-A, jaspers, and the agates, flints, and cherts). In addition to these separations, there is a division between the opals and other silicates. Generally, the opals exhibit a fracture toughness around 1, but independent of hardness. Likewise, the other silicates show a spread around 2, but again are basically independent of hardness. Another important feature to note is that the Gilson synthetic opals are harder and tougher than natural opals and are tougher than the jaspers, cherts, flints, and agates.

Table 7 lists Vickers hardness and fracture toughness, K_c, for selected materials for comparison to the natural silicates used in the study. One can readily see from Table 7 that the jaspers, agates, flints, and cherts are harder and tougher than sodium borosilicate or soda-lime glasses, and are slightly tougher than Corning 0337 glass ceramic.

Hardness and Density

Figure 2 is a plot of density and Vickers hardness. One can also observe a separation of the silicate types as seen in Figure 1. Moreover, there is a general trend for hardness to increase as density increases for the more pure types (non-jasper). The jaspers possibly are displaced to greater density because of Fe impurities and are less tough due to impurities, both Fe and relic feldspar grains.

Fracture Touchness and Density

As seen in the previous two figures one also observes a separation of types in Figure 3, but not in the same manner. However, in more than the other figures the types are more distinctly and closely grouped. The groupings show that the more dense natural silicates are tougher than the less dense opals, but the synthetic opals are tougher than all.

Table 7. VH and K_c for Selected Materials (1).

Material	Surface Condition	VH(GN/m^2)	K_c($MN/m^{3/2}$)
Sodium borosilicate glass	as poured (annealed)	5.5	0.75
Soda-lime silica float glass	as received (annealed)	5.5	0.75
Corning 0337 glass ceramic (~60 vol % crystalline)	as fired	12.7	1.6
Wesgo Al-500 alumina	as fired	14.2	3.5
Diamonite P3142-1 alumina	as fired	15.7	4.5

(1) Marion (1979).

Table 8. Fracture Toughness and Al Correlation.

#	Sample	Al	Vickers Hardness (GN/m^2)	Fracture Toughness ($MN/m^{3/2}$)
16	Bloodstone Agate	--	8.3	1.8
17	Brazil Agate	Al*	7.9	2.1
18	Fire Agate	--	8.4	1.7
19	Montana Agate	--	8.4	1.9
20	Moss Agate	--	8.2	1.8
21	Petrified Wood	Al*	8.7	1.8
22	Botswana Agate	Al*	9.1	2.3
23	Blackskin Agate	Al	9.5	2.0
24	Black Flint	Al*	9.3	1.4
25	Flint	--	8.4	1.9
26	Chert	Al	9.5	2.2
27	Oalitic Chert	--	8.5	1.4

* = Trace.

Impurities and Mechanical Properties

Upon looking at the data it was noticed that the toughest and hardest agates, flints, and cherts were those samples that also had Al present. Table 8 summarizes the pertinent information. For the 12 samples listed, six contain Al and six do not. The average hardness and K_c for the Al-containing samples is 9.0 and 2.0, respectively, and 8.4 and 1.8 for the non-Al-containing samples. Therefore, it appears that the incorporation of Al into the silicate structure could be a factor in hardness and fracture toughness enhancement.

Summary

1. Hardness and fracture toughness measurements indicate that jaspers, flints, cherts, and agates are hard and very tough naturally formed ceramic-like materials harder and tougher than Na-borosilicate or soda-lime glasses and tougher than Corning 0337 glass ceramic. The synthetic opals (diphasic) are much harder and tougher than their natural counterparts.

2. Second-phase impurities such as hematite and goethite and relic feldspar grains tend to decrease the hardness of the silicate but show no significant effect on toughness.

3. The incorporation of Al into the silicate structure of agates, flints, and cherts may enhance both hardness and fracture toughness.

4. Hardness and fracture toughness of these silicates increases as the density increases.

References

Dana, J.D. (1962). A System of Mineralogy, 7th Ed., 3, Wiley, New York. Rewritten by C. Polache, H. Berman, and C. Frondel.

Marion, R.H. (1979). Use of indentation fracture to determine fracture toughness. Fracture Mechanics Applied to Brittle Materials. ASTM STP 678, S.W. Freiman, Ed., American Society for Testing and Materials, 103-111.

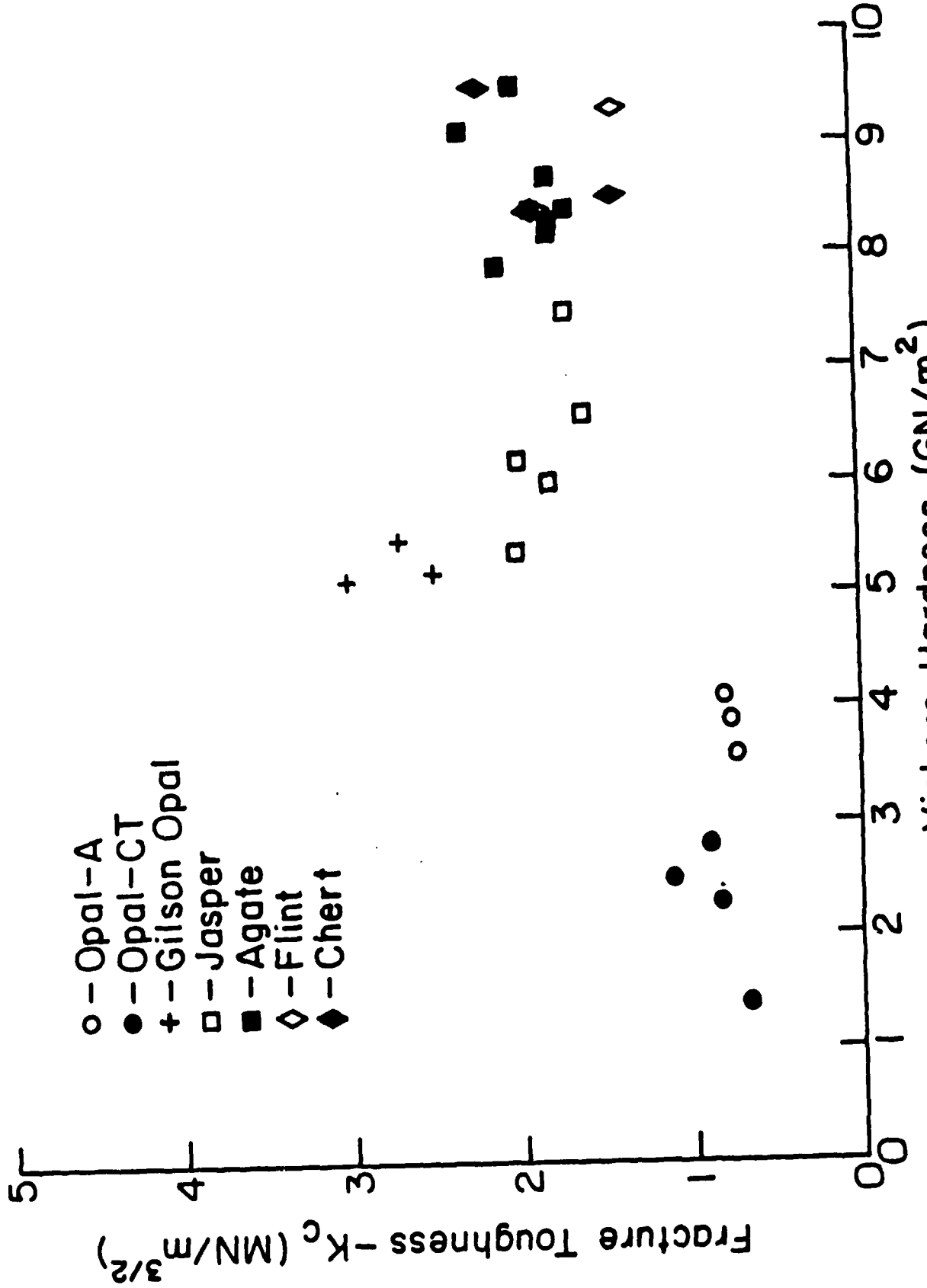
Fracture Toughness - K_C ($MN/m^{3/2}$)
Vickers Hardness (GN/m^2)
o – Opal-A
● – Opal-CT
+ – Gilson Opal
□ – Jasper
■ – Agate
◇ – Flint
◆ – Chert
0
1
2
3
4
5
6
7
8
9
10

Figure 1

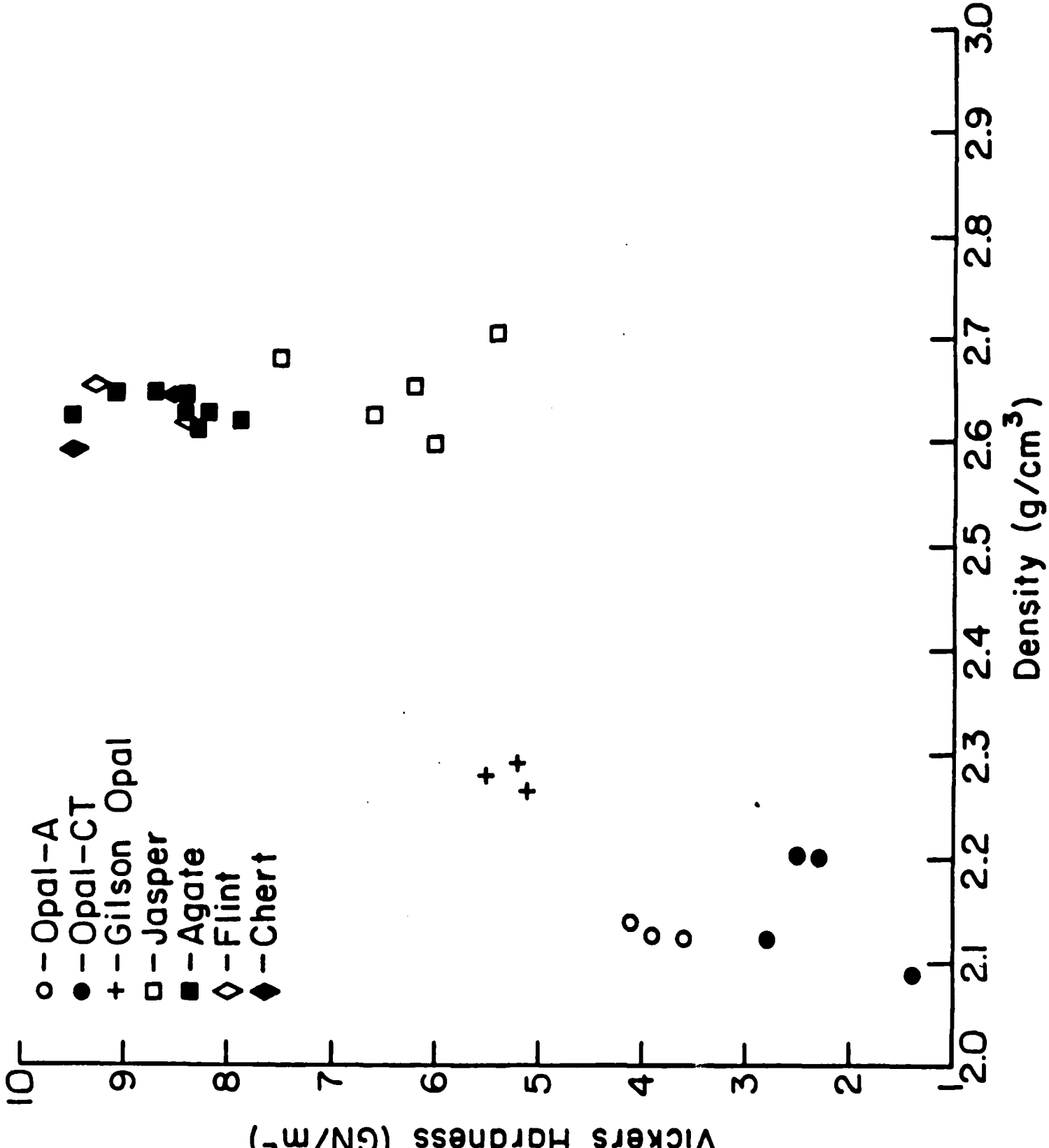
Vickers Hardness (GN/m²)
10
9
8
7
6
5
4
3
2
Density (g/cm³)
2.0
2.1
2.2
2.3
2.4
2.5
2.6
2.7
2.8
2.9
3.0
o – Opal-A
● – Opal-CT
+ – Gilson Opal
□ – Jasper
■ – Agate
◇ – Flint
◆ – Chert

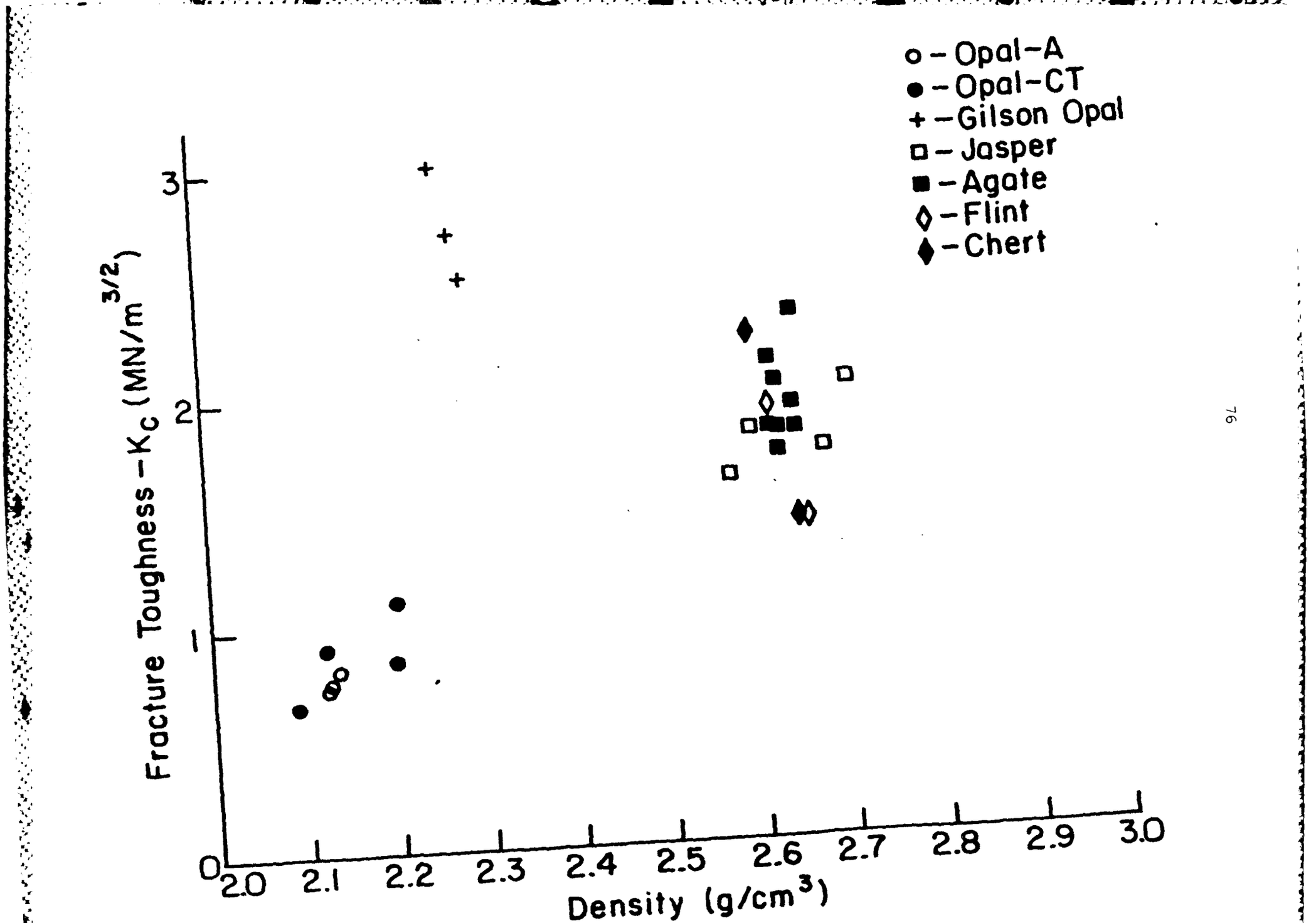
o – Opal-A
● – Opal-CT
+ – Gilson Opal
□ – Jasper
■ – Agate
◇ – Flint
◆ – Chert
Fracture Toughness – K_c ($MN/m^{3/2}$)
3
2
1
0
2.0
2.1
2.2
2.3
2.4
2.5
2.6
2.7
2.8
2.9
3.0
Density (g/cm^3)

Figure 3

Reprint #7

Titania-Silica Glasses Using a Colloidal Sol-Gel Process

246 Journal of Non-Crystalline Solids 82 (1986) 246–255
North-Holland, Amsterdam

TITANIA–SILICA GLASSES USING A COLLOIDAL SOL–GEL PROCESS

C.P. SCHERER and C.G. PANTANO

Department of Materials Science and Engineering, The Pennsylvania State University, University Park, PA 16802, USA

A colloidal sol–gel process has been developed to prepare a silica–10% titania glass for low thermal expansion substrates. The method utilizes titanium isopropoxide which is first reacted with ethylene glycol and citric acid at 120°C. This stabilizes the titanium isopropoxide against hydrolysis/precipitation so that it can be mixed with water and then used as the medium for dispersion of colloidal silica. This sol is then cast in tubes, sealed, and heated to 60–70°C to promote gelation. The gels are removed from the tubes after 2–3 days, dried in air for 24–36 h, and then sintered to 1230°C. The decomposition of the Ti–isopropoxide/ethylene glycol resin occurs at 300–350°C at which point the average pore-size increases to about 10.0 nm. The final density of the sintered gel is comparable to that reported for glasses of similar composition prepared by chemical vapor deposition (CVD). The glasses are translucent and TEM examination revales that this is due to the presence of uniformly distributed microcrystallites of anatase (< 150 Å). The coefficients of thermal expansion are intermediate between those of fused silica and a commercial titania–silica glass (Corning 7971).

1. Introduction

The preparation of low thermal expansion titania–silica glasses by the sol/gel method has been an active area of research and development [1–3] because these compositions are difficult to prepare by conventional melt techniques [4]. Although the sol/gel approach has been of practical benefit in the case of thin films [5–7], the results have been less significant in the case of bulk glasses. The major problem here – as well as in many other organometallic sol/gel processes – is the shrinkage-induced cracking. This limits the processing speed and/or the dimensions of the gels and glasses which can be obtained in practice. Thus, the chemical vapor deposition (CVD) technique [8,9] is still the only commercial method [10] used for the preparation of bulk titania–silica glasses. Nonetheless this method is time-consuming and costly and it, too, is limited with regard to the preparation of large, monolithic glass substrates.

The objective of this study was to use a colloidal sol/gel route for the preparation of these glasses. This method – which utilizes colloidal particles rather than organometallics as the oxide precursor – is much less susceptible to shrinkage induced cracking during processing [11,12]. Thus, it may be possible to prepare large, low-expansion mirror blanks in this way. In this application,

the optical properties of the glass, itself, are not of major concern; thus, the presence of structural water, closed-residual porosity, or even second phases, may be of little consequence. Rather, the processability, homogeneity and thermal expansion characteristics are the critical parameters.

An obvious means for accomplishing this task would be to gel a titania-doped colloidal silica. This doped colloidal silica could be fabricated by flame hydrolysis (e.g., the intermediate in the CVD process) or by controlled precipitation of micro gel or colloidal particles from solution. In this work, though, we have tried to develop a simple, inexpensive process. Thus, a method is herein described where a commercially available fumed colloidal silica is gelled in an aqueous solution containing a soluble titania polymer. This paper describes the chemistry of the sol, the microstructural evolution of the gel during sintering, and the thermal expansion behavior.

2. Experimental procedure

The colloidal material used for this sol-gel process was fumed silica (Degussa Aerosil) with a specific surface area of 200 m^2/g and a particle diameter of 14 nm. The titanium source was a solution made from tetraisopropyltitanate (TPT, Alpha Products). The TPT ($\sim$ 200 ml) was mixed with ethylene glycol ($\sim$ 600 ml), and then, anhydrous citric acid ($\sim$ 400 g) was added. The mixture was heated at $\sim$ 120°C on a stir/hot plate until the solution cleared and the odor of propanol vapors could no longer be detected. This step took about two hours during which time approximately 200 ml of solution evaporated. The solution was then filtered and stored at room temperature. Emission spectrometry of the solution yielded a titanium content of 2.34 wt% which is equivalent to $\sim$ 0.5 mmol. of titanium per gram of solution.

The sol was made by first mixing the titanium/glycol solution with water (1 : 1), and then adding the colloidal silica powder ($\sim$ 30.0 g per 100 ml). On the basis of the titanium/glycol solution assay, this was expected to yield an effective oxide composition of 7.5% TiO_2 and 92.5% SiO_2. The sol was homogenized in a conventional blender, and then cast in borosilicate glass tubes with an inside diameter of 12.77 mm. The tubes were capped with a plastic wrap, and were held overnight at 40°C to allow for the evolution of the bubbles that were created during the blending procedure. The temperature of the dryer was then slowly increased to 60–65°C to accomplish the gelation ($\sim$ 1 day).

The gels were cooled to near room temperature in the molds and were then extracted. There was no shrinkage during the gelation step. The gelled bodies could be dried crack-free within 24–36 h at room temperature. The shrinkage due to drying was $\sim$ 20%.

The dried gels were carefully pre-sintered to 400°C to decompose the organic resin phase without fragmenting or cracking the gel. Typically, this

schedule involved heating in oxygen at a rate of 75°C/h, with a 5°C/h rate in the critical temperature range 225–375°C to insure complete removal of the organics without carbonization. The gels were then heated to 1000°C at 100°C/h in the oxygen atmosphere to initiate the densification. The atmosphere was changed to air at 1000°C and the heating continued to ~ 1230°C to complete the densification.

The weight loss and thermal behavior of the gels were studied by thermal gravimetric analysis (TGA) and differential thermal analysis (DTA) using a Dupont Thermal Analyzer. The pore size distribution of the dried and presintered gels were measured by mercury porosimetry. The X-ray diffraction patterns were obtained using standard powder diffraction. The microstructures were examined in a transmission electron microscope using crushed fragments of the glass which were supported on a copper grid and coated with carbon. The coefficients of thermal expansion (CTE) was evaluated using a dilatometer (Theta Dilatronic Research I) equipped with a differential measuring head ($\frac{1}{2}$% accuracy).

3. Results and discussion

In contrast to pure silica sols, these titanium/glycol–silica sols are much more viscous. This characteristic is believed to be due to the presence of polymeric complexes. These polymeric species, or resin intermediates, form during the preparation of the titanium/glycol solution. Although the stepwise reaction mechanisms and final molecular weight distributions have not yet been established, the most important reactions are relatively simple and straightforward; i.e.,

(1) in the presence of a metal alkoxide, in this case tetra-isopropyltitanate, the citric acid and ethylene glycol catalytically react to form esters:

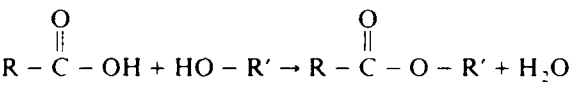

where

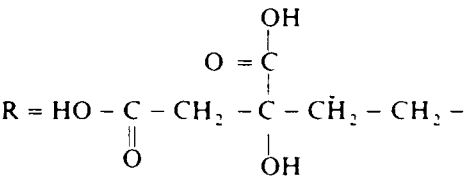

$R' = -CH_2CH_2OH$.

(2) the dihydroxy alcohol, ethylene glycol ($HOCH_2CH_2OH$), reacts with the

tetra-isopropyltitanate ($Ti(OiPr)_4$) to evolve propanol and form: glycolates, e.g.,

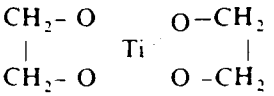

alkoxy-glycolates, e.g.,

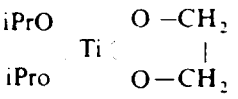

and oligomeric species thereof; e.g.,

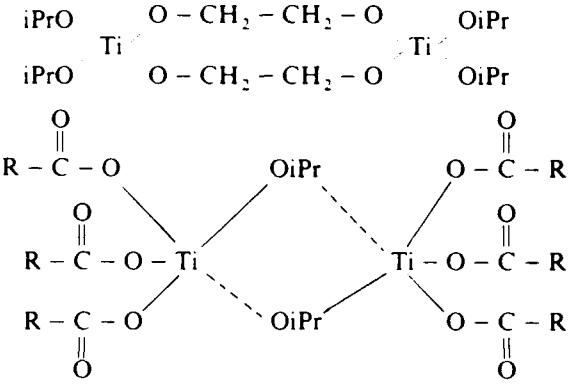

Of course, it is possible that some of the titanium ligands have been hydroxylated due to the presence of water. However, it is to be emphasized that the water (being formed as a by product of the condensation reaction (1)) is created very slowly. And due to the dilution of the Ti-complexes within the polyhydroxy alcoholic solution, as well as the prevalence of pilyesterification reactions under these conditions, the precipitation of a distinct hydrate phase is prevented. Upon completion, these reactions yield a highly polymeric solution wherein the chelates and derivatives of titanium are - for a variety of reasons - rendered much more resistant to hydrolysis during subsequent processing. These resin intermediates have also been used for the preparation of mixed-oxide powders, e.g., alkaline earth titanates and niobates [13].

The terminal hydroxyl groups on the polymer complexes render them soluble in the aqueous solution used to disperse the colloidal silica, and the chelation of the titanium by the citric/glycotic acid complexes and esters hinders hydrolysis/precipitation of titanium hydrates so that they can be uniformly distributed dring the sol preparation. More importantly, though, the terminal hydroxyls provide a mechanism for adsorption of the complexes to the colloidal silica particles via hydrogen bonding and condensation with surface silanol groups. One would also expect these polymer complexes to

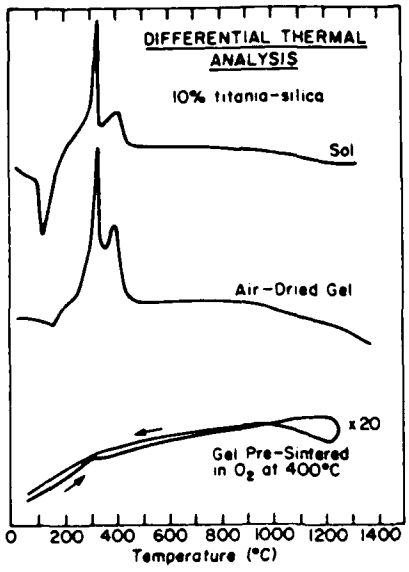

Fig. 1. The thermal decomposition behavior – in oxygen – of a freshly prepared sol, an air-dried gel and a pre-sintered gel; the exothermic features at 300–400°C are due to combustion of the organic resins.

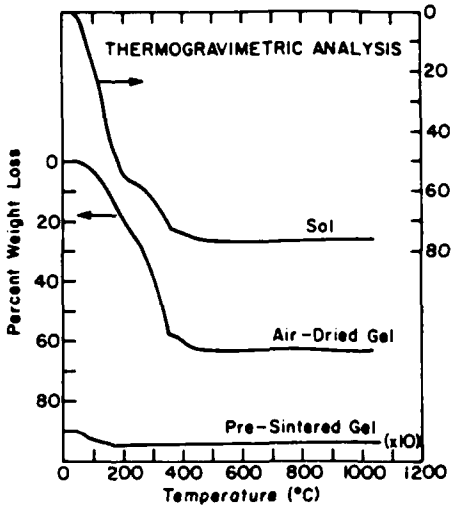

Fig. 2. The weight loss due to the evolution of water and decomposition of organic resins in the sol and gel; the pre-sintered gel is very porous, and thus, the small low-temperature weight loss is due to adsorbed water.

form bridges between the silica particles. Due to the presence of these interparticle resins, it is not surprising that the dried titania–silica gels are extremely hard and tough (at least compared to pure colloidal silica gels). After pre-sintering the dried gels – wherein these resinous complexes are decomposed – the gels are noticeably more fragile.

Fig. 1 presents DTA traces for the sol, the air-dried gel, and the gel after pre-sintering at ~ 400°C. The endothermic feature at ~ 125°C is clearly due to water, while the exothermic doublet at 350/400°C is due to decomposition of the organic resin. The TGA trace shown in fig. 2 reveals that the sol loses 75–80% of its weight, which is consistent with the batch composition (~ 40% water, 40% titanium/glycol and 20% silica). One would expect a 60% weight loss in the "water-free" gel due to the organic resins. This is qualitatively consistent with the TGA data which indicates a 60–65% weight loss in the "air-dried" gel. The lower trace verifies that pre-sintering at ~ 400°C is sufficient to remove all but traces of the organic resins. Clearly, removal of the organic resins is one of the most critical steps in the process because the decomposition of this relatively large quantity of material can lead to carbonization of fragmentation if carried out at an excessive rate.

The shrinkage behavior was studied by measuring the diameter of the gels at various stages of the drying and sintering, and also by dilatometry with a

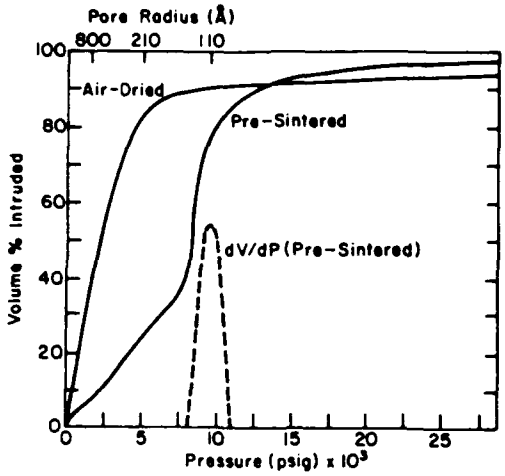

Fig. 3. The pore size distribution for the air-dried and pre-sintered gels (by mercury porosimetry of crushed specimens): the derivative is presented for the pre-sintered gel (dotted line).

constant load cell. During the drying step, these gels undergo a 20–25% shrinkage. This is not surprising since the sol contains ~ 40% water which is believed to be hydrogen-bonded at interparticle contacts [12]. Upon pre-sintering the air-dried gels at 400°C to remove the organic resins, little or no shrinkage occurs, but the density falls from 1.1 g/cc to 0.55 g/cc.

It may be especially significant that decomposition of the organic resins at 400°C does not produce any perceptible shrinkage. This indicates that the interparticle bridges and contacts formed during drying are stable to 400°C. Fig. 3 presents the pore size distributions measured in crushed samples of the dried gel (at 105°C) and the pre-sintered gel (at 400°C). The low pressure peak at ~ 80 nm is due to mercury intrusion between the gel fragments of these powdered specimens, and is not intrinsic to the gel structure itself. Any real porosity within the dried gel structure is below the resolution of mercury porosimetry. This is consistent with the idea that the pore spaces between the silica particles within the gel are filled with organic resin; pure colloidal silica gels made by the identical process - but without the titanium/glycol additions - exhibit measurable porosity centered at 10–15 nm diameter [12]. But after the 400°C resin decomposition, one notes the existence of a pore distribution centered at ~ 22 nm diameter. These undoubtedly represent pores within the gel structure, due to the loss of organics, and the measured pore size is consistent with values reported in the literature [12] for comparable colloidal silica gels heat treated at 400°C (15–19 nm diameter). The generation of this porosity (nearly 75%) during the resin decomposition, is consistent with their loss of strength.

The gels were sintered at a constant heating rate (~ 100°/h) in the dilatometer, and it was found that virtually all of the densification occurs in the range 1000–1250°C. The shrinkage behavior was further investigated by

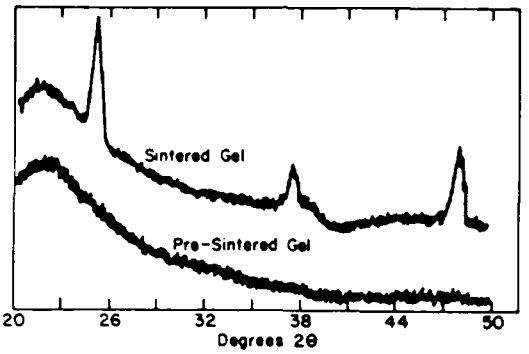

Fig 4. The X-ray diffraction patterns for the pre-sintered gel and the translucent glass obtained by sintering the gel to 1230°C.

measuring the diameter of the rods after heating at a constant rate to temperatures (T_{max}) of 1200°C, 1220°C, 1240°C and 1260°C and then holding there for four hours. The final stages of sintering (1000°C to T_{max}) were carried out in vacuum, air, oxygen or helium, but there was no observable effect of the sintering atmosphere on the total shrinkage. These experiments led to the establishment of 1230°C as the sintering temperature since additional densification was not observed at higher temperatures. The maximum shrinkage during this sintering step was ~ 30%, and so the total shrinkage from sol to glass in this system is 50–55%. The final density of the sintered gels was in the range 2.18 to 2.26 g/cc; the commercial titania–silica glass (Corning Code 7971) which contains ~ 7.5% TiO_2 has a density of 2.21 g/cc. Although the batch composition used to prepare the sol was expected to produce glasses with 7.5% TiO_2 (based upon the spectrochemical analysis of the titanium/glycol solution), the corresponding analysis of the sintered and pre-sintered gels revealed the presence of ~ 10% TiO_2.

These sintered gels are optically translucent due to the presence of a microcrystalline second phase. The X-ray diffraction (XRD) analyses are shown in fig. 4 and reveal the presence of crystalline titania (anatase) in the sintered gel. The pre-sintered gel was also examined by XRD but it was found to be X-ray amorphous. Thus, the anatase crystals form during the sintering step; unfortunately the DTA traces (see fig. 1) provide no means for establishing the crystallization temperature (due to the rather low concentration of TiO_2).

In order to determine the size and distribution of these crystals, the glasses were crushed and examined in an analytical TEM equipped with an energy dispersive X-ray analyzer (EDX). Fig. 5 reveals the presence of a second phase – approximately 13 nm in diameter – uniformly distributed in a glassy matrix. The microcrystalline nature of these second phase particles was verified by selected area electron diffraction, and the EDX analysis indicated that they are Ti-rich relative to the surrounding matrix. Thus, it is certain that these second

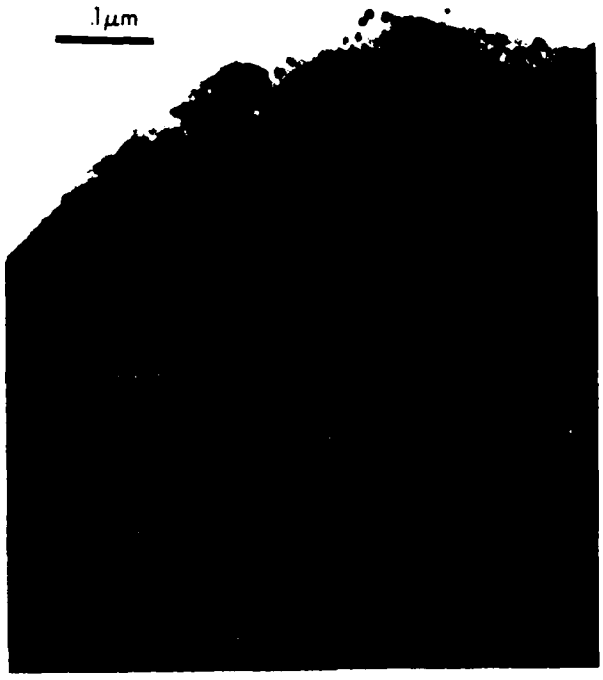

Fig. 5. TEM micrograph, obtained in direct transmission, for crushed fragments of the translucent glass.

phase particles are, in fact, the anatase crystals detected by XRD. The TEM examination of pre-sintered gels revealed the absence of any crystalline or other second phase material, and showed only the extensive porosity which characterizes the xerogel state.

It is believed that the tendency for these gels to undergo crystallization during sintering is due, in part, to their higher than optimum titania concentration, although the presence of the internal surface associated with the colloidal gel microstructure is certainly a contributing factor. Binary TiO_2–SiO_2 glasses melted with 8–12% TiO_2 show an amorphous second phase in the form of 10–20 nm droplets [4]. Upon heat treatment in the temperature range 1200–1400°C, these droplets crystallize to rutile. In the case of binary TiO_2–SiO_2 glasses prepared by flame hydrolysis, Nordberg first reported the limits of glass formation to be ~ 10% TiO_2 [10]. Later work by Schultz [8,9], however, showed that clear, X-ray amorphous glasses could be prepared up to ~ 17% TiO_2. Although an amorphous second phase was not observed in the unannealed glass, it was suggested that the glass compositions in the range 10% to 16% TiO_2 were "metastable" wherein TiO_2-rich zones could precipitate out in the form of phase separated regions and/or 6-coordinated Ti. It was shown

that heat treatment of these "metastable" glasses leads to internal rearrangements (e.g., changes in Ti coordination and/or amorphous phase separation) and crystallization (glass → anatase → rutile) which can be used to control the density and thermal expansion. It is most interesting to note that more recent studies [1-3] of TiO_2-SiO_2 glass formation, using organometallic sol/gel approaches, show only the formation of anatase crystals upon heat treatment. Altogether this suggests that anatase precipitates from "highly metastable" glasses such as those prepared by flame hydrolysis and sol/gel, whereas conventional melting leads to more stabilized glasses - often exhibiting an amorphous microphase - which yield rutile upon heat treatment.

The thermal expansion behavior was evaluated using a dilatometer with a differential measuring head. The glasses were run against a silica reference standard ($CTE_{25-960°C} = 3.5 \times 10^{-7}$ °C^{-1}) and a contraction was noted in the temperature range 25°C to 900°C. Thus, in spite of the limited sensitivity of this type of dilatometer ($\frac{1}{2}$%), it is clear that these gel-derived 10% titania-silica glasses have a lower expansion coefficient than fused silica. A titania-silica glass (Corning 7971-$CTE_{25-1000°C} \approx 2 \times 10^{-7}$ °C^{-1}) was used to better calibrate the contraction relative to silica. The best estimate of CTE that could be made with these data suggests an average value of $\sim 2.1 \times 10^{-7}$ °C^{-1} for the sol/gel glasses.

4. Summary and conclusions

A process has been developed wherein a colloidal fumed-silica is gelled in an aqueous solution containing polymeric titanium/glycol complexes. A wide variety of other aqueous and non-aqueous titanium solutions were evaluated, but these often led to hydrolysis/precipitation of titania-hydrates, poor gelling behavior, gas evolution and decomposition during the gelation and drying, or excessive granulation and cracking of the gel upon drying. The key features of the solution process described here are: (1) the titanium/glycol solution is water soluble and therefore can be used in the "conventional" processing of colloidal silica sols, (2) the polymeric titanium species - although not yet fully characterized - are stabilized against hydrolysis/precipitation during preparation of the sol, as well as during gelation and drying, (3) these polymeric titanium complexes have an abundance of hydroxyl groups which can hydrogen bond to surface silanol groups on the colloidal silica surfaces and eventually form interparticle bridges, and (4) the polymeric nature of the titanium/glycol species not only make the sol and wet-gel easier to handle, but because they are essentially resin intermediates, they impart a hardness and toughness to the dried gel which further facilitates the processing. The critical steps in the process are the pre-sintering (for removal of the organic resons) and the final sintering of the gel to produce a dense glass which is sufficiently homogeneous to yield near-zero thermal expansion. Obviously, the sintering must entail some diffusion of titanium into the colloidal silica particles to form

the 4-fold coordinated titanium sites which are required for low-expansion behavior. Ideally, though, some of this titania-silica network formation and homogenization will occur during gelation since the silica which dissolves in the aqueous sol can complex with the Ti species, and together, they may be adsorbed or re-deposited within the gel structure (e.g., during interparticle neck growth).

Although the dried and pre-sintered gels were amorphous, crystallization was observed in these ~ 10% TiO_2 glasses during sintering to the pore-free state. This leads to translucency and less than optimal thermal expansion behavior. Nonetheless, it was already shown [8,9] that careful heat-treatment and microcrystallization, at least in the case of CVD derived glasses, can be used to control the final thermal expansion of TiO_2-SiO_2 glasses. Thus, we believe that additional study of the densification step in this process, and better control of the TiO_2 concentration during the sol preparation, can lead to optimization of the thermal expansion behavior. Some preliminary studies, wherein these 10% TiO_2 gels were vacuum hot pressed, produced tinted - but transparent - glasses with the lowest thermal expansion coefficients yet achieved ($\sim 0.5 \times 10^{-7}$ °C^{-1}).

It is worth mentioning, finally, that in contrast to the organometallic sol/gel approach to TiO_2-SiO_2 glass formation, this colloidal route is less expensive, more expedient, and at the same time, has the potential to produce large monolithic pieces. The eventual application of a "double-dispersion" procedure [12] in this system could further reduce the drying shrinkage, and thereby, may represent an important avenue for future investigation.

The authors gratefully acknowledge the Air Force Office of Scientific Research (F49620-85-C-0069) for financial support of this study, and helpful discussions with G. Geoffrey and B. Gordon.

References

[1] K. Kamiya and S. Sakka, J. Mater. Sci. 15 (1980) 2937.
[2] B.E. Yoldas, J. Non-Cryst. Solids 38 (1980) 81.
[3] C.J.R. Gonzalez-Oliver, P.F. James and H. Rawson, J. Non-Cryst. Solids 48 (1982) 129.
[4] D.G. Ostrizhko and G.A. Pavlova, IZV. Akad. Nauk SSR, Neorg. Mat. 6 (1970) 74.
[5] H. Schroeder, Phys. Thin Films 5 (1969) 87.
[6] C.J. Brinker and M.S. Harrington, Solar Energy Mater. 5 (1982) 159.
[7] B.E. Yoldas, Appl. Optics 21 (1982) 1960.
[8] P.C. Schultz, J. Am. Ceram. Soc. 59 (1976) 214.
[9] P.C. Schultz and H.T. Smyth, in: Amorphous Materials, eds., Douglas and Ellis (Wiley, London, 1972) p. 453.
[10] US Patent 2326059 (1943); see also Low Expansion Materials Bulletin (Corning Glass Works, 1969).
[11] E.M. Rabinovich, D.W. Johnson, J.B. MacChesney and E.M. Vogel, J. Non-Cryst. Solids 47 (1982) 435.
[12] E.M. Rabinovich, D.W. Johnson, J.B. MacChesney and E.M. Vogel, J. Am. Ceram. Soc. 66 (1983) 683.
[13] US Patent 3330697.

Manuscript #3

Colloidal Sol/Gel Processing of Ultra-Low Expansion TiO_2/SiO_2 Glasses

COLLOIDAL SOL/GEL PROCESSING OF ULTRA-LOW EXPANSION TiO_2/SiO_2 GLASSES

DENG ZAIDE, ELSE BREVAL and CARLO G. PANTANO

Department of Materials Science and Engineering, The Pennsylvania State University, University Park, PA 16802, USA

Abstract

A series of titania-silica glasses with 0-9% TiO_2 were fabricated using a sol/gel process. The sol was prepared by dispersing colloidal silica fume in an aqueous solution of titania which was synthesized through the acid-catalyzed hydrolysis of titanium isopropoxide. The sols gelled in 2-4 days, and then were dried for 6-8 days. The dry gels were sintered at 1450-1500°C to produce clear, dense, microstructure-free glasses.The gels underwent a total shrinkage of ~50% to yield glass rods about 50 mm long and 5 mm in diameter, or glass discs about 4 cm in diameter and 5 mm thick. The drying step was most critical in the production of crack-free specimens.

In the gel, the transmission electron microscope (TEM) revealed the presence of 1-5 nm rutile microcrystallites uniformly distributed within a network of colloidal silica particles. After sintering to 1450-1500°C, though, an amorphous, homogeneous structure was created. Fourier transform infrared spectroscopy (FTIR) verified the formation of an amorphous solid-solution of titania and silica after sintering.

The thermal expansion of the glasses was measured using a differential dilatometer. The average linear coefficients of thermal expansion (CTE) varied between $+5x10^{-7}$ and $-.2x10^{-7}$ c^{-1} in the range 0 to 9% TiO_2. The glass with 7.2% TiO_2 exhibited a zero thermal expansion coefficient at 150-210°C. The hysterisis in CTE on heating and cooling was of the order .01-.02 ppm.

1. Introduction

It is well known that 5-10% TiO_2/SiO_2 glasses are very refractory and possess very low thermal expansion coefficients (1-3). Unfortunately, they are exceedingly difficult to fabricate. The melting temperatures are in excess of 1700°C, and the glassmelts are quite susceptible to phase separation and devitrification upon cooling (4-5). The glasses can be prepared by the flame hydrolysis technique, but the cost and availability has limited their more widespread application (1-2,6-7). A number of reports have shown that the organometallic sol/gel method can be used to prepare glasses in this system, but in this case, the processing times and cracking problems have been severe limitations (8-10).

This paper describes a colloidal sol/gel approach for the preparation of TiO_2/SiO_2 glasses over the composition range 0-10% TiO_2. They can be processed in 7-10 days, and to date, have been fabricated in the form of rod, tube and plate up to 50 mm in size. The glasses are clear, fully dense and microstructure-free. Most importantly, they exhibit thermal expansion characteristics which match those of glasses prepared by flame hydrolysis.

2. Synthesis

The general approach in this sol/gel process is to disperse colloidal silica fume in a 'titania' solution. The stability and chemistry of the titania solution is most important. The titania species must be soluble so that a homogeneous dispersion and gelation of the silica fume can be achieved. Since the silica fume is most effectively dispersed in aqueous solutions, the development of an aqueous titania solution was sought. An earlier publication (11) showed that a titanium glycoxide solution (prepared by hydrolysis and polyesterification of titanium isopropoxide in ethylene glycol/citric acid at 120°C) was effective for the uniform dispersion of silica fume, and also yielded a tough, resinous gel. But, carbonization of the residual glycoxides was difficult, and this led to crystallization during sintering.

In the present study, the hydrolysis and peptization of titanium isopropoxide in a variety of simple acids (namely, nitric, hydrochloric, and acetic) was evaluated for the preparation of an acidic titania solution whose hydrocarbon content was minimal. It was found that a clear, stable

titania solution could be prepared by first mixing titanium isopropoxide (Alfa Products) with acetic acid, and then adding water. After stirring for 30-60 minutes, the solution would clear. This titania solution was found to be stable at room temperature for 2-3 days.

The silica fume (Degussa Aerosil 200) was dispersed in the titania solution using a conventional blender. The solids content of these titania-silica sols was held constant at 20%. The titanium isopropoxide concentration was varied in the solution to control the TiO_2/SiO_2 ratio. The sols were cast in molds to produce rods, discs and tubes, and these were sealed in plastic. The gellation would occur within four days at 25°C, but could be accelerated to two days at 60°C. The gels were then removed from the molds and slow-dried (usually one week) at 25°C on a teflon sheet. The dried gels were always heat-treated in air at 500°C for ~30 minutes to remove adsorbed molecular water and to carbonize residual acetate groups. Thermogravimetric analyses revealed a 3-4% weight loss at 25-125°C (due to water), and another 1-2% weight loss at 250-450°C (due to residual acetates).

It was found that sintering is best accomplished using a very rapid heating rate (20-50°C/min) with plateaus at ~1200-1250°C and ~1450-1500°C. The temperature is held at 1200-1250°C because the shrinkage rate is highest there. This permits the structural water to escape, and thereby minimizes the tendency for bloating at higher temperatures. The temperature is then raised to 1450-1500°C where the glass becomes fully dense and clear. Differential thermal analyses suggested that a correlation exists between the titania content and the presence and breadth of an exotherm at 1200-1400°C. Presumably, this is due to a reaction between silica and titania, but a quantitative interpretation is not yet available. There is no question that the gels with the higher titania contents are more difficult to sinter.

It may be especially significant to note that if the gel is sintered to 1200°C in He, and then to 1450-1500°C in air, the clarity of the glass is noticably improved and the tendency towards bloating at higher temperatures is further reduced. The fact that the gel turns blue-purple after the 1200°C He treatment suggests that titanium redox may play an important role in the final stages of sintering. Figure 1 illustrates these points.

The preparation of crack-free glasses is most dependent upon the drying step. The wet gel is very weak, and therefore, is very susceptible to cracking during mold release and/or drying. The linear shrinkage is about 24% during drying. The only problems encountered in sintering the gel to glass are due to bloating and this can be easily controlled through the He presintering and/or the dehydration treatments. The linear shrinkage is about 32% during sintering, and virtually all of this occurs between 1000°C and 1200°C. In this study, 50 mm glass rods (5 mm in diameter), 40 mm diameter glass discs (5 mm in thickness) and glass tubes were successfully and reproducibly fabricated.

3. Characterization

All of the glasses were optically clear and x-ray amorphous after sintering. The density was 2.19 to 2.20 g/cc for all the glasses; Corning's Code 7971 (with ~7% TiO_2) is fabricated by flame hydrolysis and has a reported density of 2.20 g/cc. Table 1 shows that the $\%TiO_2$ has no systematic effect on the density.

The composition of selected glasses was determined by spectrochemical analysis and also electron microprobe analysis; these data are also included in Table 1. It can be seen that the titania concentration is within 2-3% of the nominal value (based upon the Ti-isopropoxide composition in the original sol). This indicates that the hydrolysis of Ti-isopropoxide in the acetic acid solution was nearly complete and that little titania was evolved during sintering. The compositional homogeneity was evaluated using a wavelength-dispersive electron microprobe. A 5 μm electron beam was used to measure the TiO_2 and SiO_2 concentration at 60 individual points. The spatial variation in composition was of the order $\pm$.2 % TiO_2 at this scale. This is comparable to the value obtained for the Corning 7971 glass, and probably corresponds to the instrumental precision rather than any real compositional nonuniformity. It verifies, at least, that gross variations in titania distribution are not present. Finally, note that the glass with 7.2% TiO_2 (nominal) actually contains closer to 7.0% TiO_2; it is shown later that this glass exhibits near zero thermal expansion.

The gels and glasses were extensively characterized in the analytical TEM, but only a brief summary can be presented here. The dried gels showed networks of the spherical silica particles

AD-A185 482 EXPLOITATION OF THE SOL-GEL ROUTE IN PROCESSING OF CERAMICS AND COMPOSITES(U) PENNSYLVANIA STATE UNIV UNIVERSITY PARK MATERIALS RESEARCH LA R ROY 2/2

UNCLASSIFIED 10 JUL 87 AFOSR-TR-87-1193 F49620-85-C-0069 F/G 11/4 NL

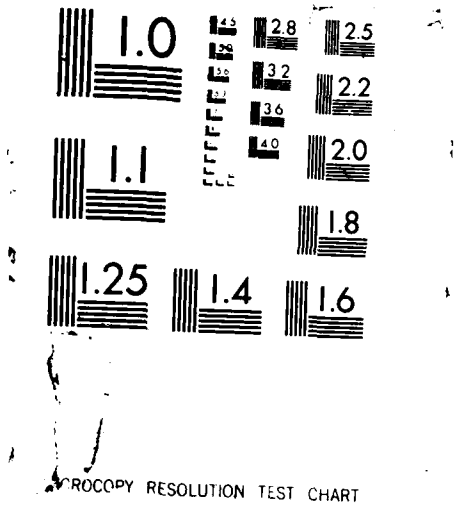
1.0
2.8
2.5
3.2
2.2
3.6
4.0
1.1
2.0
1.8
1.25
1.4
1.6
ROCOPY RESOLUTION TEST CHART

(~10-20 nm in diameter). The TiO_2 was found in the form of rutile microcrystals of the order 1-5 nm in size. They could be readily highlighted within the amorphous silica gel network using a dark field image of the 2.5 Å rutile electron diffraction line. This is shown in Figure 2a and reveals that the titania distribution is rather uniform when viewed over areas of the order 2 μm. It should be noted that only those crystallites properly oriented for reflection can be seen in this micrograph. The uniformity of their distribution is even more apparent upon 'rocking' the sample to bring other crystallites in and out of the proper diffraction condition. At higher magnifications, the location of the crystallites between the amorphous silica particles can be observed (Figure 2b). The crystallites are very fine and seem to coat most of the silica particles; in some regions, though, clusters of the crystallites can be seen.

After sintering to 1200-1250°C, the TiO_2 rutile crystallites were transformed into TiO_2 anatase crystallites. These crystallites were of the order 5-10 nm in size and were uniformly distributed in an amorphous silica matrix. Naturally, these crystals were more prevalent in the glasses whose $\%TiO_2$ was higher, and there was some indication that the He atmosphere enhanced their formation. In the 9% TiO_2 glasses for example, the anatase could be detected by x-ray diffraction. After the final densification at 1450°C-1500°C, the presence of crystallites was not observed. Many crushed fragments and ion-beamed thin sections of the 7.2% TiO_2 glasses, in particular, were examined; all were found to be free of any microstructure. In the 9% TiO_2 glasses, an occasional anatase crystal (10-30 nm) would be encountered. Apparently, the titania crystals dissolve at 1450-1500°C where the mobility of the Ti ions is sufficient to create a homogeneous amorphous structure.

The gels and glasses were further characterized using Fourier transform infrared spectroscopy (FTIR). The upper spectra in Figure 3 is for the dried gel. Only the silicon-oxygen vibrations associated with the amorphous silica fume can be observed in this region. The titanium vibrations in the crystalline oxide cannot be seen here due to their six-fold coordinations. The middle spectra shows the appearance of a new band after the gels are sintered at 1450-1500°C. This 945 cm^{-1} band is also observed in Corning's 7971 glass, and has been attributed to the

vibration of titania in four-fold coordination with oxygen (12). Thus, it seems clear that the titania - originally dispersed between the silica particles - has dissolved in the silica to create an amorphous solid solution.

It is noteworthy that the 945 cm^{-1} [TiO_4] band begins to appear even after the 1200-1250°C heat-treatment. This suggests that most of the anatase observed in the glasses heated only to 1200-1250°C may form on cooling; i.e., the TiO_2-SiO_2 solution has already been created, at least in part, at 1200-1250°C. The spectra and expansion properties are identical whether the gel is sintered to 1250°C, cooled and then reheated to 1450-1500°C, or sintered in one cycle to 1450-1500°C with a hold at 1250°C to change atmosphere. These observations further verify that the titania dissolves in the silica matrix at 1450-1500°C.

4. Thermal Expansion

The expansion curves for the various glasses are presented in Figure 4. These were measured on ~4 cm long samples in a differential dilatometer using Corning's 7971 for reference. The data was calibrated using the expansion curve reported by Schultz (2) for 7971. The expansion curves for these sol/gel-derived glasses appear to be more linear than those reported for glasses prepared by flame hydrolysis (2,7). This observation is consistent with the results of Hench et al. (13), who report that alkoxide-derived SiO_2 glasses exhibit more linear thermal expansion than fused silica. It is also worth mentioning that there was scarcely a .01 ppm hysterisis in the expansion curves on heating and cooling.

The average linear coefficients of thermal expansion (CTE) were determined over three temperature ranges and these are plotted in Figure 5. The values for Corning's SiO_2 (7940) and TiO_2-SiO_2 (7971) are superimposed. It is clearly evident that the expansion values, and their dependence upon composition, are consistent with the data reported for glasses prepared by flame hydrolysis (2,6,7). The 'zero-expansion' sol/gel composition is ~7.2% TiO_2 (nominal). (Note: Additional measurements of the CTE for the 7.2% and 9.0% TiO_2 glasses were obtained through an independent laboratory and those verified the data in Figure 5.)

5. Summary

It has been shown that microstructure-free glasses in the TiO_2-SiO_2 system can be prepared using a diphasic colloidal sol/gel approach. The FTIR data provided direct evidence that the TiO_2 and SiO_2 form a solid solution during the heat-treatment, and the TEM verified that the final structure is dense, amorphous and homogeneous at the 5-10 nm level. The thermal expansion behavior is consistent with these characteristics, and comparable to the properties of glasses prepared by flame hydrolysis. A range of glasses with CTE between $+5x10^{-7}$ and $-.2x10^{-7}$ $°C^{-1}$ were fabricated by varying the TiO_2 between 0 and 9%. The CTE of the 7.2% TiO_2 composition was zero at 150-210°C, and was within .01 ppm of zero between 110 and 500°C.

The authors gratefully acknowledge the Air Force Office of Scientific Research (F49620-85-C-0069) for financial support of this study. We also thank Theresa Guiton for the FTIR spectra.

6. References

[1] N. E. Nordberg, U.S. Patent 2,326,059 (1943).
[2] P. C. Schultz and H. T. Smyth, in: Amorphous Materials, eds., Douglas and Ellis (Wiley, London, 1972) p. 453.
[3] G. J. Copley, A. D. Redmond and B. Yates, Phys. Chem. Glasses, 14, (1973) 73.
[4] L. N. Kozlova, B. V. Tarasov and K. I. Chepizhnyi, Steklo, 3, (1968) 6.
[5] D. O. Ostrizhko and G. A. Pavlova, IZV. Akad. Nauk SSR, Neorg. Mat. 6 (1970) 74.
[6] Low Expansion Materials Bulletin (Corning Glass Works, 1969).
[7] P. C. Schultz, J. Am. Ceram. Soc., 59 (1976) 214.
[8] K. Kamiya and S. Sakka, J. Mater. Sci., 15 (1980) 2937.
[9] B. E. Yoldas, J. Non-Cryst. Solids, 38 (1980) 81.
[10] C.J.R. Gonzalez-Oliver, P. F. James and H. Rawson, J. Non-Cryst. Solids, 48 (1982) 129.
[11] C. P. Scherer and C. G. Pantano, J. Non-Cryst. Sol., 82 (1986) 246.
[12] H. R. Chandrasekhar, M. Chandrasekhar, and M. H. Manghnani, Solid State Comm., 31 (1979) 329.
[13] L. L. Hench, at the Third International Conference on Ultrastructure Processing, San Diego, CA, February, 1987.

Table 1. Properties of Titania-Silica Sol/Gel Glasses

$\%TiO_2$ (nominal)	0	2.9	5.1	6.1	7.2	8.0	9.0	Corning 7971
Density gm/cm^3	2.202	2.199	2.199	2.207	2.200	2.191	2.202	2.192
Analyzed % TiO_2								
• Spectrochemical	-	-	4.92	-	7.01	-	8.85	-
• Electron Probe*	-	-	-	6.15±0.21	7.01±0.22	-	-	7.38±0.23

* The average and standard deviation of 60 individual measurements; the beam was 5 μm in diameter and was stepped in 5 μm increments.

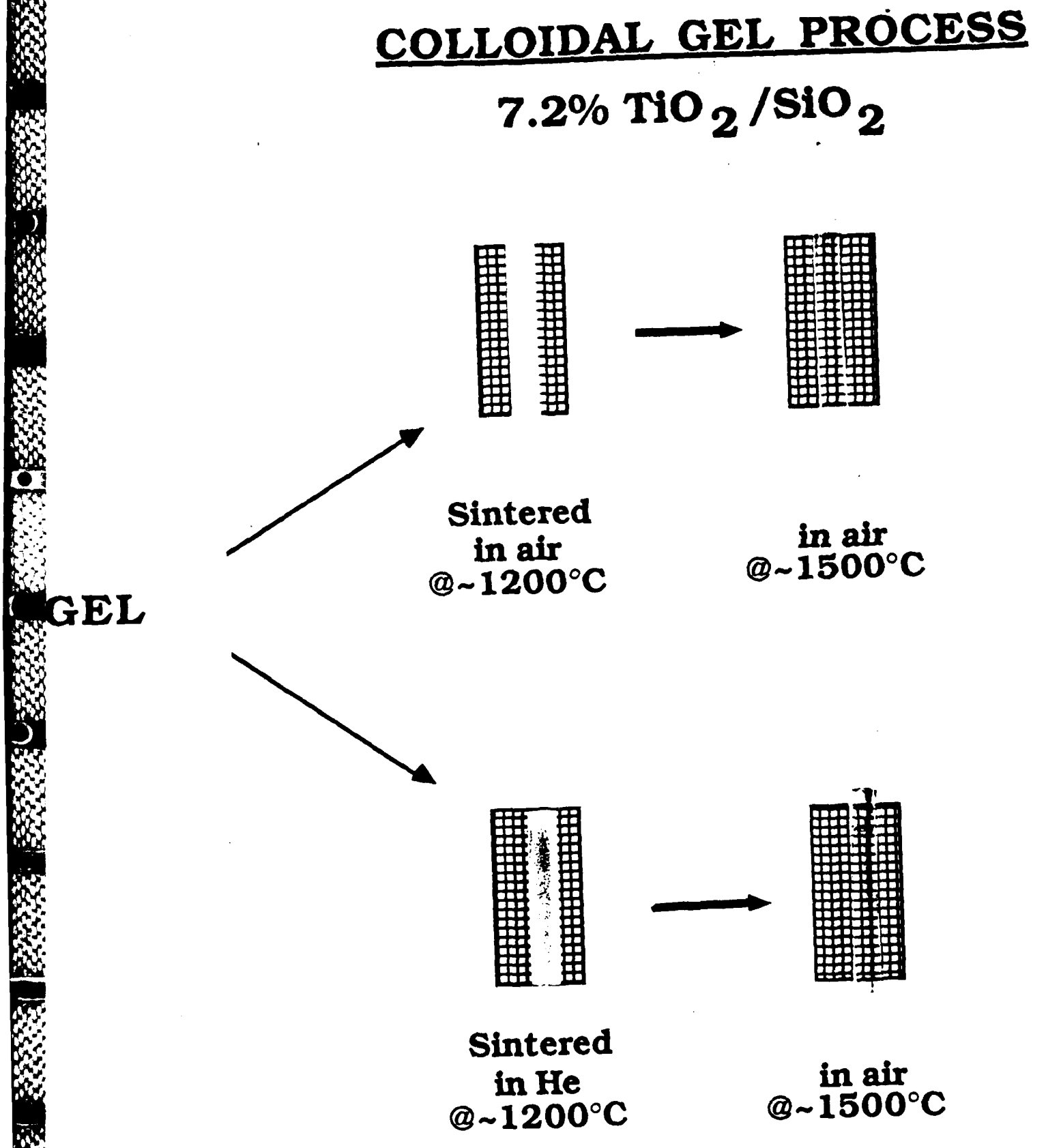

Figure 1. The effect of heat-treatment temperature and atmosphere upon the colloidal gel-to-glass conversion; the gel heated to 1200°C in He is distinctly blue-purple.

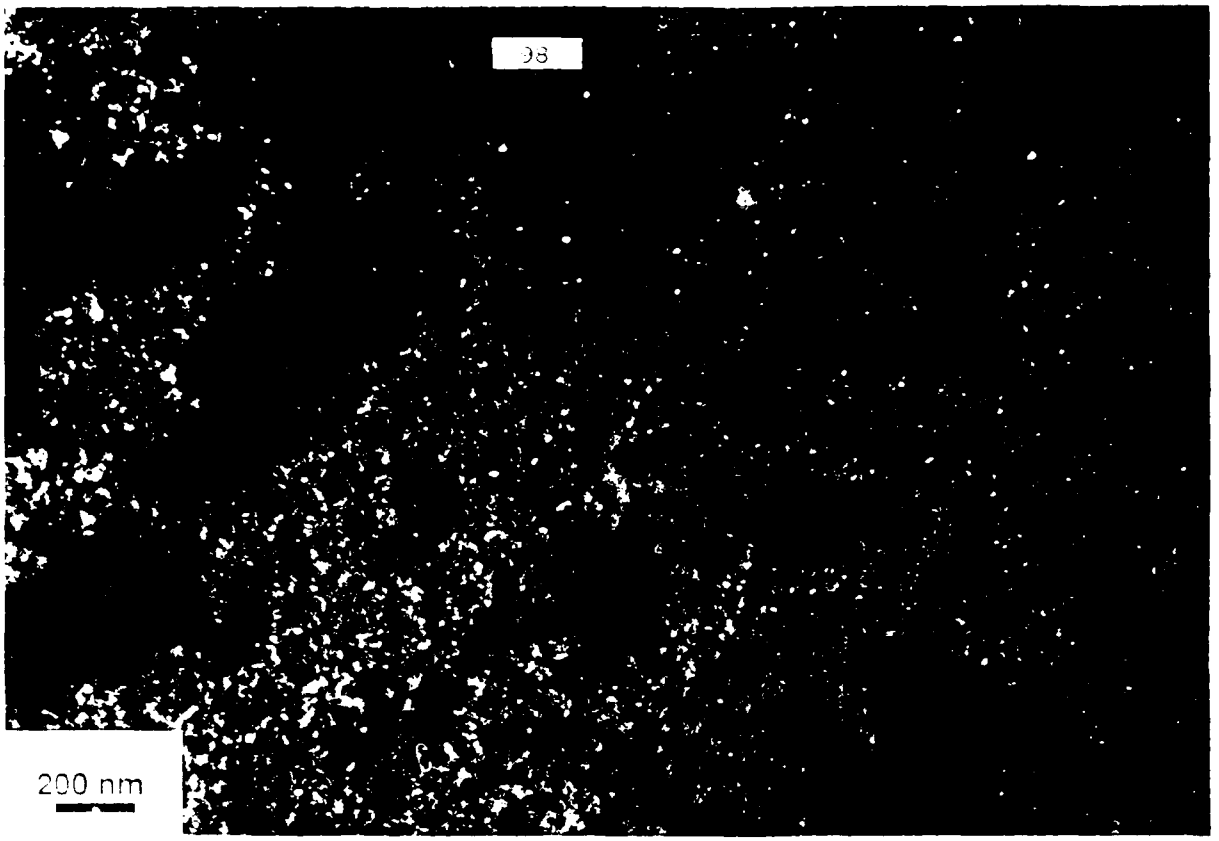
98
200 nm

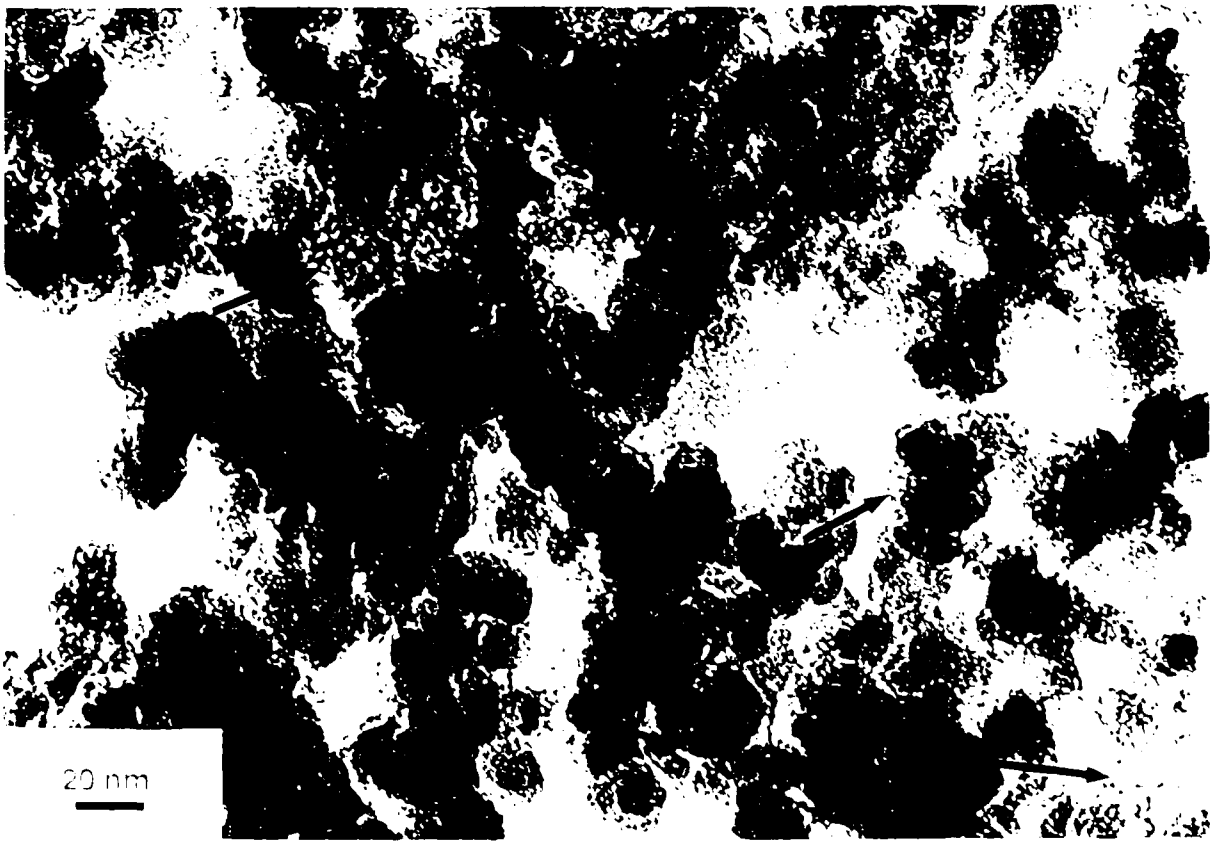
20 nm

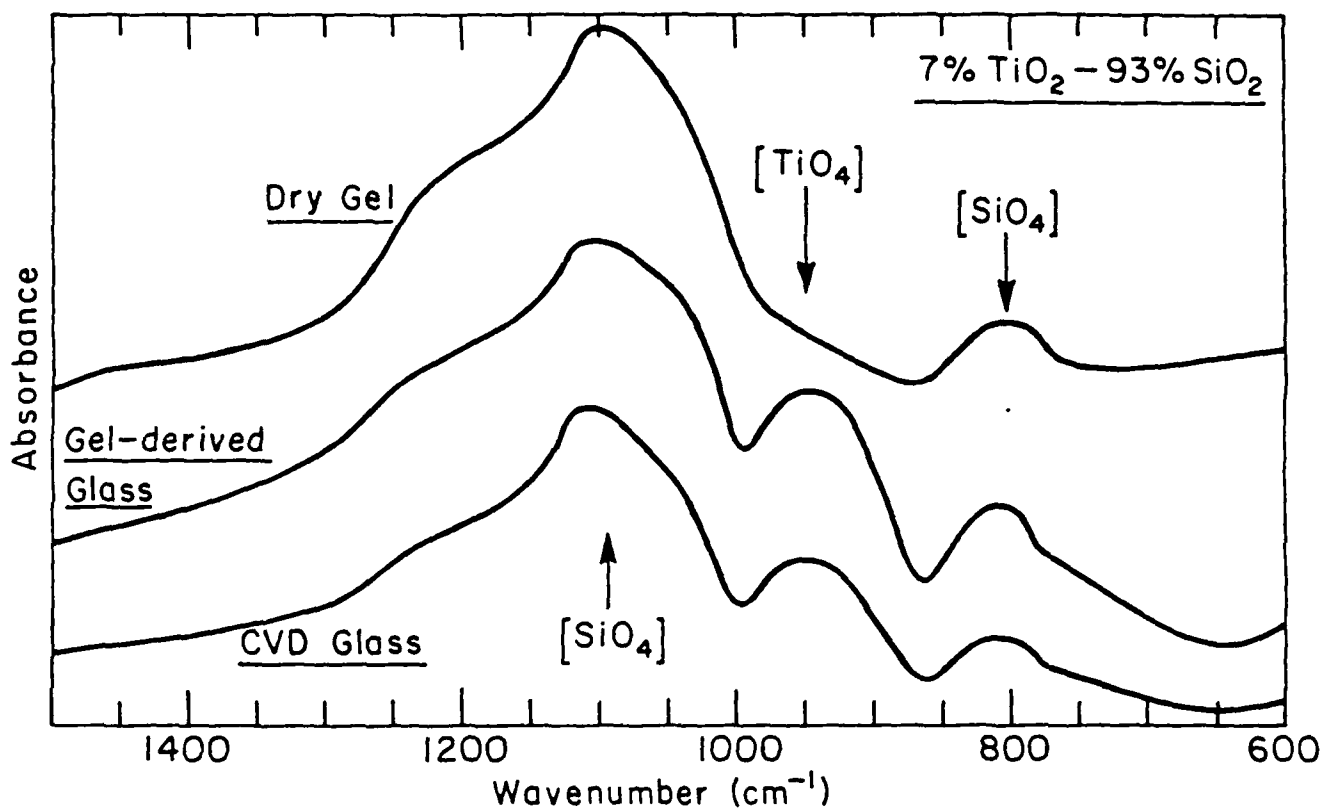

Figure 3. Fourier-transform infrared (FTIR) absorption spectra of the colloidal gel (upper), the gel after sintering to a dense glass (middle), and Cornings 7971 glass prepared by flame hydrolysis.

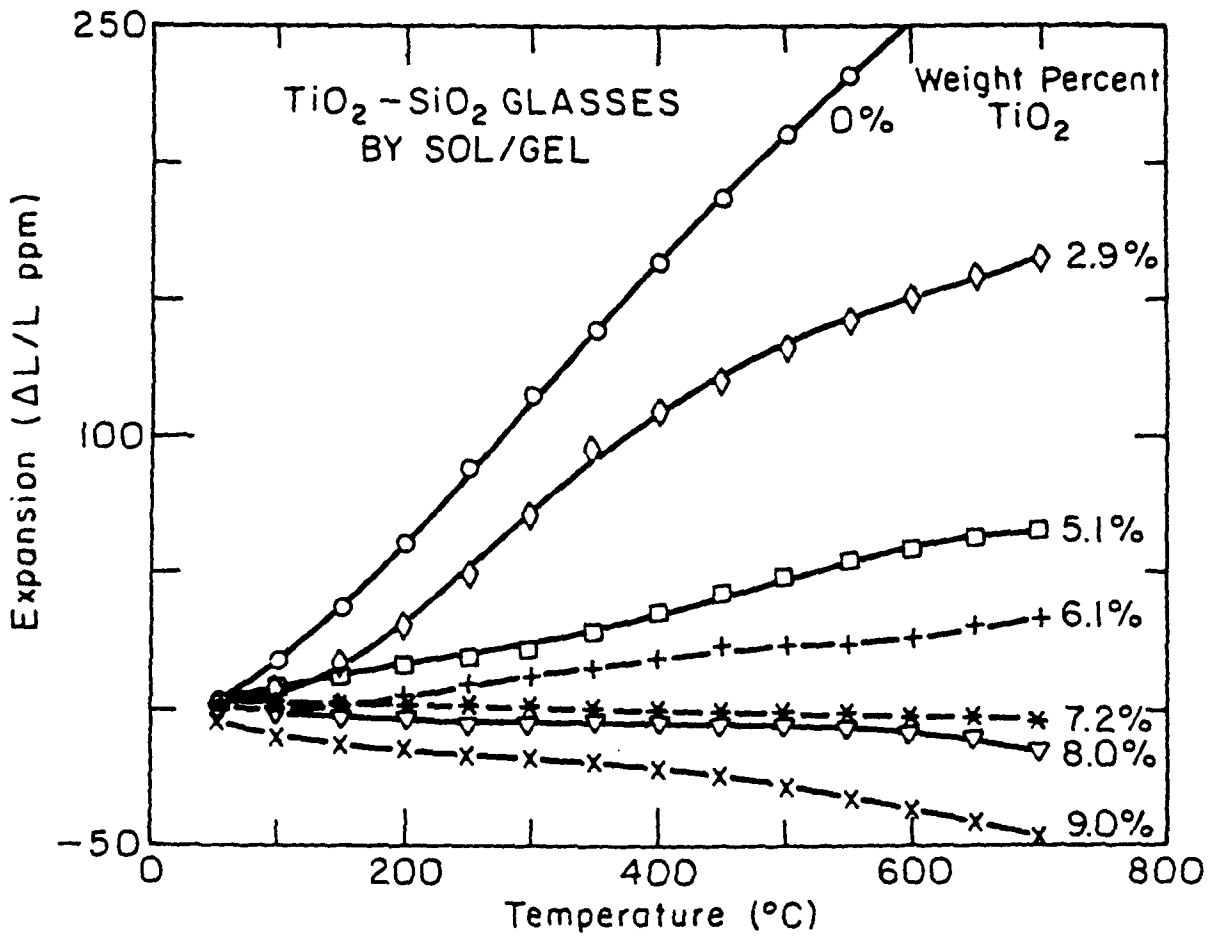

Figure 4. Thermal expansion curves for titania-silica glasses prepared by the colloidal sol/gel method: obtained using a differential dilatometer with Corning's 7971 for reference.

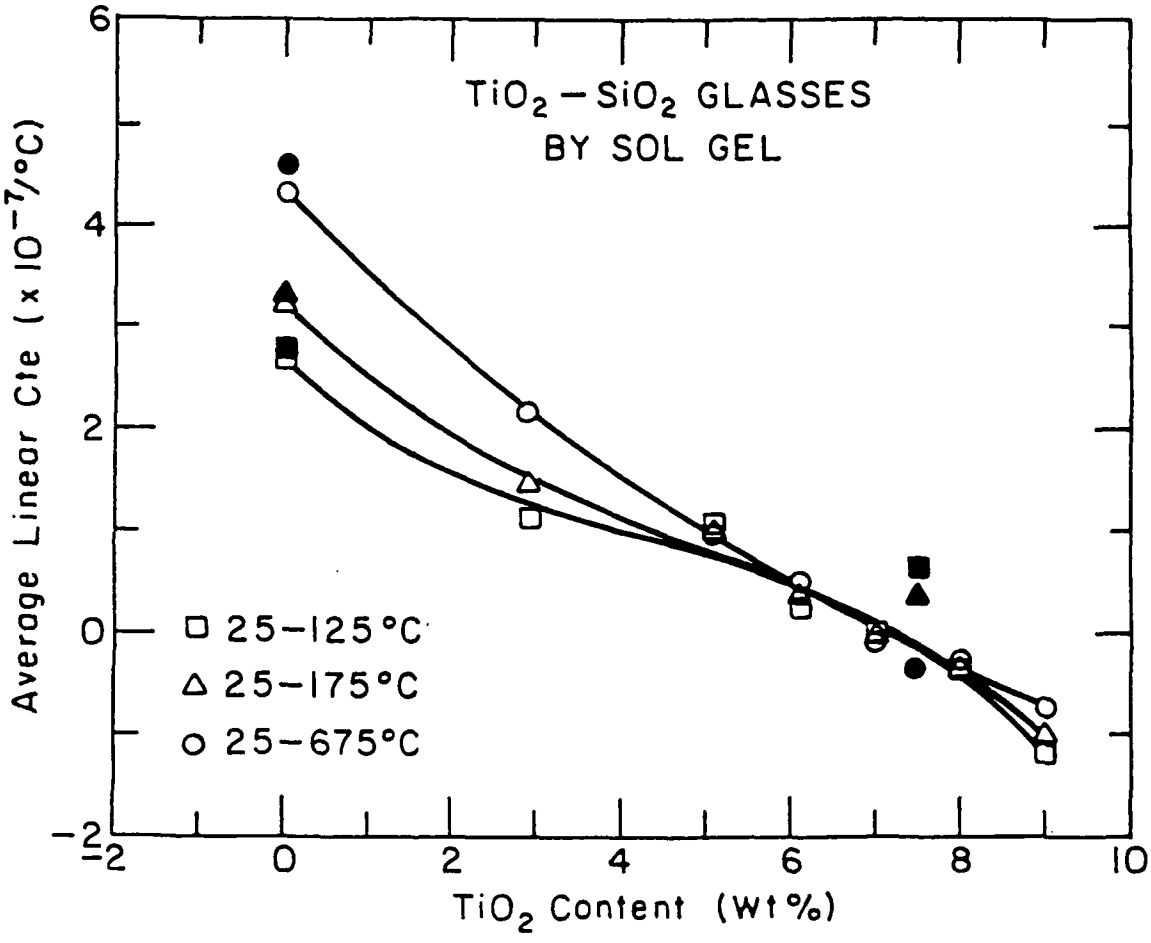

Figure 5. The relationship between the average linear coefficient of thermal expansion (CTE) and the titania content in the sol/gel derived glasses; the values reported for Corning's 7940 (0% TiO_2) and 7971 (7.4% TiO_2) are superimposed in the 'filled' symbols.

END

DATE

FILMED

DEC.

1987